Sentinel-HR Phase 0 Report

Julien Michel, Olivier Hagolle, Jean-Marc Delvit, Martin Thierry, Lebegue Laurent, David Laubier, Jean Philippe Malet, Legenne Jérome, Joël Michaud, Vinasco-Salinas Juan, et al.

Sentinel-HR Phase 0 Report

March 28, 2022

Julien MICHEL (CESBIO/CNES DTN/CD/CB)
and
Sentinel-HR Mission Advisory Group

Ref: DTN/CD/CB-2022.0002072

Contents

Chapter 1

Introduction

Sentinel-HR is a phase 0 study of a systematic observing remote sensing mission working at a metric resolution. Its mission is focused on small scale change detection, although its conception allows innumerable usages. The study was conducted by CESBIO on behalf of CNES, it started on September 2020 and ended in late 2021. This report describes the outcomes of the study.

1.1 Proposed Sentinel-HR mission

The proposed Sentinel-HR mission is an **optical, sun-synchronous earth imaging mission** which is similar to Sentinel2 in that it provides **systematic, repetitive worldwide acquisitions with constant viewing angles**, allowing to foster long time-series with high radiometric and geometric quality. It would therefore complement Sentinel2 or Sentinel2 NG by bringing higher resolution observations (1 to 2.5 meters) on a regular basis.

For economic reasons, it seems difficult to combine all the characteristics of Sentinel-2, with a 5-fold increased resolution. For this reason, Sentinel-HR trades revising time for higher resolution. The proposed mission would offer a **spatial resolution of 2 meters**, with a **revisit time of 20 days**, with the 4 spectral bands that are already acquired at 10m on Sentinel2 : Blue, Green, Red and Near Infra-Red, with a similar radiometric quality.

The aim of this trade-off is to enable the monitoring of high resolution changes that are out of reach for the current Sentinel2 constellation alone and probably also for the next generation of Sentinel-2.

In addition, Sentinel-HR would perform perform **systematic Digital Surface Model acquisition**, with a target accuracy of 4 meters CE90. As Sentinel-HR is a mission dedicated to change detection, changes in elevation are important to complement the changes in radiometry and give a full insight on the amount and nature of observed changes.

Sentinel-HR is a Sentinel mission at heart: it aims at a long mission lifetime in order to guarantee data availability, create deep time archive, and enable earth observation services. In the same spirit than the other Sentinel missions, we advocate for a free and and open-data model.

Sentinel-HR main specifications are shown in table 1.1.

Coverage	All lands and coasts (similar to S2)
Ground Sampling Distance	$\leq$ 2.5 meters
Revisit time	20 days
Spectral bands	Blue, Green, Red, Near Infra Red (similar to S2 10m bands)
Viewing angles	Constant Nadir (at center of swath)
Stereoscopic capability	Systematic with height accuracy better than 4m CE90
Orbit	Sun-synchronous
Tasking	no tasking, instrument always on
Mission lifetime	7 years or more
Proposed launch date	2028
Products	Analysis Ready, free and open data

Table 1.1: An overview of proposed specification for Sentinel-HR

1.2 Position with respect to other foreseen missions

1.2.1 Position with respect to Sentinel2 NG

We think that with one of the options studied in this report, a launch date in 2028 could be reached if the funding of the mission was to be decided in 2022. However, in the eventuality of a failure to obtain the funds, it is interesting to compare Sentinel-HR with Sentinel2-NG.

The Sentinel2 missions has recurrent satellites planned until 2035 approximately. Those satellites will have exactly the same specifications as Sentinel 2A and Sentinel 2B. Note that in terms of specifications, Sentinel-HR trades Sentinel2 revisit time for higher resolution, in approximately the same ratio. In 2035, an evolution of the Sentinel2 mission, called Sentinel2 NG, should be launched by ESA. This mission is currently in phase-A, with Target (lower bound) ad Goal (upper bound) specifications as shown in table 1.2.

Specification	Target	Goal
Atmospheric correction bands resolution	60 m	30 m
Other bands resolution	10 m	5 m (for 6 bands)
Optional panchromatic band		2.5 m
Number of bands	$\approx$ 16	
Revisit	2-3 days	

Table 1.2: Extract of foreseen specifications for Sentinel2 NG

With a maximum number of 3 satellites, increasing the spatial resolution and the number of bands, improving the revisit time and adding a 2.5 meters panchromatic band is a lot of constraints for the design of the satellites and mission, and for the overall mission cost.

We advocate that Sentinel-HR would be a better option, by dedicating separate satellites to the resolution increase and especially to the 2 meters target, and focusing Sentinel2 NG on the revisit time. Sentinel-HR would therefore act as a companion mission for Sentinel2 NG. It is also important to note that a large panchromatic band may be insufficient for the user needs, and that Sentinel-HR would instead offer four high radiometric quality spectral bands that can be tuned to exactly match those of Sentinel2 or Sentinel2 NG.

1.2.2 Position with respect to Copernicus Contributing Missions

Copernicus contributing missions, in the European glossary, are commercial satellite missions (sometimes funded by the member states), whose data can be bought by Copernicus to serve the interests of European users. Table 1.3 shows some of the available contributing missions. Note that Planet Doves, and RapidEye satellites are not included, and neither is Airbus Defense and Space SPOT6/7 or hypothetical UryheDaily constellation, since the resolution of the multi-spectral bands is too coarse to fulfill Sentinel-HR mission. CO3D case is presented in section 1.2.3.

Mission	Nb. Satellites	Swath (km)	MS GSD (m)	Capacity/day (M.km²)
Pleiades	2	20	2.4	1
Pleiades Neo	4	14	1.2	2
Worldview 2 & 3	2	13	1.2	1.2
Planet Skysat	21	6	1	0.4
Total				4.6

Table 1.3: Some Very High Resolution missions that are part of Copernicus Contributing missions

Can Copernicus Contributing Missions meet the requirements of Sentinel HR ? As presented in section 1.1, Sentinel-HR is a Copernicus mission at heart: it aims at global, systematic, long-term observations in order to provide stable ground for the development of value-added services. Copernicus Contributing Missions, on the other hand, are a collection of privately owned constellation, with commercial prospects at heart and very heterogeneous lifetimes.

In section 3.1.2, we estimate that Sentinel-HR would acquire 5.94 Mkm² per day, which exceeds the current total acquisition capacity of all missions listed in table 1.3. This means that even buying the full available capacity can not meet the requirements of Sentinel-HR, even if we let aside heterogeneity of sensors and lifespan, and without acquiring systematic stereoscopic pairs for 3D reconstruction.

Restricting the target area to Europe (and losing major use cases such as monitoring of glaciers 2.1) may be seen as a solution to this problem, but unfortunately, the acquisition capacity of Contributing Missions will also be reduced, since capacity is uniformly distributed around earth. For instance, figure 1.1 shows all the Pléiades acquisitions over France for April 2021, regardless of their cloud coverage. We can see that only around 20% of the area is covered.

In order for Contributing Mission to meet the requirements for Sentinel-HR, capacity would therefore have to be drastically increased, and long term planning of the different missions life should be carefully handled in order to guarantee a gap-free acquisitions plan over several years. This capacity increase and synchronization will require substantial commitment from Europe in terms of data buy, in order to convince private investors funding. Effort will have to be put in data harmonization in order to deliver a single consistent product from all those missions. And this plan is still not considering two key features of Sentinel-HR : guaranteed constant (or near constant) viewing angle, which would limit the possibility for constellation owners to sell part of orbital resources to private customers, and 3D systematic acquisition, which would require even bigger capacity increase.

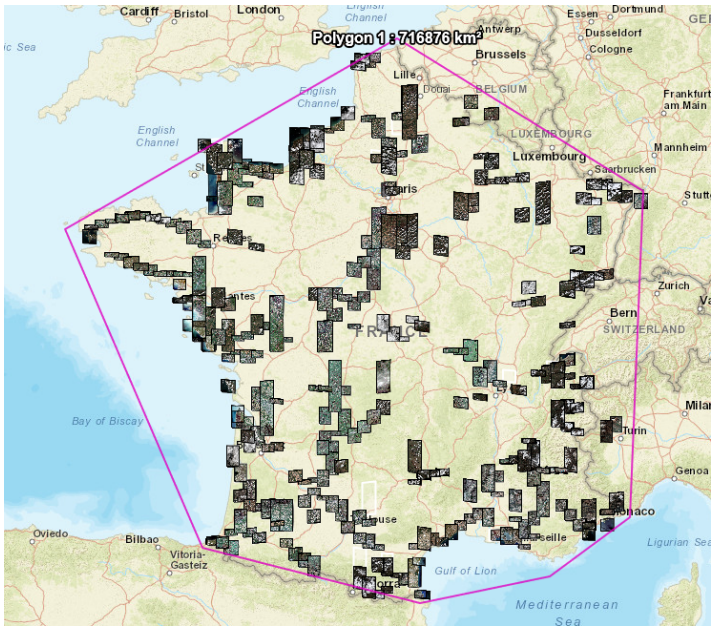

Figure 1.1: Acquisitions by Pleiades 1A and 1B over France for the three first weeks of April 2021. Although all these images are great and locally useful, probably less than 20 % of the French surface is covered. (from Airbus geostore catalog).

Copernicus Contributing Mission are therefore a valuable tool for local provisioning of VHR images, but it can not meet the requirements for Sentinel-HR, by far.

1.2.3 Position with respect to CO3D

CO3D [LCHL+20] is a mission proposed by CNES and developed with Airbus Defense and Space, aiming at providing a Digital Surface Model of the world landmass between S60° and N70° with 1 meter relative accuracy and 4 meters absolute accuracy. In addition to this DSM, CO3D products will also provide 50 centimeters images in Near Infra-red, red, blue and green bands. The DSM will be computed by stereo-reconstruction from simultaneous stereo images acquired by a constellation of at least two pairs of low-cost 50 cm resolution satellites flying at 502 kilometers on the same sun-sychronous orbit and equiped with matrix sensors. Each satellite has a footprint of 7x5 km² (lxh) and performs a step and stare acquisition scheme. Pairs of satellite will have the ability to perform simultaneous stereo acquisitions with a B/H of 0.2, which can be useful when imaging moving objects such as waves or vehicles. Satellites are small, and 4 of them fit in the Vega launcher, leaving half of the space available for another passenger. CO3D is currently being developed with a launch expected mid-2023.

Here we must distinguish between the planned CO3D mission and the CO3D concept off-the-shelf satellites.

1. Current CO3D mission

   The current CO3D mission uses 2 pairs of satellites and will consist in two phases. First phase is a 18 months demonstration aiming at assessing the system performances over two areas; France (0.5 Mkm²) and an area of interest of 27 Mkm² covering middle-east and north Africa. Those areas will therefore be prioritized over commercial activities

and completion of DEM. After 18 months, the mission enters a second phase dedicated to commercial exploitation. It will therefore act as an additional VHR capability to complement those listed in table 1.3, with a daily capacity of 0.8 Mkm² per day (or 0.4 Mkm² for a DSM involving 2 satellites). A part of this capacity will be dedicated to the monitoring of 40 glaciers 3 times a year, as well as some sites for snow cover monitoring, and other requests for revisit are possible at a fair price, for a maximal total coverage of 5Mkm² annually. It should also be stressed that if revisit is feasible in theory for a few sites, it will be very hard to guarantee small or constant viewing angles due to constraints from tasking.

In that perspective, current CO3D mission is similar to other VHR missions with respect to Sentinel-HR : it will offer a sharper resolution than required, but is not meant for systematic revisit with constant or near-constant nadir observations. Additionally its acquisition capacity can not meet the requirements for Sentinel-HR. However, it is noteworthy that it can provide the Digital Surface Model as a standard product out of the ground segment, which makes it very unique with respect to the other VHR missions. DSM quality is expected to be far better than what Sentinel-HR could offer with a low-baseline ratio instrument. Last it should be stressed that the radiometric quality is not the heart of the mission (see section 3.2.1).

2. Re-using CO3D conception for Sentinel-HR

   However, CO3D has been designed from the start as an extensible constellation. We could therefore inquire whether Sentinel-HR specifications could be met by mean of buying dedicated additional CO3D satellites. With the current revisit requirements and the 50 cm resolution, this would probably require a large amount of satellites. However, should we adapt their orbit and make a few adjustment to the instrument, it seems that a constellation of 12 or even 9 dedicated satellites could meet the requirements, benefiting from all the work that has already been achieved on this recurrent satellites line. This solution for Sentinel-HR is presented in section 3.2, as an alternative to building two ad-hoc satellites.

1.2.4 Importance of the 3D component of Sentinel-HR

It is also important to stress that, even if numerous Very High Resolution ($< 1m$) commercial satellites can offer stereo or multi-view acquisitions to their client, none of them offers the systematic and global acquisition of DSM that Sentinel-HR will provide. With Aster mission planned to end in September 2023, we will loose the ability for global monitoring of elevation changes on a regular basis and Sentinel-HR would allow to enable some sort of continuity of service, which is of tremendous importance for long term monitoring of earth at a time when the effects of global climate change become more and more impacting. This is highly demanded with a much better revisit by the scientific community. For instance, a group of 23 renowned scientists from the international glaciers, volcanoes and solid earth community wrote a letter to the Landsat Next engineering team to request for a stereo capability of this mission. To our best knowledge, this requirement is still under investigation by the Landsat Next engineering team.

1.2.5 Importance of a Free and Open data policy

The Sentinel-2 mission is receiving a unprecedented success for a earth observation mission in Europe : in 2020, between 8000 and 10000 users downloaded data every month on the Copernicus data distribution centre, an increase by 15% compared to 2019 [KC21], as shown in figure 1.2. And these statistics to not account for the number of users downloading data from the European DIAS or the collaborative ground segments, including PEPS and THEIA in France. They also don't include the users that work online with the data in cloud infrastructure at Sinergise, Google Earth Engine or Amazon Web services.

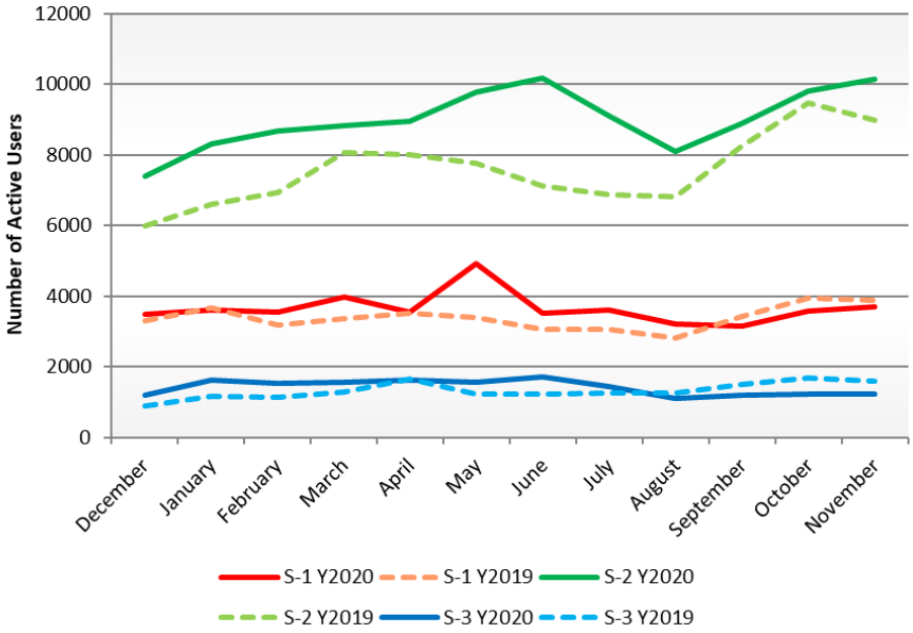

Figure 1.2: Active user trend per mission in 2019 and 2020 (source [KC21])

This rather unexpected success, knowing the low uptake of remote sensing data until the Copernicus era, results in the development of a lot of services, in the domains of land cover, agriculture, incitement of good agricultural practices, land planning, ecosystem monitoring, coastal surveillance, risk evaluation and post-catastrophe evaluation...

This success is due to the combination of several features :

- Sentinel-2 acquisitions are systematic
- data are free and openly accessible
- the data quality is high, and the mission has become a reference
- the revisit (5 days) and resolution (10m), are well tailored for a lot of usages

Among these features, the systematic free and open acquisition is a key one. The Landsat history, shows how the change of policy from a paying data policy to a free and open one completely changed the situation, as shown in figure 1.3 extracted from [WMC+12].

Having access to free and open data is of course essential for research and development purposes, to lower the cost of development to start a new service or application, or to apply

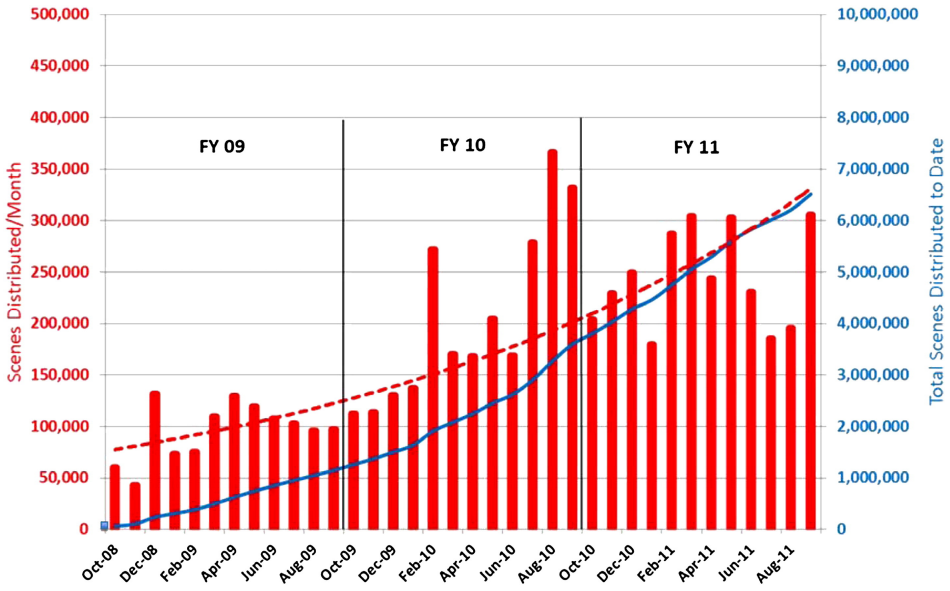

Figure 1.3: Monthly summary of scene downloads from the EROS Data Center, covering the period from October 2008 (opening of the Landsat archive) to September 2011, further delineated by US Government fiscal year. (source: [WMC+12])

to non-commercial applications such as the monitoring of the health of our planet ecosystems. It is also essential to allow the demonstration of feasibility of applications at large scale, such as the production of land cover maps over a whole country, or the monitoring of deforestation. It is also essential to deliver public services such as the monitoring of snow cover, the change of coastlines with time, or the global detection of water bodies.

Free and open data are also essential for educational purposes, within student projects, or for public awareness objectives, and it may also be used by journalists.

Thanks to the free and open data policy, the acquisition costs are shared for all users, and if an image is useful for monitoring coastlines and deforestation in two different projects, it is not necessary to pay it twice.

But the best argument can be found in a report by the French parliament [FM18]. « It is not the sale of data that creates its value, it is its circulation ». To justify this change of policy, the report states that : « Free dissemination and reuse of sovereign geographic data implies that the production of sovereign geographic data must be financed by the state subsidies, if not by the sale of the data. If the open data business model is empirically verified, a return to the public purse will be achieved by the taxes of the additional wealth created by the release of data. »

1.3 The phase 0 study

1.3.1 Objectives

Objectives of the phase 0 were stated as follows:

- Investigate and refine users requirements for the Sentinel-HR mission with the help of a Mission Advisory group in order to assess the benefits of this mission with respect to

other foreseen missions

- Provide a coarse design of the mission in order to assess its cost and feasibility
- Investigate methodology and readiness level of the hybridation between Sentinel-HR and Sentinel2 and Sentinel2 NG
- Communicate outcomes to ESA in the frame of the preparation of Sentinel2 NG

1.3.2 Organisation

The phase 0 study has been conducted and coordinated by **Julien Michel** (CNES/CESBIO, DSO/SI//CB), with the help of **Joel Michaud** (CNES, DIA/PF) and **Olivier Hagolle** (CNES/CESBIO, DSO/SI//CB).

1. CNES Human Resources

   Technical contributions have been made by :

   - **Thierry Martin** (DSO/DV/IFL) for the preliminary orbitography study of the ad hoc satellites configuration presented section 3.1.2
   - **Clément Dudal** (DSO/RF/ITP) for the analysis of telemetry requirements presented section 3.1.3.
   - **David Laubier** (DSO/SI/IN) for the instrument design proposition of the ad hoc satellites configuration presented section 3.1.4.
   - **Renaud Binet** (DSO/SI/QI) for the low-baseline 3D simulation and performance assessment study of the ad hoc satellites configuration presented in section 3.1.5.
   - **Laurent Lebègue** (DSO/OT/CXI) for the design and preliminary study of the CO3D extension configuration presented in section 3.2.

   Several suggestions and technical advice regarding the hybridation methodology have been proposed by **Jordi Inglada** (CNES/CESBIO, DSO/SI//CB) during the course of the study.

2. Other CESBIO resources

   The super-resolution part of the hybridation study has begun with the 6 months internship of **Juan Vinasco-Salinas** at CESBIO, funded by ANITI. **Juan Vinasco-Salinas** worked 6 additional months on the comparison of hybrid products methodologies presented in chapter 4 through a CNRS contract under Sentinel-HR project funding.

3. Financial Resources

   Of the 50 k€ budget allocated to the study, 50% has been used for funding the low-baseline 3d simulation and performance estimation delegated to CS-SI in the frame of its current contract with CNES, and 50% has been used to fund a 6 months short term contract for **Juan Vinasco-Salinas** at CESBIO, to help with the design and experimentation of the hybridation workflow.

4. Mission advisory Group

   A large part of the study heavily relied on an informal **Mission Advisory Group**, composed of **benevolent** scientists and users that dedicated their time to contribute to use cases and user requirements, and **should be greatly thanked for that**:

Name	Affiliation
Anne Puissant	LIVE, UMR 7362 CNRS / Université de Strasbourg
Antoine Lefebvre	Kermap
Etienne Berthier	LEGOS
Rafael Almar	LEGOS
Erwin Bergsma	CNES labo-OT
Jean-François Faure	Maison de la télédétection, UMR Espace Dev, IRD
Gerard Dedieu	E2L
Jean-Philippe Cantou	IGN
Jean-Philippe Malet	CNRS/EOST et ForM@Ter
Philippe Maisongrande	CNES DIA
Thomas Corpetti	LETG
Stephen Clandillon	ICUBE-SERTIT/Université de Strasbourg
Pierre Maurel	Maison de la télédétection, TETIS, INRAE
Jean-Marc Delvit	CNES labo-OT
Antoine Lucas	IPGP
David Sheeren	DYNAFOR UMR 1201 INRAE / Toulouse INP
Jérémie Mouginot	IGE
Hervé Yesou	ICUBE-SERTIT/Université de Strasbourg
Christelle Iliopoulos	CNES labo-OT

Table 1.4: Composition of the Mission Advisory Group

1.3.3 Timeline

- The informal Mission Advisory Groups met 4 times during the course of the study:

  Kick-Off Meeting 2020.07.06

  Progress Meeting 2020.11.25

  Progress Meeting 2021.02.12

  Progress Meeting 2021.05.25

  Final Meeting 2022.01.20

- The internship on super-resolution took place at CESBIO between 2020/10 and 2021/04
- The 3D simulation and performance assessment study took place between 2021/05 and 2021/09

1.4 Outline of this report

The report is organised as follows.

Chapter 2 describes the use cases of Sentinel-HR identified by the Mission Advisory Group, for a set of themes ranging from glacier monitoring to disaster recovery. Use cases describe target indicators, required coverage and update frequency, as well as readiness level. Benefits of Sentinel-HR as well as potential limitations are identified.

Chapter 3 presents the coarse preliminary design and the associated costs, for two options: one by designing a pair of ad-hoc satellites for the mission, the other by extending the

CO3D constellation with a set of dedicated satellites. Since the first option may require to perform low-baseline stereo-reconstruction, the associated section also contains outcome of a 3D simulation and performance assessment study conducted with Sentinel-HR characteristics using a CNES in-house tool.

Chapter 4 focuses on research conducted at CESBIO during the phase 0 in order to demonstrate the feasibility of hybrid imagery products combining Sentinel-HR with Sentinel2 (NG). This chapter presents two main approaches, Single Image Super-Resolution and Spatio-temporal fusion, as well as some considerations on how to turn those methods into an operational ground segment.

Last, chapter 3.1.6 will present the main outcomes of each of those three aspects of the phase 0 study, and identify perspectives for Sentinel-HR.

Chapter 2

Sentinel-HR use cases

Use cases have been collected during the first semester of 2021. Themes have been selected by the Mission Advisory Group, and member of the group have been designated to coordinate the contributions on each theme. Some coordinators gathered contributions from fellow colleagues outside of the Mission Advisory Group. A common template has been used for all use cases in order to collect consistent information across themes. The template insisted on identifying key indicators enabled by Sentinel-HR, as well as their expected accuracy and target coverage and update frequencies. Limitations of Sentinel-HR and position with expected contemporary missions were also investigated.

Altogether, 11 use cases were identified and investigated. Table 2.1 shows an overview of those use cases, with a summary of the associated indicators, target coverage, and update frequency. It is noteworthy that many indicators relates to Essential Climate Variables or Essential Bio-diversity Variables, and that all themes play a role in one or more Sustainable Development Goals.

Target coverage areas ranges for less than a million km^2 for specific targets like glaciers or volcanoes to large portions of emerged land for the monitoring of cities, water bodies, or herbaceous ecosystems. It should be stressed that only a global coverage mission will be able to fully address the diversity of target areas and provide global insight on each theme.

In terms of update frequency of indicators, most of them range from quarterly to yearly update, which seem compatible with the kind of revisit that Sentinel-HR would offer if complemented by Sentinel2 (or Sentinel2 NG) observations. It should be noted that this update frequency should not be directly interpreted as the required satellite revisit, as indicators may require several observations or depend on external factors for the update.

2.1 Monitoring of glacier geometric changes: area, volume and velocity

Contributors: Berthier, Etienne (LEGOS); Dehecq, Amaury (IGE); Paul, Frank (Univ Zurich) and Kääb, Andreas (Univ Oslo)

2.1.1 Summary

Glaciers are considered as iconic indicators of climate change. Their state of health can be evaluated using their extent, their surface velocity or their volume, best all three variables

Theme	**Indicator**	**Coverage**	**Update**
Glacier	Elevation time series, changes	0.7 Mkm²	3-6 months
	Map of displacement		1-2 months
	Map of extent		3-5 years
Ice sheets	Ortho-images of outlet glaciers	Coastal Greenland	**Weekly**
	Elevation time series	+ Antartica	
	Map of displacement		
	Elevation changes		Annual
Water bodies	Water Bodies Extent (WBE)	All emerged lands	Quarterly
	Occurrence of water		
	Volume variations		
	Water leaving reflectance		
	Ice coverage and duration		
Urban	Changes at urban parcel level	All rapidly growing	Quarterly
	Start and end dates	cities	
	Structural metrics		
	Characterization of change process		
Urban vegetation	Individual trees map (crown >2m)	800 cities in Europe	Quarterly
	Height, structural attributes	with $\geq$ 50 000 hab.	
	Vegetation strata, composition	$\approx$ 751 871 km²	
	Phenological cycle		
Herbaceous	Structural configuration metrics	40% of earh's land	Annual
Ecosystems	Structural composition metrics	20% in Europe	
	Functional metrics		
Agricultural parcels	Structural features	7% of emerged lands	Yearly
	Dynamic features		Growing season
Forest	Location, structure, dynamics	4 billions Ha	3-5 years
Trees outside forest	Function	unenvely distributed	Montly
Erosion	Landslide mass wasting scarp surf.	N.A.	Quarterly
Sediment transport	Scarp depth and deposit volume		
	Exported sediment at river outlet		
	Vegetation recover rate		
	Dune field evolution, dune height		
Land-Sea	Shoreline map	All coastal areas	Seasonal
Topo-bathymetry	Intertidal topography		to annual
	Topography, bathymetry		
Geo-hazard	Domain specific indicators	Volcanoes: 0.1 Mkm²	Quarterly
		main tectonic areas	
	Ground motion, DSM	moutain regions	
	Volume variation	Intertropical zone	
Crisis	Up-to-date background imagery	All emerged lands	Annual
Risk recovery	Flood extent and depth		
	Vegetation and LULC dynamics		
	Ground displacement		
	DSM changes		

Table 2.1: Overview of indicators by theme, with target coverage and update frequency.

combined. Accurate, frequent, and consistent high resolution ortho-images from Sentinel-HR (referred to as [HR] below) would contribute to update global glacier inventories and measure accurately their flow velocities. A stereo capability (referred to as [HRS] below), along with the frequent revisit, would be a real game changer for glaciology, especially for estimating glacier volume changes globally and at different time scales (from seasonal to multi-annual).

2.1.2 Context

Glaciers are key indicators of climate change as they react very strongly to small but continuous trends in atmospheric forcing. They are thus considered as an essential climate variable (ECV) by GCOS (Global Climate Observing System) and are an important component of the IPCC reports. They also act as a natural water tower, providing liquid water in spring and summer, the time of the year when it is most needed for irrigation and water consumption, among others usages. Glaciers distinct from the ice sheets contribute significantly (about 25%) to the present-day rise in global sea level. Moreover, glaciers are an ever-changing source of natural hazards, threatening nearby communities and livelihood in remote mountain regions. In particular, newly developing and/or rapidly growing pro-glacial lakes that can burst catastrophically require frequent monitoring at high-spatial resolution. In this context, Sentinel-HR could dramatically improve our capacity to monitor glacier changes at an unprecedented spatio-temporal resolution.

2.1.3 Objectives

1. Target indicators and expected accuracy

    - [HRS] Elevation time series over all glaciers on Earth, every 3 to 6 months, with a vertical accuracy better than 5 m for individual measurements, i.e. pixels of 10 m by 10 m.
    - [HRS] Elevation changes aggregated for individual glaciers and entire mountain ranges 2 to 4 times per year with expected accuracy of $\approx$ 0.5 to 1 m.
    - [HR] Map of surface displacement every 1 to 2 months with an accuracy of 0.5 m and a resolution of 20-30 m over as many glaciers on Earth as possible, with a focus on significant dynamic variations, surrounding steep high-mountain topography. Whereas small glaciers require high spatial resolution, rapid flow and rapid changes require a high repetition rate (currently done using Planet data).
    - [HRS] Accurate mapping (typically 2 to 3 m in planimetry) of glacier extents every 3-5 years. Sentinel-HR high image resolution (compared to 10 m for Sentinel-2) would be a strong added value to identify accurately and unambiguously the complex boundary of retreating and down-wasting glaciers, often obscured by debris cover.

2. Target coverage and update frequency

    According to the Randolph Glacier Inventory version 6.0 (RGIv6), there are almost 220 000 glaciers on Earth covering in total over 700 000 km^2 with a concentration towards the poles where satellite orbits converge and revisit is more frequent. Glaciers are globally distributed but regionally concentrated with sizes ranging from 0.01 to about 10 000

km². For optimal monitoring, this size spectrum requires high spatial resolution and a wide swath (or several satellites in formation). The revisit depends on the parameter of interest as well as the monitoring goals (inventory, change assessment / trends, special events). It ranges from a 5 to 10 year revisit for glacier inventories (typical length changes near the terminus is about 10 m / year, but it has to be measured before the first snowfalls) to, ideally, a near daily revisit when following the evolution of flow velocities during glacier surges (typical displacement of surface features reach 10+ m / day). In general, seasonal (elevation changes, velocity mapping) to annual (frontal length change) revisits are well-suited. Of course, cloud free images are needed.

3. Methodological insights

   Our starting product would be the ortho-images and DSMs [HRS] derived from the raw Sentinel-HR images.

   (a) Elevation changes [HRS] After co-registration of all DSMs to a unique reference DSM off glacier [NK11], volume change would be obtained using classical DSM differencing [PBK+15] or using advanced methods for processing time series such as Gaussian Process regression [HMB+21b].

   (b) Flow velocities [HR] From well-co-registered orthorectified images, velocity maps can be obtained by applying image correlation techniques [HK12, DGG+19]. Time series of repeat images, combined with stereoscopic view [HRS] enable development and application of novel high-precision techniques that rely on entire stacks of images, involving not only temporal redundancy but also geometric redundancy from different views to reduce the effects from elevation errors [AK17, AK20] .

   (c) Glacier inventories [HR] Glacier inventories form the base of all glacier-specific calculations, be it their mass balance [HMB+21b], their flow velocities [FSM+16a], their thickness distribution [FHF+19] or modelling of their future evolution [HBM+19]. Creating glacier outlines from satellite images follows a well-established semi-automated workflow but requires manual editing in the post-processing stage [PBK+15]. A higher spatial resolution (compared to Landsat, ASTER or Sentinel-2) is particularly beneficial at this stage to achieve accurate results [PWK+16].

4. Current readiness level

   (a) Elevation changes [HRS]

   The amplitude of the seasonal elevation cycle on glaciers varies according to the degree of continentality and is in the order of 1-3 meters. It is nowadays possible to measure these subtle changes in elevation from very high-resolution images (Figure 1) such as Pléiades or Worldview [BBM+17], but only for specific targets, given the limited data availability. A mean seasonal cycle seems to be captured for large regions from 30 m DEMs derived from 15 m ASTER images but these promising results need to be validated [HMB+21a] and do not capture the large inter-annual variability. There is currently a lack of a snow-free DEM over the stable terrain surrounding glaciers to facilitate proper co-registration of all DEMs on a common snow-free reference. Given its high temporal revisit and after a few years in orbit, Sentinel-HR could contribute to build this snow-free DEM by selecting snow-free images (and DSM) in the catalogue.

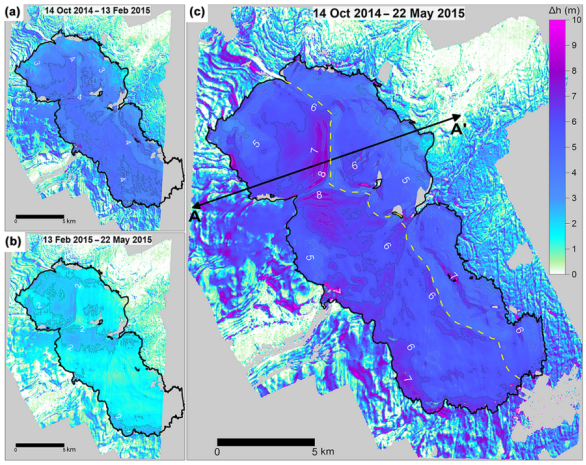

Figure 2.1: Winter accumulation for an Icelandic ice cap based on Pléiades and WV2 data. Panel c shows the entire winter (October to May) while panels a and b show sub-periods. From [BBM+17].

(b) Flow velocities [HR & HRS]

Thanks to Sentinel-2 and Landsat 8 images, global glacier velocity maps are currently generated on a regular basis, typically from images acquired about 1 year apart [DGG+19] [MMR+19], but increasingly over much shorter time periods when glaciers are flowing fast [AK17]. One limitation of these maps is the fact that images are orthorectified using freely available external DSM (SRTM, GDEM, AW3D30, TanDEM-X) that are asynchronous with the images and that the space agencies (ESA / USGS) are using different DEMs and ground control points (GCPs). In consequence, there are shifts between Landsat and Sentinel-2 data that complicate their joint use. Moreover, the strong surface elevation changes over time leads to systematic errors in the flow field (Figure 2). As the DSM will be available simultaneously with Sentinel-HR image acquisition [HRS], an improved quality of the calculated 2D velocity fields can be expected.

5. Glacier inventories [HR]

Currently, glacier inventories are refreshed only at irregular time interval, in the best cases every five to ten years. They often also lack a well-defined time stamp, being generated from images acquired a few years apart. There are several reasons for that, one of them being the difficulty to obtain cloud and snow free high-resolution images to accurately map (automatically or manually) the glacier limits. Given its frequent revisit, Sentinel-HR could be an invaluable source of cloud and snow free images to update inventories. Annual frequency would make sense for the fastest retreating glaciers (including calving glaciers). For the global inventory, an update every 5 years would be sufficient. A bottleneck could be the manpower needed to check and improve manually these inventories. Methodological developments, in particular artificial intelligence methods, neural networks and cloud processing together with the availability of suitable imagery from Sentinel-HR, might help to overcome these hurdles.

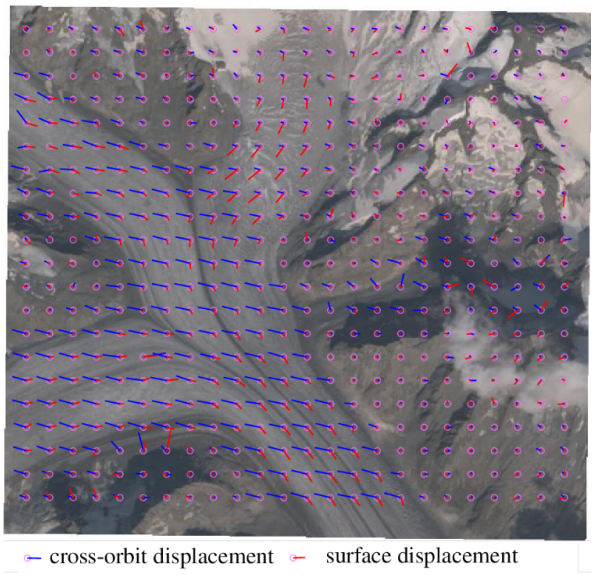

Figure 2.2: Sentinel-2 displacements over Aletsch Glacier, Swiss Alps. Cross-track displacements are shown in blue (with an erroneous flow direction), surface displacements in red.

2.1.4 Benefits expected from Sentinel-HR data

Sentinel-HR would be unique by providing simultaneously metric imagery and DSM. For glacier studies, the stereo capability would be a breakthrough for two main reasons:

- the elevation change from DSM differencing is a climate signal itself as it allows deriving seasonal glacier volume change and ultimately glacier mass balance, a direct indicator of climate change impacts. No mission in orbit or planed currently allows estimating glacier volume change or mass balance globally with a seasonal frequency and at high resolution. Current sub-metric missions are commercial, acquire images on-demand and follow a logic of "targets". This is useful for a case study approach, but not for global monitoring. So far, metric to decametric resolution missions rarely have stereo capabilities. ASTER is one of the exceptions but the sensor is getting old, will not be replaced and its spatial resolution (15 m), or its geometric and radiometric (8 bits) accuracy are not sufficient for estimating the subtle seasonal elevation changes on glaciers.

- Sentinel-HR would provide frequently "real" ortho-images, generated from a DSM that is synchronous to the image itself. This would avoid image distortions due to the rapid obsolescence of any DSM on a constantly evolving glacier topography. Such ortho-images would be the basis for improving the present day capability to derive velocity fields from Sentinel-2 or Landsat-8 images. They would also be useful to create glacier inventories with a better quality (as interpretation of glacier features is facilitated at higher resolution) and follow glacier frontal changes on a yearly basis, allowing to largely extend the sample of field measurements and obtain a globally more representative picture of climate change impacts.

2.1.5 Limitations of Sentinel-HR specifications

As explained above, the stereo capability is key for glacier applications. We can accept a coarser resolution (between 2 and 3 m) if the B/H is increased. A 20-day revisit will ensure a cloud free image probably every trimester and also will help to acquire images with minimal snow, close to the end of the melt-season. An even higher repeat frequency would increase the chance of cloud-free image acquisition further. This can likely be best achieved with a second satellite.

2.2 Monitoring of ice sheets changes: volume and velocity

Contributors: Mouginot Jérémie (IGE), Etienne Berthier (LEGOS), Romain Millan (IGE)

2.2.1 Summary

Since the 1990's, mass-loss rates increased significantly for the ice sheets due to large impact of retreat, acceleration of marine-terminating outlet glaciers, and increased surface melting due to warmer air temperatures [SFG$^+$20, MRB$^+$19, KHC$^+$20]. Despite regional-scale climate change, the spatial and temporal pattern of flow velocities and down-wasting of these glaciers is rather complex [MJSH12]; pointing out the need for more detailed, comprehensive repeat observations in order to better understand their response mechanisms to external forcings from the ocean and the atmosphere. The current temporal and spatial resolution of the altimeters (CryoSAT-2/ESA, IceSat-2/NASA) limits our ability to resolve with enough details, on a large scale, the current elevation changes in these areas of complex topography located at the boundary between the ice and the ocean.

The high resolution, revisit and stereo-capabilities of Sentinel-HR would be instrumental to provide continuous time series of glacier elevation. It would also provide accurate and frequent ortho-images to measure their flow velocities and observe at the high temporal and spatial resolution the surface condition experienced by the ice sheets at the interface between the ice and the ocean (albedo, crevassing, melt-water).

2.2.2 Context

Ice sheets are acknowledged by the World Meteorological Organization (WMO) and the United Nations Framework Convention on Climate Change (UNFCCC) as an Essential Climate Variable (ECV) needed to make significant progress in the generation of global climate products and derived information. Besides their strong impact of their mass loss on sea level, another potential environmental impact is the modification of climate due to changes in surface albedo, freshwater fluxes, orography and shifts in vegetation cover. These changes may impact local climate and atmospheric and ocean circulations. In this context, Sentinel-HR combined with Sentinel-2 could dramatically improve our capacity to monitor ice sheet changes at an unprecedented spatio-temporal resolution.

2.2.3 Objectives

1. Target indicators and expected accuracy

- High resolution ortho-images of all spectral bands over outlet glaciers of Greenland and Antarctica, from March to October every week, with horizontal accuracy of 0.5 pixels.
- Elevation time series over outlet glaciers of Greenland and Antarctica, from March to October every week (when solar illumination permits), with a vertical accuracy better than 5 m for individual measurements, i.e. for 10 m by 10 m pixels.
- Surface displacement time series over outlet glaciers of Greenland and Antarctica, from March to October every week, with an accuracy of 0.5 m and a resolution of 50 m.
- Long-term (inter-annual) elevation changes over the coastal sectors of Greenland and Antarctica with expected accuracy of $\approx$ 1 m over the lifetime of the mission.

2. Target coverage and update frequency

   Together, the Antarctic and Greenland ice sheets contain more than 99 percent of the freshwater ice on Earth. The Antarctic Ice Sheet extends almost 14 million square kilometres. The Greenland Ice Sheet extends about 1.7 million square kilometres, covering most of the island of Greenland. To make a difference compared to existing or planned systems, Sentinel-HR should focus on the coastal regions of Greenland and Antarctica.

   Two monitoring goals are identified for the ice sheets : long-term (interannual) and seasonal evolution. The long-term evolution requires monitoring at least once every year (at the same time of the year) in order to follow the global trend in ice discharge into the ocean and the volume change of the ice sheet. The information is used to derive their mass balance. Monitoring the seasonal evolution allows for describing the outlet glacier evolution at a weekly to monthly time scale and is needed to capture the large fluctuations (speed can increase a twofold factor and surface elevation can vary by +/- 30m) that occur at the glacier terminus during the melt season. This is especially true for Greenland outlet glaciers, but also some sectors of Antarctica such as the Antarctic Peninsula or the Amundsen Sea Sector.

2.2.4 Methodological insights

Our starting product would be the DEMs and ortho-images derived from the raw Sentinel-HR images.

Elevation changes Fine DEM co-registration and correction using filtered altimetry data [SAM$^+$16, SJD$^+$19]. This filtered altimetry would be located off glacier (e.g nunataks) or on non-changing areas from well-defined freely available external DSM (SRTM, GDEM, AW3D30, TanDEM-X, Copernicus). Additionally, other sources of altimetry (e.g. lidar) acquired simultaneously could be used. After co-registration, volume change would be obtained using classical DSM differencing or using an advanced approach such as SERAC [SC12].

Flow velocities From well-co-registered orthorectified images, velocity maps can be obtained by applying image correlation techniques [FSM$^+$16b, HK12, MRSM17].

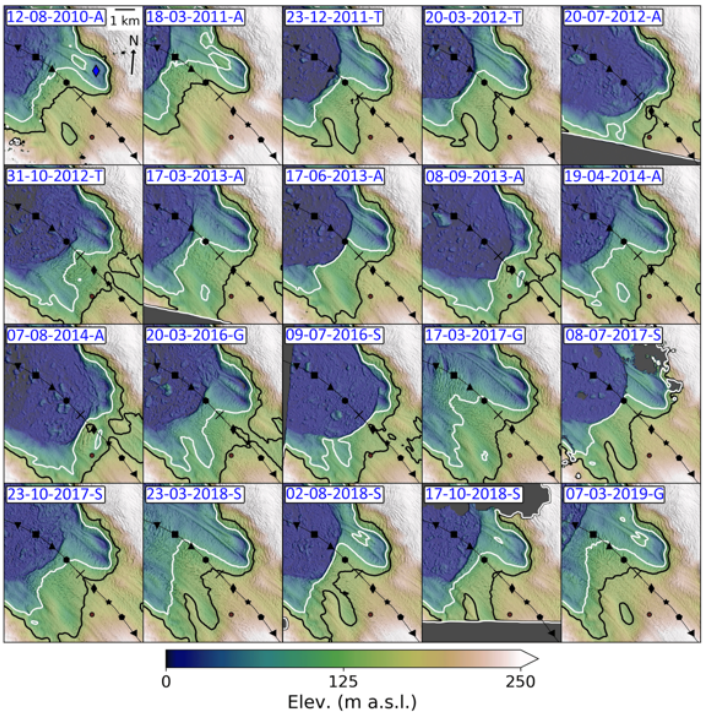

Figure 2.3: Colour-shaded relief maps for a subset of DEMs. Elevation contours of 150 (black) and 100m (white) bound the approximate transition from grounded to floating ice. The letter after the date-string (DD-MM-YYYY) indicates the DEMs source (A: ASP WorldView; T: TanDEM-X; S: SETSM WorldView; and G: GLISTIN) (adapted from [JSSF20])

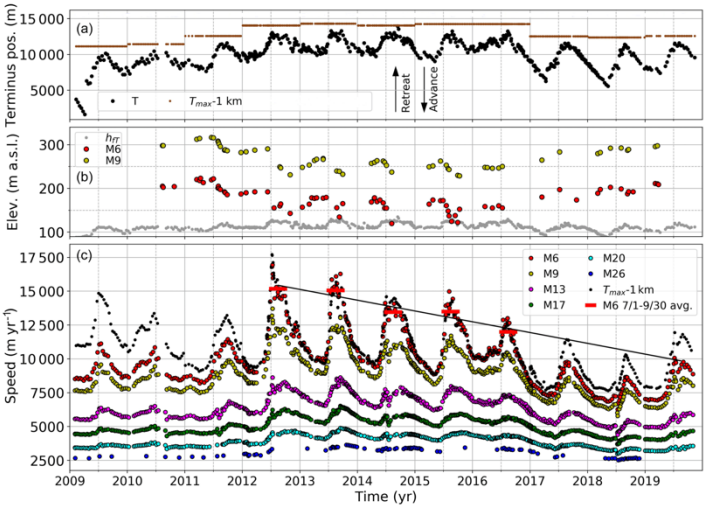

Figure 2.4: (a) Terminus position (T: black circles) and position 1km upstream of annual minimum terminus extent (Tmax1km: brown dots). The blue squares indicate when a rigid mélange was present in front of the terminus at the locations indicated by the blue boxes in Fig. 1. (b) Elevations of the points M6 (red) and M9 (gold) extracted from all available DEMs along with the inferred flotation height, hfT (grey), at the terminus. (c) Surface speeds through time extracted from a TerraSAR-X/TanDEM-X velocity time series, with a few points from summer 2019 derived using COSMO-SkyMed data (adapted from [JSSF20])

2.2.5 Current readiness level

1. Elevation changes

   The amplitude of the seasonal elevation cycle on outlet glaciers in Greenland are mainly linked to rapid changes in ice flow that occurs during the summer season. The increased extension during the summer speed-up can locally produce near-terminus dynamic thinning of $\approx$ 30m/yr. It is nowadays possible to measure such changes in elevation from high resolution images such a Pléiades or Worldview or SAR single pass interferometry (SP-InSAR) such as TanDEM-X [JSSF20], **but only for specific targets**, given the data availability.

   Over the ice sheets, the Sentinel-HR would focus on outlet glaciers and areas of complex topography, where the horizontal resolution of the altimeters (CryoSAT-2, IceSat-2) limits our ability to resolve with enough details the current elevation changes, as demonstrated over outlet glaciers Greenland or the Antarctic Peninsula using high-resolution SP-InSAR repeat digital elevation models from TanDEM-X [FSW$^+$18, KJS$^+$17] .

2. Flow velocities Thanks to Sentinel-2 and Landsat-8 images, global glacier velocity maps are currently generated on a regular basis [MRSM17]. One limitation of these maps is the fact that images are orthorectified using freely available external DSM (SRTM, GDEM, AW3D30, TanDEM-X) that are asynchronous with the images. As elevation has sometimes changed strongly on glaciers, this can lead to systematic errors in the flow field. As the DSM will be available simultaneously with Sentinel-HR image acquisition, an improved quality of the calculated 2D velocity fields can be expected.

2.2.6 Benefits expected from the Sentinel-HR data

Sentinel-HR would be unique by providing simultaneously metric imagery and DSM. For ice sheet studies, this would be a breakthrough for two main reasons:

1. For large ice displacements and large elevation changes, on the order of tens of meters, unprecedented simultaneous and frequent horizontal displacements and elevation changes would be routinely available by combining displacement maps and elevation models. This implies that the integration of measurements of horizontal ice flow and simultaneous elevation changes over short time scales offers great potential for understanding and predicting the rapid loss of glacier volume over longer time scales [FBC$^+$17]. Today, there is no sensor or mission to make such simultaneous measurements of horizontal displacement and altitude changes. Such conclusions must be drawn from temporal measurements that are often very disconnected from the variation in glacier flow and thickness, the main bottleneck being the absence of surface elevation measurements with a temporal repetition frequency of the same order as horizontal displacements.

2. Current satellite altimetry data with radar (CryoSat-2/ESA) or lidar (IceSat/NASA) sensors have significant gaps in the complex topography of the ice sheets due to the inherent limitation of horizontal spatial resolution and/or the inability to track the rapidly changing topography [MLS$^+$16]. Detailed observations of changes in surface elevation provide important new information on the diversity of spatial and temporal response of outlet glaciers to changing boundary conditions. The Sentinel-HR mission

will be able to fill key gaps in global ice sheet monitoring by providing comprehensive and spatially detailed measurements of changes in surface elevation of outlet glaciers of the ice sheets at well-defined epochs. These measurements will be used to complement other lower resolution sensors to derive the volume change of ice sheets over the mission duration and significantly improve global and regional estimates of their contribution to sea level rise.

2.2.7 Limitations of Sentinel-HR specifications

The stereo capability is key to make a difference compared to existing observations over the ice sheets.

A 20-day revisit will ensure to obtain enough cloud free images. For the ice sheets where overlap between adjacent orbits becomes higher, it would still be beneficial to acquire images for every orbit to increase the chance of cloud-free image acquisition further and increase the frequency of revisit below 20 days.

2.3 Monitoring of water bodies

Contributors: Yésou Hervé (ICUBE-SERTIT/Université de Strasbourg), Crétaux Jean-François (LEGOS / CNES), Ferrant Sylvain (CESBIO)

2.3.1 Summary

Access to and management of water, a vital resource, have become crucial issues that will be increasing in the context of global change and are causing tensions in many regions. The 2030 Sustainable Development Goals identify water and its management as crucial for providing the economic, social and environmental well-being of the present and future generations. Water surfaces, such as lakes or large reservoirs, essential elements of the chain as primary resource storage (SDG 2-6), host of biodiversity (SDG 14-15) and due to their role as climate sentinel (SDG13), are targets of great interest. In this context, earth observation data is called upon to play an important role in assessing and monitoring this resource, with potentially an important role in assessing and monitoring the water characterization parameters like height, extent and radiance, temperature. Therefore, small lakes, pounds, very important at local scale both in terms of available resource and biodiversity are not considered at large scale. Actually, the access to information to these water bodies is limited both by the swath, revisiting time and cost of VHR imagery. Sentinel-HR can also provide valuable insight for monitoring water bodies; taken into account large to small ones.

Moreover, when assessing the total surface over the continents covered by lakes and reservoirs, a large portion is still not well identified due to their smaller size [VKST14]. In any case, the fraction of water available for human use -agriculture, domestic use, industry, hydroelectricity, recreation, etc- is minimal: a few thousandths of the total quantity of water on Earth. Monitoring this available quantity is therefore a major issue for humanity. In the framework of climate change this is however a crucial information for several reasons: shallow and very small lakes contain in their sediment a high concentration of greenhouse gas (GhG) that can be re-emitted in the atmosphere if these lakes are shrinking [WSVS09]. The knowledge of carbon budget has still some uncertainty due to GhG originating from these very small water bodies. Most of the re-emission is also done in the margin of lakes, where a monitoring of

changing lakeshore at high resolution would allow improving the carbon budget generated by lakes. Global warming also provokes some new phenomena that dramatically transform landscape at different scales. In the Siberian plain, the melting of the permafrost causes the appearance of an incalculable number of small lakes and swamps which mix with peat bogs whose limits are difficult to detect. In mountain areas, glacier outburst floods (GLOFs) have become very frequent, for example in Himalaya. Small lakes are created in the spillways of glaciers, which can give way under pressure and cause serious damage in the form of floods or landslides. As an example, in Kyrgyzstan, there are about 2000 very small (less than 0.1ha) mountain lakes with for most of them a great risk. [J10] In addition, under more temperate climatic zones, there are numerous hill reservoirs, all over the world, that are also rarely taken into account when exploiting satellite imagery such as Landsat 8 -Sentinel or weakly described despite their crucial role in agriculture. For all these small objects, it becomes necessary to observe the evolution at high resolution and the current sensors do not allow it globally.

2.3.2 Objectives

1. Target indicators and excepted accuracy

   The first derived indicator corresponds to the water bodies extent (WBE) that can be expressed as the presence of water (on a map), or as the total areal extent of a water body (a single number). The main difficulty encountered is the definition of the target: are we willing to extract only open water, or do we have to consider that the bordering inundated vegetated wetlands are full-fledged of the lake ? indeed, this edge effect increases drastically for small WBE.

   The second indicator corresponds to the Water leaving reflectance (water colours). It provides information on dissolved (organic) and particulate matter (phytoplankton, minerals, detritus). In addition, it links to lakes as sources/sinks of Carbon, heat trapping potential, seasonal stratification. Most of the studies over lakes are actually exploiting historical MERIS and MODIS data, and more recent S3 OCLI imagery. HR and VHR such as Sentinel2, and the foreseen Sentinel NG and HR would be more acute for small water bodies WLR monitoring (selection of pure water pixels from S2 and S2NG and or Modis based on S2HR WBE). Of course, for this we would rely mainly on Sentinel-2, but the refined knowledge of the edges will enable knowledge of the surface.

   A third indicator of water bodies is the volume, or the variations of volume. Water bodies volume dynamics can be handled in two ways, associating WBE with water height (from in situ data or satellite altimetry) or WBE with topography. For this volume approach, the Sentinel-HR, Digital Surface Model (DSM) acquisition capabilities have also to be considered. The high X, Y resolution, associated with a moderate Z error would allow to generate DSMs over large area, to monitor flood prone lakes to small hilly reservoirs.

   Indicators therefore include:

   - Water Body Extent (expressed either in Km2 or Ha)
   - Occurrence of water (on a quarterly, 6 months or annual basis)
   - Volume variations when WBE associated with Water height, or DEM bathymetry
   - Water leaving reflectance (water colours)

- Ice coverage and duration

2. Target coverage and update frequency

   The revisit with 20 days is as already noticed too weak to capture alone the dynamic of the water bodies based on a single mission. But studies shall be conducted to estimate the gain of the fusion of HR WBE with Medium Resolution High Temporal Revisit derived water masks time series in arid and semi-arid areas where the WBE highly fluctuate. For less variable WBE, in temperate areas or for permanent river monitoring, a 20 days revisit Sentinel-HR WBE would allow identifying pure water pixel from lower resolution but more frequent satellite observation to better extract Water leaving reflectance, and lead studies at higher resolution thanks to the multispectral capacities of Sentinel-HR.

   Those indicators should be monitored for changes on a quarterly basis.

2.3.3 Methodological insights

During the last 25 years, there have been many water body extraction approaches from multispectral imagery (Figures 2.5 and 2.6). [YQY+20] divided these approaches into three levels:

> "[...] pixelwise classification, object-based image analysis (OBIA) and subpixel fraction estimation. Pixelwise approaches directly extract the pixels associated with water body areas, mainly considering the spectral characteristics of targets. OBIA groups the adjacent pixels with similar features into homogeneous clusters, which provides valuable information, including spectral, textural, shape, and spatial relationships. Subpixel fraction estimation considers the mixed pixels in remote sensing images and estimates the fraction of water bodies in each pixel using the spectral mixture analysis (SMA) method. However, the relevant methodologies fall into two categories depending on whether training samples are needed. The sample-based approach relies on the training dataset for supervised classification at both the pixel and object levels or on pure endmember selection to derive the subpixel water body fraction. The rule-based approach is based on prior knowledge of the target and background instead of the known sample data [...] Among the rule-based approaches, water indices and binary thresholding-based methods are characterised by easy implementation and a high calculation efficiency and are thus widely utilised (Table 2), especially in large-scale and time series analyses. Water indices differentiate the water bodies (normally with positive values) from the background (tending to negative values). Many water indices have been designed to enhance the separation between water bodies and other land cover types table 2.6"

1. Current readiness level

   The extraction of water surfaces exploiting optical Imagery with High Temporal Revisit missions at high or medium resolution recently reached a high Technology Readiness Level. Numerous processors have been set up, based on various techniques: thresholding, clustering, classifications ...

Training samples	Different levels	Literature	Methodology	Main water bodies
Sample-based methods	Pixelwise supervised classification	(Acharya et al., 2016)	Decision tree	River and lakes
		(Deng et al., 2017)	Decision tree	Urban lakes
		(Isikdogan et al., 2017)	Deep learning	Inland surface water
		(Mueller et al., 2016)	Regression tree	Across Australia
		(Sun et al., 2015)	Support vector machines (SVMs)	Urban water bodies
		(Tulbure and Broich, 2013)	Classification tree algorithm	Western Australia
		(Verpoorter et al., 2012, 2014)	Supervised classification	Global lakes
		(Jakovljević et al., 2018)	Supported vector machine (SVM) classifier	Open water bodies
		(Tulbure et al., 2016)	Random forest	Australia
	Object-based supervised classification	(Bayram, 2013)	Spectral indices	Shorelines
		(Yang and Chen, 2017)	Spectral indices	Urban water bodies
	Subpixel mixture analysis	(Pan et al., 2016)	Mixed land-water pixel extraction using SMA methods	Urban water bodies
		(Rover et al., 2010)	Combined with regression-tree technique	Lakes, wetlands and small water bodies
		(Zhou et al., 2014)	Spectral mixture analysis combined with multiscale extraction	Rivers
Rule-based methods	Spectral indices	(Arvor et al., 2018)	Time series indices	Small water reservoirs
		(Avisse et al., 2017)	Water and vegetation indices	Small water reservoirs
		(Campos et al., 2012)	Sample-based thresholding	Seasonal and permanent water
		(Cian et al., 2018)	Minimum, maximum and mean of the NDVI throughout the entire stack of images	Flood mapping
		(Du et al., 2016)		Venice coastland
		(Fisher et al., 2016)	Indices and thresholding	Eastern Australia
		(Ogilvie et al., 2018b)	New water index	Small water bodies
		(Yamazaki et al., 2015)	Comparing popular water indices	Global water body map
		(Yang et al., 2018)	Water indices and temporal analysis	Urban water bodies
		(Feng et al., 2016)	Refined by constrained energy minimization Terrain metrics and prior coarse-resolution water masks	Global inland water
	Object/cluster-based image analysis	(Chen et al., 2017)	Segment images using an active contour model	Glacial lake outlines
		(Mitkari et al., 2017)	Combined with band indices	Glacial lakes
		(Sivanpillai and Miller, 2010)	Unsupervised ISODATA algorithm to generate clusters	Water bodies
		(Xie et al., 2016b)	k-means/ISODATA to generate clusters	Lake and river
		(Zhang et al., 2013)	Object-oriented image analysis and edge detection	Coastlines

Figure 2.5: Water body extraction methodologies from multispectral imagery (from [YQY+20])

Water indices	Literature	Bands
Normalized difference water index (NDWI)	(Gao, 1996)	NIR, SWIR
Normalized difference water index (NDWI)	(McFeeters, 1996)	Green, NIR
Modified NDWI (MNDWI)	(Xu, 2006)	Green, SWIR
Automated water extraction index (AWEI)	(Feyisa et al., 2014)	Blue, Green, NIR, SWIRs
Multi-spectral water index (WuWI)	(Wang et al., 2018)	Blue, Green, NIR, SWIRs
Normalized difference mud index (NDMI)	(Bernstein, 2012)	Narrow bands with wavelengths of 795 nm and 990 nm
WI_{2015}	(Fisher et al., 2016)	Green, Red, NIR, SWIRs
NDWI built-up index (NDWI-DB)	(Li et al., 2016)	Blue, SWIR
Tasseled Cap Wetness (TCW)	(Crist, 1985)	Blue, Green, Red, NIR, SWIRs
Normalized difference vegetation index (NDVI)	(Zhu and Woodcock, 2012)	Red, NIR
$NDWI_{nm}$	(Xie et al., 2016b)	Composed of a visible band and an infrared band
Enhanced water index (EWI)	(Wang et al., 2015)	Green, Red, NIR, SWIR
Simple water index (SWI)	(Malahlela, 2016)	Blue, SWIR
LBV transformation	(Zhang et al., 2017)	Green, Red, NIR, SWIR

Figure 2.6: Water indices designed for water body detection (from [YQY+20])

One of the first work at large scale for the French community was carried out by [VKST14] then CESBIO teams developed their own approaches, as well as ICUBE SERTIT and CNES with the SURFWATER processor.

The actual level of TRL is around 6 to 7 depending of the chain. Level 8 seems to be addressed by the Surfwater processor. But preliminary studies (to be consolidated worldwide) show that averaging Sentinel-1 water masks on a 20 days basis strengthen the water mask products over France [PL21]. Systematic negative bias on WBE are found for optical data (<10%) and radar data (<20%) for similar reasons: the spatial resolution of the sensor that erode the shore, balanced by false positives - bare sand soils detected as water with SAR data and dark objects and shadows with optical data. It results in an erosion of WBE from the shore and differences in water occurrence maps from radar and optical data. Fusion of Sentinel-1&2 water masks together with appropriate ancillary data are foreseen to limit negative bias and improve our capacity to map WBE dynamics for many climate and hydrological context. The Sentinel-HR mission would be an opportunity to improve those methods by decreasing the erosion of water bodies limits impacted by spatial resolution of nowadays multi-temporal sensors.

For instance, the Indian Rainwater Harvesting System (RHS) is an essential source of surface water in upstream agricultural areas. It is composed of hundreds of thousands of Small Reservoirs (SR) often disconnected from any perennial rivers. Quantifying and monitoring the surface and volume of this RHS is a challenging task given the small size of the reservoirs. It requires high-resolution data for accurate volume estimation. Figure 2.7 shows the surface water fluctuation over this semi arid region detected by Landsat mission (Global Surface Water), with water masks from January 2018 from Sentinel-1 and Sentinel-2. Even if many of the water body maximal extents can be higher than 6ha, the surface to be detected is often below 3 ha.

A spatial water stress monitoring system based on S1 and S2 is foreseen to be of interest. A first ESA project has been funded in 2019 to spread the Sentinel-1 derived water masks over the Hyderabad region, Telangana, India, through a smartphone application to provide a proxy of surface water stressors to Hyderabad region citizens. From this very first attempt to reach water users and stockholders, the research objectives have moved to the estimation of volume dynamic as it is the biggest users' expectation.

Combining HR Pleiades DEM acquired when regional RHS is empty with those data allow accurate volume retrieval. A first regional estimate of the RHS volume in the Telangana reaches 29mm of capacity [Pas21a]. It is lower than the accumulated potential capacity of 126 large dams referenced by the National Registry of Large Dam estimated to 113mm, but represents the surface water resource for upstream farming systems during the dry season. The accuracy of RHS storage dynamic methods using available global DEMs is evaluated in a second study [Pas21b]. Among DEM precision, the WBE accuracy is crucial to get accurate volumes stored in the RHS, which could be highly improved with Sentinel-HR WBE products and stereoscopy capacities.

2.3.4 Benefits expected from the Sentinel-HR data

Sentinel-HR will provide the necessary information to monitor the small to large water bodies, with an emphasis for the small water bodies, in term of spatial resolution coverage. Indeed,

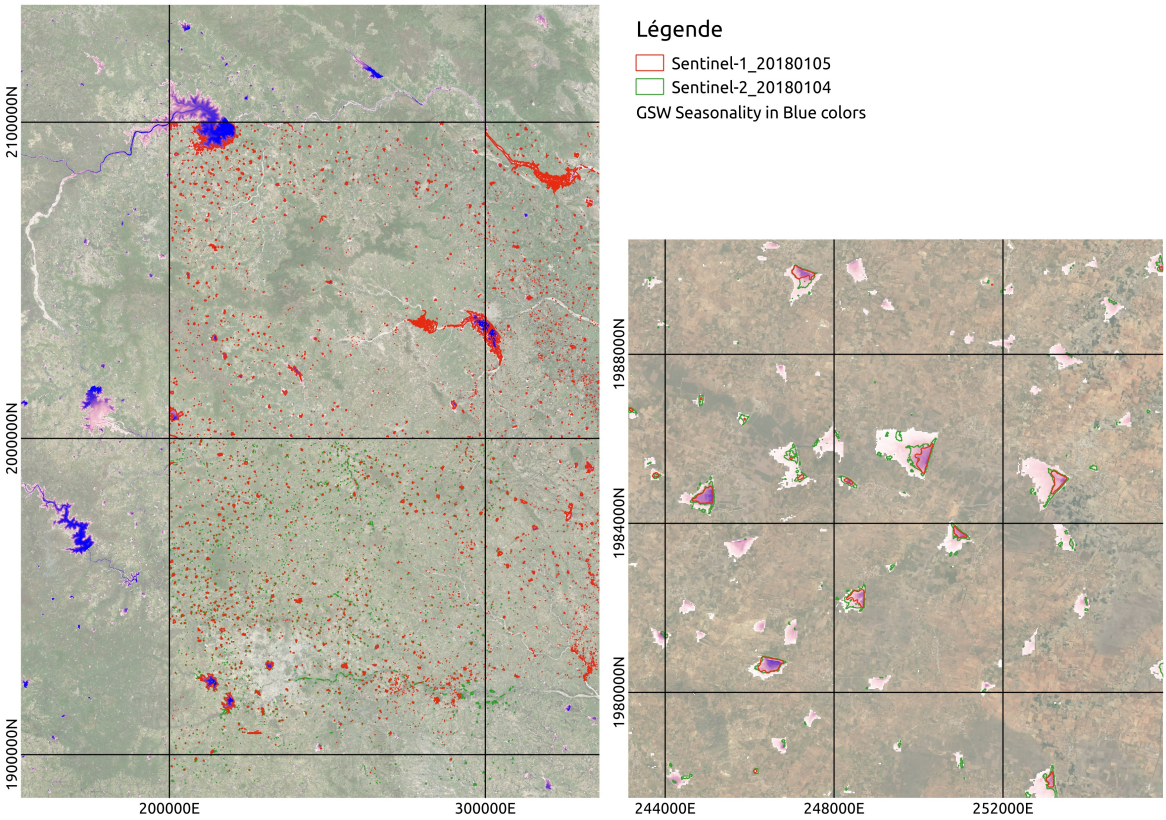

Figure 2.7: Comparison GSW Pekel and WBS derived from Sentinel 1 and Sentinel2 [Pas21a]

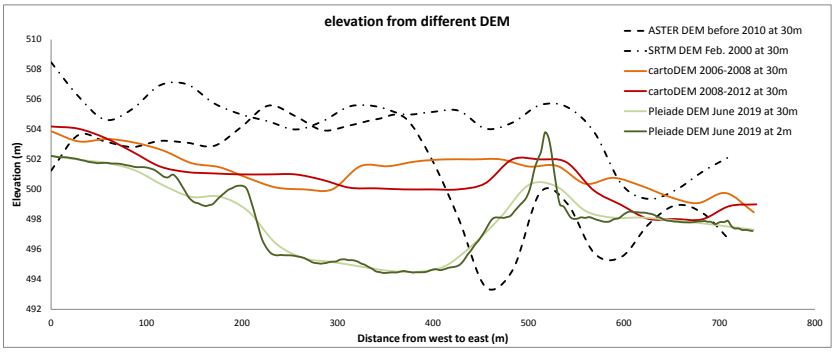

Figure 2.8: Comparison of HR and VHR DEM elevation [Pas21b]

even Sentinel2-NG foreseen spatial resolution of 5m will likely be insufficient for the smallest water bodies detection and mapping.

However, the revisit at 20 days of Sentinel-HR is not the most convenient. The dynamic of reservoirs, large or small, is much faster than 20 days especially in many semi-arid and arid area in the world where the development of surface water monitoring systems is crucial. In other temperate areas, cloud coverage will decrease drastically and randomly this observation frequency. Nevertheless, the S2HR WBE could be used in to identify and correct S2 NG and Landsat Next, or SWOT derived WBE time series over small water bodies.

CO3D imagery would be suitable for the production of the indicators VHR DEM that would be exploited in order to derive available stocks in the reservoirs, a crucial complementary information to the volume variations for water resource management. However, CO3D goals are not an automatic global coverage, but rather an on-demand tasking, after a first phase aiming at gathering a complete DTM over France and an area in middle east. So, the joint exploitation of WSE derived from Sentinel-HR and VHR DEM over sensitive areas such as India and Central Asia is not expected in a short-term future. As a result, the availability of the stereoscopic mission in Sentinel-2 is an important feature.

2.3.5 Limitations of Sentinel-HR specifications

Despite its innovative and important features, Sentinel-HR does not fully answer to two constraints for water surface detection and monitoring:

- the 20 days revisit is too small to monitor the water bodies dynamic. The hybridation of Sentinel-2 and Sentinel-HR might answer this need.
- The spectral coverage, limited to the VIS and NIR: For water detection and color measurements purposes SWIR bands would have been welcome

For DSM generation, the expected accuracy of Sentinel-HR could be a little too low to catch small altitude variations in flood prone areas as well for reservoir volume monitoring in small hill areas. At this level of the mission elaboration, there are missing elements to the End Users, to handle properly the DSM quality.

2.4 Urban monitoring

*Contributors: * Anne Puissant, LIVE, UMR 7362 CNRS / Université de Strasbourg

2.4.1 Summary

Urban growth is a worldwide phenomenon and the rate of urbanization depends on the countries. It can be fast in developing countries like Brazil, India, China where it is mainly driven by unorganized expansion, increased immigration, rapidly increasing population, and it is slower in western cities in Europe. Whatever the context, land use and land cover changes are considered one of the central components in current strategies for managing natural resources and monitoring environmental changes. Urban growth is responsible for a variety of urban environmental issues like decreased air quality, increased runoff and subsequent flooding, increased local temperature, deterioration of water quality, reduction of biodiversity, etc. Remote sensing is an important source of information for urban expansion analysis based on

its high spatial and temporal accuracy and consistency. Moreover, remote sensing data are very useful because of their synoptic view, repetitive coverage, and real-time data acquisition. Sentinel-HR will provide new insights for urban mapping and monitoring because of its large coverage and very high spatial resolution well suited to the high heterogeneity and complexity of this ecosystem. Consistent monitoring of urban changes to help urban planning and management for all urban areas in the world will be possible. Also, very high resolution and systematic stereo-acquisition could also offer the possibility to improve the detection and the characterization of urban changes.

2.4.2 Context

Growing urban sprawl (dispersed urban development) is a serious concern worldwide for a number of environmental and socio-economic reasons. It presents a major challenge with regard to making land use more sustainable, and this was highlighted by the International Year of Soils 2015. Since 2008, half of the planet's population has been living in cities and agglomerations, and this proportion is increasing at a rapid pace (UN, 2006; UNFPA, 2007). The global human population is likely to continue to increase rapidly, which will lead to a continued population shift from rural to urban areas and to significant additional land uptake for urban expansion (Montgomery, 2008; Gerland et al., 2014; UN, 2014).

The increasing urban sprawl in Europe is causing landuse conflicts and is posing a major threat to sustainable land use. Nearly 73 % of the European population lives in cities, and this proportion is projected to reach 82 % by 2050 (UN, 2012). While there are several regions (e.g. eastern Germany) in which the human population is not growing, the expansion of built-up areas has continued in most regions of Europe, even in regions in which the population has declined (Haase et al., 2013; Rienow et al., 2014).

In many cities, urban changes (sprawling, densification), on the one hand, is an indicator of social, economic, and political growth, whereas, on the other hand, it has negative impacts on agricultural land and the greenery of the city. Urban expansion also causes landscape transformations and degradation through fragmental and ecological changes.

At present, remote sensing has been recognized as a valuable technique for viewing, monitoring, analyzing, characterizing, and mapping urban growth and expansion. It has therefore been widely used in detecting and monitoring urban changes on various scales with useful results (Wu et al., 2016; Karanam et al., 2017, Pesaresi et al., 2016; Corbane et al., 2017).

The Sentinel-HR characteristics will be very useful to monitor urban changes at a fine scale to characterize the morpho-type of urban changes. The systematic stereo-acquisition could also offer the possibility to monitor urban changes in terms of height of buildings at a parcel level. Automatically monitoring newly constructed building areas is essential for efficient land resource management and sustainable urban development, particularly in the rapidly urbanizing country.

2.4.3 Objectives

1. Target indicators and excepted accuracy Automatically monitoring newly constructed building areas (at a parcel level) is essential for efficient land resource management and sustainable urban development, particularly in the rapidly urbanizing country.

   Time-series multi-view high-resolution optical satellite images can provide fine spatial details for clearly detecting and characterizing urban changes. Such monitoring at a

parcel level (few ten meters) could be effective based on this list of target indicators expected every six months, with a metric accuracy and a unique view angle:

- Detection of a change at a parcel level (ten meters)
- Structural metrics on changes (surface, etc)
- Characterization of the change process (expansion, densification, transformation, etc)
- Characterisation of the landcover/use changes (artificialisation, encroachment of wasteland, greenness, etc)
- Identification of the patterns of changes (type of urban fabrics or urban land use structure)
- Start and End date of the change
- Duration of the change

2. Target coverage and update frequency

   The need to monitor and control urban changes, although primarily a local or regional responsibility, is more and more reflected at the European policy level (e.g. the 2011 Roadmap to a resource efficient Europe (EC, 2011a), as part of the Europe 2020 Strategy and the Seventh Environment Action Programme (7EAP). There is an urgent need to assess the extent of urban change processes in Europe in a consistent and comparable way, and to provide relevant evidence that can aid the development of European policy with regard to built-up areas. It is also important to better control the spatial arrangement and utilisation intensity of built-up areas each year. From 2000 to 2006, Europe lost 1 120 km2 per year of natural and semi-natural areas (of which, on average, almost 50 % was arable or cultivated land) to urban or other artificial land development (EEA, 2011). There is a high probability ($>$ 75 %) that large areas (totalling approximately 77 500 km2) of the European continent will be or have been converted to urban areas between 2000 and 2030 (Seto et al., 2012). Moreover, this need is particularly essential for cities in the rapidly urbanizing country where urban development is at a phase at which structure are currently evolving and can potentially still be modified. The target coverage thus concerns all cities with a rapid growth of population.

2.4.4 Methodological insights

Numerous researchers have addressed the problem of accurately monitoring land-cover and land-use change in a wide variety of environments. Usually land uses and urban growth in remote sensing involves the analysis of two registered, aerial or satellite multi-spectral bands from the same geographical area obtained at two different times. Such an analysis aims at identifying changes that have occurred in the same geographical area between the two dates considered (Radke et al., 2005).

Remotely sensed imagery, with the notable advantages of the various spectral, spatial, and temporal resolutions, as well as the wide coverage, is increasingly utilized to investigate urban land expansion (Ban et al., 2017; Ban and Yousif, 2012; Del Frate et al., 2008; Gamba et al., 2006; Grey et al., 2003; Lefebvre et al., 2016; Mertes et al., 2015; Taubenböck et al., 2019, 2012; L. Wang et al., 2012; Zhou et al., 2018). Recently, the availability of high-resolution (with a spatial resolution $<$5 m) satellite data, e.g., IKONOS, QuickBird, WorldView-1/2/3,

Pléiades-1A/1B, ZY-3 01/02, GF-1/2, TerraSAR-X, and COSMOSkyMed, is opening up new avenues for dynamic urban monitoring at a very fine scale (Bouziani et al., 2010; Leichtle et al., 2017; Marin et al., 2015; Mendez Dominguez et al., 2019; Pacifici et al., 2007; Zhang et al., 2017).

Generally, change detection can be conducted at bi-temporal (i.e., identifying the differences of two images at a time) or multi-temporal (i.e., time-series analysis with multiple images) timescales (Coppin et al., 2004). While bi-temporal methods have been widely adopted (Gamba et al., 2006; Bovolo and Bruzzone, 2007; Xian et al., 2009; Teo and Shih, 2013), multi-temporal methods have shown great potential for providing a more in-depth understanding of land-cover dynamics in recent years (Zhu, 2017). The inclusion of spatial/contextual information (e.g., texture, structure, and spatial relationships) has often been considered to complement the spectral features and suppress false alarms (Bruzzone and Bovolo, 2013). Examples are the gray-level co-occurrence matrix (GLCM) (Lefebvre and Corpetti, 2017), wavelet decomposition (Celik and Ma, 2011), morphological profiles (MPs) (Falco et al., 2013; Mura et al., 2008), and edge features (Rowe and Grewe, 2001). Song et al. (2016) adopted a logical function to model the impervious surface cover change, and then extracted the change magnitude, timing, and duration over a 27-year span (Sexton et al., 2013). More recently, Li et al. (2018) developed a temporal segmentation method based on linear regression, and identified the urban land conversion sources (i.e., vegetation, water, and bare soil) during 1985–2015. These methods can characterize the urban land expansion process as three continuous stages (pre-change, change, and post-change), based on sufficiently dense time-series. Furthermore, object-based change detection, which focuses on image objects instead of individual pixels, is more effective for analyzing multi-temporal high-resolution images, due to its superiority in both facilitating the multiscale modeling of spatial information and mitigating the "salt-and-pepper" effect induced by registration errors, spectral variability, and imaging conditions (Chen et al., 2012; Hussain et al., 2013).

Particularly, in the domain of high resolution urban change detection, vertical features have been increasingly studied (Che et al., 2018; Leichtle et al., 2017; Mendez Dominguez et al., 2019; Qin, 2014; Stal et al., 2013; Tian et al., 2014; Yang et al., 2017). By contrast, LiDAR can deal with this issue but they usually have a limited coverage due to the high cost. In this regard, high resolution stereo optical images hold great potential for retrieving 3D information with fine shape details at a low cost. However, time-series and multi-view high-resolution optical satellite images have not yet been investigated for urban change detection.

Many researchers have proposed multi-temporal or time-series change detection algorithms for moderate-to-coarse resolution images (Huang et al., 2010, Kennedy et al., 2010, Verbesselt et al., 2010) and continuous change detection and classification (Zhu and Woodcock, 2014). Most of these algorithms have been developed for vegetative ecosystems, which may experience multi-directional changes (e.g., forestry disturbance or recovery), and thus they are not suitable for monitoring urban land expansion, since this is typically unidirectional (i.e., the inverse change is unrealistic) (Schneider, 2012).

In contrast to planar features (e.g., spectrum, texture, and structure), vertical features can provide three-dimensional (3D) information for describing off-terrain objects (e.g., buildings) (Li et al., 2020), and thus they have been widely applied to urban change detection (Qin et al., 2016).

The vertical features can provide three-dimensional information when describing complex urban scenes, and thus deserve comprehensive investigation. Nevertheless, in the current literature, vertical features from multi-view high-resolution optical satellite imagery, as well

as their joint use with planar features, have seldom been considered for urban change detection Most of the existing high-resolution change detection methods have been designed for use with bi-temporal images, while multi-temporal images have rarely been considered. In this context, the time-series information has not been fully exploited for the change detection. Moreover, the previous studies have usually failed to identify the timing of the changes, owing to the lack of time-series information.

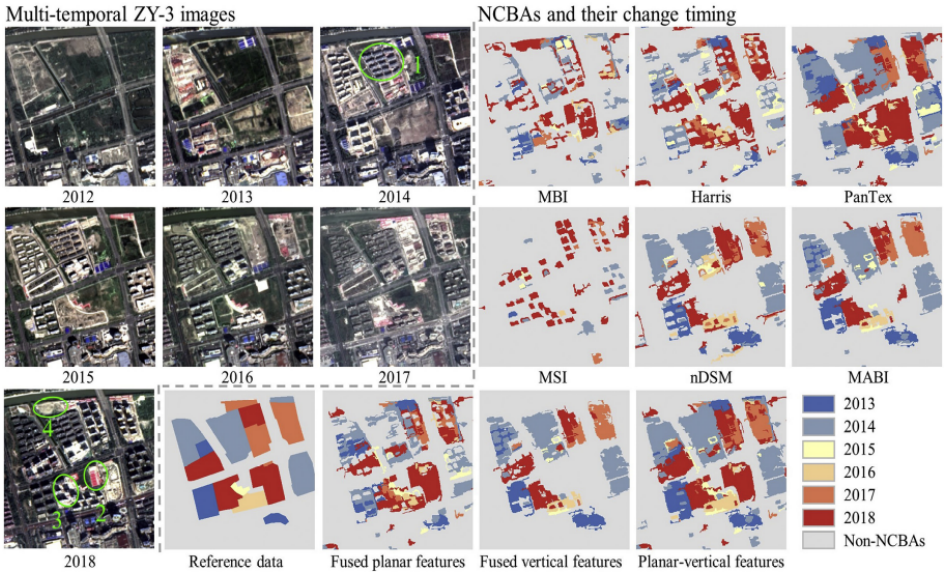

Figure 2.9: An example (1 km by 1 km) of the NCBAs and their change timing results for the different feature combinations in Shanghai (Huang et al 2020)

2.4.5 Benefits expected from the Sentinel-HR data

Sentinel-HR will provide the necessary coverage, spatial resolution, and revisit to monitor urban changes on world cities. The 20 days revisit will make yearly monitoring achievable, and spatial resolution will be good enough for urban change detection at a parcel level.

High revisit will be interesting to identify the timing of the changes and will give relevant information for urban planners and decision-makers.

The systematic stereo acquisition will offer the possibility to provide three-dimensional (3D) information for describing urban objects.

2.4.6 Limitations of Sentinel-HR specifications

The height accuracy for the stereo acquisition is a potential limit for monitoring urban changes, particularly if cities are structured with small, heterogeneous and complex parcels. Spatial resolution is also a key factor for urban buildings detection. Performances will be better if spatial resolution is in the lower range (close to 1m).

2.5 Monitoring of urban vegetation

Contributors: Anne Puissant, LIVE, UMR 7362 CNRS / Université de Strasbourg, Jean Nabucet, LETG, UMR 6554 CNRS / Université de Rennes 2

2.5.1 Summary

Urban vegetation plays a crucial role in mitigating urban environmental problems by providing a range of essential ecosystem services, such as reducing air pollution, moderating temperatures, reducing storm water runoff and storing carbon but also conserving biodiversity. Sentinel-HR will provide a new insight for urban vegetation due to both its large coverage and high spatial resolution. Consistent monitoring of urban vegetation for all urban areas in the world will be possible. Also, revisit time will allow for intra-annual monitoring of urban vegetation health and help detect damages with a monthly accuracy.

2.5.2 Context

Urban vegetation is considered as an important component of urban ecosystems playing an important role in improving urban environments. Urban vegetation can reduce urban air pollutant concentrations, sequestrate atmospheric CO2, reduce storm water runoff, mitigate the urban heat island effect and provide habitats for a variety of organisms. Mapping and monitoring urban vegetation is crucial for forecasting, and managing urban vegetation at landscape scale for urban planning to improve the urban environment. This is also one of the 17 goals defined in the 2030 Agenda for Sustainable Development, adopted by all United Nations Member States in 2015. The collection of accurate and timely urban vegetation indicators is very useful for urban managers to maximise urban vegetation benefits (urban ecosystem service) and to protect and manage urban environments. Some initiatives in this domain such as shown in France with “Nos villes vertes” or “Green City Lab” are currently proposed respectively by aerial imagery and by Pléiades imagery and can therefore not be extended or repeated very often. Sentinel-HR with its large coverage and short enough revisit time will be very useful to provide spatio-temporal maps of urban vegetation with a high spatial resolution allowing to analyse the phenological cycle of vegetation and thus monitor vegetation hydric and health conditions.

2.5.3 Objectives

1. Target indicators and excepted accuracy

   A first expected target is to distinguish urban trees and herbaceous vegetation. Then, for urban tree analysis, two types of metrics can be derived with the Sentinel-HR mission: (1) structural metrics allowing to characterise the configuration of urban vegetation (canopy surface, height, morphology, spatial configuration) and (2) functional metrics allowing to describe the behaviour of habitats (phenology, seasonal cycles, and anomalies). For herbaceous vegetation, expected targets are described in the Herbaceous Ecosystem Use Case.

   Indicators include:

   - Individual tree location in urban areas for all trees with a crown larger than 2m

- Urban vegetation structural attributes (canopy cover and spatial configuration, height)
- Estimation of tree height
- Identification of vegetation strata (tree – shrub – herbaceous vegetation)
- Composition (in term of richness, species and biodiversity)
- Phenological cycle of vegetation with metrics (start of season, end of season, etc)

2. Target coverage and update frequency

   There are currently over 800 cities in Europe with more than 50 000 inhabitants according to a report from the Netherlands Environmental Assessment Agency from 2016. According to the same report, 4% of the total land area of the European Union is occupied by cities (176 910 km²) and this figure goes up to 17% if including towns and suburbs (751 871 km²).

   Those indicators should be monitored for changes on a quarterly basis.

2.5.4 Methodological insights

With the increasing availability of satellite images, numerous methods have been developed to retrieve the urban vegetation. These methods may be supervised or not and are often uniquely based on spectral values of pixels [XSY08]. However, with VHR images, the spectral values of objects of the same type become more heterogeneous and it may become necessary to use new features such as texture or neighbourhood to improve the results of classifications [TP05, SBO+09]. Rather than using a per-pixel classification, object- based image analysis has been proposed as an alternative [Bla10]. These approaches allow pixels to be re-grouped within homogeneous segments and a large set of features to be computed, which can be spectral, textural, contextual or spatial [MFA07, BJTW11]. The use of these approaches for the detection of urban vegetation allows increased performance compared to per-pixel approaches [CKKM08, ZFJ10]. Rule-based classifications are often used to retrieve the vegetation from VHR images [ASG+11, VDG11]. The relevant features and thresholds are often determined by trial and error, which can be very time-consuming and is strongly influenced by the knowledge of the expert [BDS14]. Supervised classifications with statistical learning techniques have provided good results for the detection of urban trees cover [CKKM08, ZFJ10, TLH13, PRS14]. These methods have the advantage of being easily reproducible, regardless of the study site or the image considered. However, to obtain good results with a supervised algorithm, it is often necessary to collect large amounts of training data, particularly for the most heterogeneous classes [CS02] or require representative training data which allow to consider the whole diversity of the space or the classes studied [FM04]. Active learning methods have been proposed and generally allow to obtain more accurate results than with simple random sampling [TRP+09].

To summarise, VHR imagery have made it possible to provide information on the structure and biophysical properties of the vegetation on a plot or even intra-plot scale [DRM+18] and also in intra-urban areas in order to differentiate between tree and herbaceous strata [PRS14, NRD+15, RPSL16, Nab18]. More recently, multi-temporal images, even with coarser spatial resolution (Landsat HRS optical images), have been (re)exploited to map structural attributes of urban vegetation and analyse their changes [RPZ+17]. [GBALB20] has shown interesting results in mapping the health of some urban alignment species with Sentinel-2

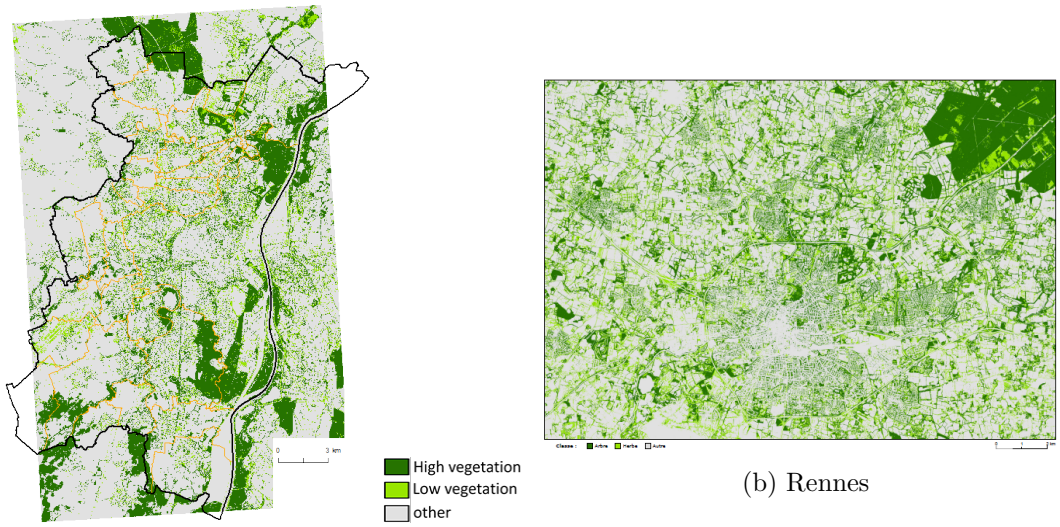

(a) Strasbourg

(b) Rennes

Figure 2.10: Example of urban vegetation on Strasbourg and Rennes with Pléiades imagery cite:rougier2016comparison

imagery. [FMW+20] evaluate also the potential of THRS satellite images (WorldView-3) to detect tree health classes measured in the field but only with single-date or bi-date images.

2.5.5 Current readiness level

An experiment has been conducted by LIVE to map urban vegetation based on a object-oriented approach in two classes (high and low vegetation) with Pléiades imagery on Strasbourg and Rennes (Figure 2.10 [RPSL16]). This experiment has shown that an accurate map can be achieved with a precision greater than 0.8 for high vegetation (urban trees) and a lower accuracy for low vegetation which are often part of complex areas (urban park or wasteland).

An other experiment conducted by LETG evaluated the contribution of DSM built with stereo-pair images to extract urban vegetation [Nab18]. Results reveal that stereo-pair images combined with texture information improve extraction of urban trees but some difficulties appear for small objects such as isolated trees or fine alignments.

Kermap processes 20cm resolution aerial imagery provided by the National Institute of Geography, which were acquired during a period of 5 years and obtain a map “Nos Villes Vertes” website. In this experiment an accurate map can be achieved (a precision greater than 90% is advertised). The current map therefore exhibits time discrepancies and is not fresh enough to evaluate recent public policies. The methodology readiness level is good but lacks wide systematic coverage at metric spatial resolution with intra-annual revisit.

2.5.6 Benefits expected from the Sentinel-HR data

Sentinel-HR will provide the necessary coverage, spatial resolution, and revisit to monitor urban vegetation. The 20 days revisit will make quarterly monitoring achievable, and spatial resolution will be good enough for urban vegetation (high and low). High revisit will be interesting to analyse phenological cycle of vegetation and to detect anomalies due to hydric

or temperature stress in intra-annual analysis. Sentinel NG foreseen spatial resolution of 5m will likely be insufficient for this use case, even if the addition of a 2.5m panchromatic band is being discussed.

The systematic stereo acquisition will offer the possibility to accurately delimit new urban trees. The maximum error (CE90) of 4m in height accuracy should allow detecting most of them and considerably improve this monitoring. CO3D imagery would be suitable for the production of the indicators but, as of now, the tasking of the constellation is not oriented toward automatic global coverage, but rather to on-demand tasking.

2.5.7 Limitations of Sentinel-HR specifications

Spatial resolution is a key factor for isolated tree detection. Performances will be better if spatial resolution is in the lower range (close to 1m).

The spectral resolution, limited to 4 channels in Sentinel-HR, can also limit studies aiming to detect ecological habitats or identify community assemblages and/or species.

2.6 Herbaceous ecosystems

Contributors: Pierre-Alexis Herrault, UMR 7362 CNRS / Université de Strasbourg, Pauline Dusseux, UMR 5194 CNRS / Université Grenoble Alpes

2.6.1 Summary

Herbaceous Ecosystems (HE) are continuous low-lying vegetation including natural and semi-natural grasslands, grasses and moors. They also may include a low tree density and shrubs depending on the use and the colonisation dynamic they are facing. They play a vital role in regulating the global carbon cycle, as well as supporting plant and animal biodiversity. Sentinel-HR will provide new insights for HE mapping and monitoring because of its large coverage and very high spatial resolution well suited to the high heterogeneity of these ecosystems. Moreover, consistencies with the current Sentinel 2 missions (similar tiling) will help to characterise intra-annual vegetation cycles at a very high spatial resolution. Systematic stereo acquisition might also offer the possibility to improve discrimination between herbaceous and woody vegetation in heterogeneous vegetation mosaics.

2.6.2 Context

HE mapping and monitoring with remote sensing products are crucial issues for understanding their spatio-temporal dynamics over large territories. Because of a high spatial/temporal heterogeneity and of the dynamics of use and encroachment they are facing, high spatial and temporal resolution are often required. Nonetheless, current optical missions with high/moderate revisit time such as Sentinel 2 or Landsat show some limitations to characterise their spatial heterogeneity at a very fine scale. At the same time, VHRS multispectral missions such as Pleiades or WorldView only provide punctual acquisitions in the same year and are not oriented toward automatic global coverage. Sentinel HR will fill these gaps and will be complementary to current and future existing satellite data sources.

In particular, the Sentinel-HR mission may have a great potential in the context of the European Union Biodiversity Policy. The Habitats directive (92/43/EEC) pointed up the

obligation for Member States to establish a network of Special Areas of Conservation (SACs) which, together with the Special Protection Areas (SPAs) designated under the Birds Directive (79/409/EEC), constitute the Natura 2000 network. Annex 1 of the Habitats Directive includes several Herbaceous Ecosystems. The Habitats Directive requires continuous monitoring of the status of species and extent of habitats in each Member State (within and outside Natura 2000 sites), with a regular update of the results.

Hence, the Sentinel-HR characteristics will be very useful to monitor Herbaceous ecosystems through different aspects :

- Characterising the **spatial heterogeneity** of HE in terms of composition and configuration. Such analysis can be performed from a landscape scale to a local and specific area
- Measuring the seasonal behaviour of micro HE and consequently their **temporal heterogeneity** (in terms of productivity or phenology for example).
- Improving the delineation between woody and herbaceous ecosystems in vegetation mosaics. This latter point is particularly important for HE where dynamics of encroachment were largely underlined such as in mountain areas.

2.6.3 Objectives

1. Target indicators and expected accuracy

   In an ecological perspective, two major types of metrics can be derived with the Sentinel-HR mission. First, the structural metrics allow characterising the configuration (morphology, spatial configuration) and the composition of HE (type, diversity, etc). Secondly, the functional metrics describe the behaviour of habitats (productivity, phenology, etc.) and these variables are proxies for habitat function over a relatively short period (seasonal cycles).

   (a) Structural Metrics
      i. Configuration (Landscape and patch scale)
         - Surface
         - Connectivity
         - Complexity/Simplification
      ii. Composition (Landscape, patch and plot scale)
         - Habitat type (phytosociological units, practices (grazing pressure))
         - Habitat diversity
         - Species diversity
         - Species dominance

   (b) Functional Metrics (Landscape, patch and plot scale)
      - Productivity
      - Phenology

2. Target coverage and update frequency

Grasslands cover about 40% of the earth's land surface and are therefore among the largest habitat type over the globe [SRB05]. At the European scale and according to the last CORINE Land Cover (CLC) inventory, herbaceous ecosystems represent around 20% of the territory. Synergies between Sentinel-HR and Sentinel 2 for the mapping and monitoring of HE will allow an annual update of their spatio-temporal evolution. Indeed, these productions could be used as management tools, for example in mountain areas where the closure of open landscape is significant for several decades. Spatialising and characterising, on a regular basis, HE evolution, will allow the development of effective habitat management and restoration practices.

2.6.4 Methodological insights

In order to derive indicators from HE, the herbaceous layer must first be extracted from the satellite data sources. The classification methods used to map HE types and/or HE heterogeneity can be supervised or unsupervised and is mostly based on the spectral values of pixels. With VHRS data such as the future mission Sentinel-HR, spectral heterogeneity increases with increasing spatial resolution making complex the use of per-pixel methods. In this context, the Object Based approach (GEOBIA) has been proposed [CW18] and aims to firstly obtain prior homogeneous segments. Segments are then classified with spectral and spatial features. Rule based methods are regularly used to assign labels to each segment that can be very time consuming and strongly influenced by experts. Recently, Superpixel approaches have been proposed and showed promising results. They aim to extract spectrally homogeneous regions, but that includes another constraint: the segments should all have similar sizes, and should be equally distributed throughout the image. Superpixels have advantages to have the scale between the pixel level and the object level so most structures in the image are well conserved in the classification outputs [ASS$^+$12].

The Supervised methods (machine learning) have been successfully proposed to map herbaceous land cover types at different scales. They are easily reproducible, regardless of the study site, because of low amount of input parameters. The quality of results is strongly dependent on the selected features (themselves dependent on the mission characteristics) and the available learning samples to calibrate the classification model. In this context, Features selection models have been proposed [LFG17]. Other approaches consist of optimising learning samples (such as Active Learning) to avoid problems due to limited training sets [HSP$^+$19]. Recently, the emergence of Convolutional Neural Networks offered new possibilities with the development of Semantic Segmentation models (e.g U-NET architecture). Although they have been only used a few times to map herbaceous land cover types (see [KEF19]), preliminary results for some study cases are spectacular both in terms of quality of detection and homogeneity of outputs. One current limitation to a larger use so far remains the availability of sample reference observations for identifying and learning the decisive image features. Given these latter issues, a continuous approach (including no classification step) has been proposed which contrasts with the above-mentioned discrete vision. These works are based on the spectral variation hypothesis (SVH), which assumes that the spectral dispersion in the image (NDVI, texture, or reflectance values) is correlated with the heterogeneity of the habitat patches in the landscape. Many approaches have been proposed to quantify spectral heterogeneity and relate it to alpha and beta diversity [RBC$^+$10]. They include (1) dispersion-based metrics, which rely on calculations of the standard deviation or the coefficient of variation of pixel values; (2) spectral distance-based metrics, which involve

an initial classification of pixels with non-supervised methods, such as K-means methods, to describe similarities between spectral classes. Landscape heterogeneity is then calculated with diversity indices (e.g. Shannon, Rao; [RSB+21]). Results suggest that spectral heterogeneity is an effective and quickly produced proxy of biodiversity; however, the quality of its output is strongly dependent on (1) the characteristics of satellite or airborne sensors; (2) scale-matching problems between the remotely sensed and field-based diversity data, and (3) the types of species diversity measures.

2.6.5 Current readiness level

The structural description of HE has been largely investigated for many years [ACD+16]. At the landscape scale, existing works primarily consist of classifying different HE types following their spectral and temporal dimension. Most of them rely on multispectral sensors with high/medium revisit time (Satellite Image Time Series, SITS). For example, several classes of grass and moors were distinguished with Landsat data in semi-arid and Mediterranean regions (overall accuracy 74.5%; [SLP+15]) . Sentinel 2 data were also used to produce the French Land Cover Map OSO (CESBIO) with different herbaceous land cover types. Among the detected class, Grass and Shrubs displayed a low classification score (Recall < 0.65). One of the recommendations remains in the use of VHRS images in combination with SITS in order to extract decisive features for the classification problem, but few acquisitions are often available at close dates from the target scene (Figure 2.11). About Habitat Composition mapping, SITS also allowed largely improving results, namely because of the capabilities to detect seasonal changes. Furthermore, some limitations appear when it comes to link in-situ and satellite data because of scale matching problems leading to strong limitations to describe the habitat composition. Exact spatial and temporal synchronisations between in-situ and satellite dates showed promising avenues but such surveys are difficult to implement [FLD+20]. At the plot scale, most of the studies aim to investigate species composition on the basis of the spectral variation hypothesis [RCL04]. Results show that spectral heterogeneity is a reliable proxy to investigate species diversity over large territories. Nonetheless, most of the aforementioned works were performed with hyperspectral data issued from field spectroradiometer/airborne sensors that limit the spatial and temporal coverage of these applications.

Figure 2.11: Spatial resolution comparison (false color composite: R = NIR, G = RED, B = GREEN) among QuickBird (A; res. spat = 0.65m), RapidEye (B; res. spat = 5m) and Landsat-8 (C; res. spat = 30m) covering a managed natural grassland conservation site in the west of Berlin, Germany (Courtesy: Dr Michael Förster) [ACD+16]

High revisit satellite missions are required to derive functional metrics about HE. Consequently, the spatial scale with which it is possible to monitor HE is strongly dependent on the spatial resolution of the SITS. For example, a recent study demonstrated the usefulness of

S2 data to calculate phenological metrics of salt marsh for a dutch barrier island [VMD+18]. These works pave the way to provide crucial information on spatial patterns and inter-annual trends of phenology. The retrieval error is variable and can be partially attributed to the occurrence of several species within a pixel resulting in mixed spectra [VMD+18]. The finer spatial resolution of Sentinel reduces this effect compared to medium/high resolution series like MODIS. Nonetheless, most of the monitored salt marsh are floristically diverse which implies that phenological metrics for 10m grid cells still relate to the phenology of the vegetation community rather than of individual plants.

Another difficulty remains in the distinction between herbaceous and woody strata in vegetation mosaics, particularly in temperate heterogeneous ecosystems. LIDAR data are often privileged because of its capability to provide vertical measurements allowing for a better distinction of vegetation strata [WBE+08] and studying the dynamics of encroachment [MTZ+20]. Nonetheless, such acquisitions are timely and costly consuming over large territories making their use complex for operational studies.

2.6.6 Benefits expected from the Sentinel-HR data

- Sentinel-HR will provide the necessary coverage, spatial resolution and revisit to estimate the configuration/composition of HE from the landscape to a local scale. The 20 days revisit will make seasonal monitoring achievable and spatial resolution will allow for a metric scale description.

- Synergies between the Sentinel-HR and Sentinel 2 missions will be possible (similar tiling) and help to characterise intra-annual cycle of vegetation for different herbaceous habitat types. With a revisit of 20 days, Sentinel-HR will provide only a few clear dates a year for a given location, which seems insufficient for a precise monthly interpolation of missing data for instance. Sentinel 2 data will be crucial to guide this interpolation and allow deriving an intra-annual cycle of vegetation at VHRS.

- The systematic stereo acquisition will offer the possibility to accurately delimit the encroachment of HE by trees and shrubs. The maximum error of 3m in height accuracy should allow detecting most of them and considerably improve this monitoring. For this task, the CO3D mission would be suitable for a production of such indicators but this mission is not oriented toward automatic global coverage.

2.6.7 Limitations of Sentinel-HR specifications

Limitations identified for the Sentinel-HR mission are of varying degrees :

- The time revisit (20 days) can considerably limit our capability to reconstruct the intra-annual cycle of HE. This limits the availability of cloud free images over the year and a 20 days revisit can contribute to missing some abrupt and rapid changes. Synergies with S2 data can partly fill this gap but studies aiming to evaluate these possibilities are still under way.

- The spectral resolution, limited to 4 channels in Sentinel-HR, can also limit studies aiming to detect ecological habitats or identify community assemblages and/or species. Indeed, several studies showed the importance of using additional spectral channels such

as Red-Edge or MIR (for water content) bands to detect herbaceous land cover types or to improve the woody/herbaceous distinction.

- The height accuracy for the stereo acquisition is also a potential limit for studies aiming to improve the herbaceous/woody separation in heterogeneous vegetation mosaics, namely for small sized trees.

2.7 Monitoring agricultural parcels

Contributors: Jean-François Dejoux (CESBIO), Julien Michel (CESBIO)

2.7.1 Summary

Monitoring agricultural parcels is key to a wide range of ecological and economical issues. On the ecological side, crops have their own part in carbon cycle and water budgets, and agricultural practices have a direct impact on surrounding ecosystems (SDG15). On the economical side, they of course contribute to food security (SDG2). In Europe, controlling crops is a pillar of Common Agricultural Policy, helping to control subsidies to farms. In other parts of the world, where agricultural practices are less industrialised and administratively managed, crops tend to be smaller and less distinctive, and the higher resolution of Sentinel-HR would make a great difference in their mapping and monitoring.

#TODO: Olivier ref taille des parcelles

2.7.2 Context

1. Static structural elements at intra-annual scale

   (a) Woody plants within parcel

   Trees within crops are already addressed in 2.8 use case. Meadow mixed with woody plants are also of great interest. They can exist in various forms such as mixed orchards or mixed pastoralism, in almost all parts of the world. Traditional systems are in general heterogeneous on small parcels. More modern systems can be larger and resemble plantations of trees. Despite being very interesting from an ecological point of view, those systems are threatened and decreasing rapidly, one of the reason being the complex management and man power they require. Better knowledge and identification of those systems is therefore of great interest in order to protect and develop them.

   (b) Woody plants and semi-natural systems around parcels

   A better knowledge of the surrounding environment of crops is required to assess the impact of the surrounding on crop yield one hand, and on the other hand to evaluate the impact of agricultural practices on surrounding ecosystems. If current mapping capacity can be sufficient for crops and forest, complex semi-natural systems such as hedges, isolated trees, fallow, and heterogeneous mix of those remain a challenge, for which Sentinel-HR can be of great interest.

   (c) Anthropic structures within and around parcels

   There exists a wide range of anthropic structures within and around parcels. Sentinel-HR could help to characterize some of those small or thin objects and

help to better characterize agricultural practices (pathways, terraces...), agro-environmental infrastructures (grass bands, mix between grass and woody plants ....), and blue and green corridors.

(d) Crops limits

In the case of adjacent crops without any material limit, only differences in crops type or stage allow to distinguish them. Sentinel-HR would enable a more precise localisation of the limits. Depending on the level of administrative information on crops limit in a country, the existing inventory might not be precise or complete enough.

2. Functional and dynamic elements at intra-annual scale

(a) Rows

Estimating rows orientation, number of rows and intermediate cultures between rows during growing season could be of interest, to monitor agricultural practices as well as to enhance radiative transfer models by better taking into account directional effects (see figure 2.12), and in turn improve estimates of bio-physical variables.

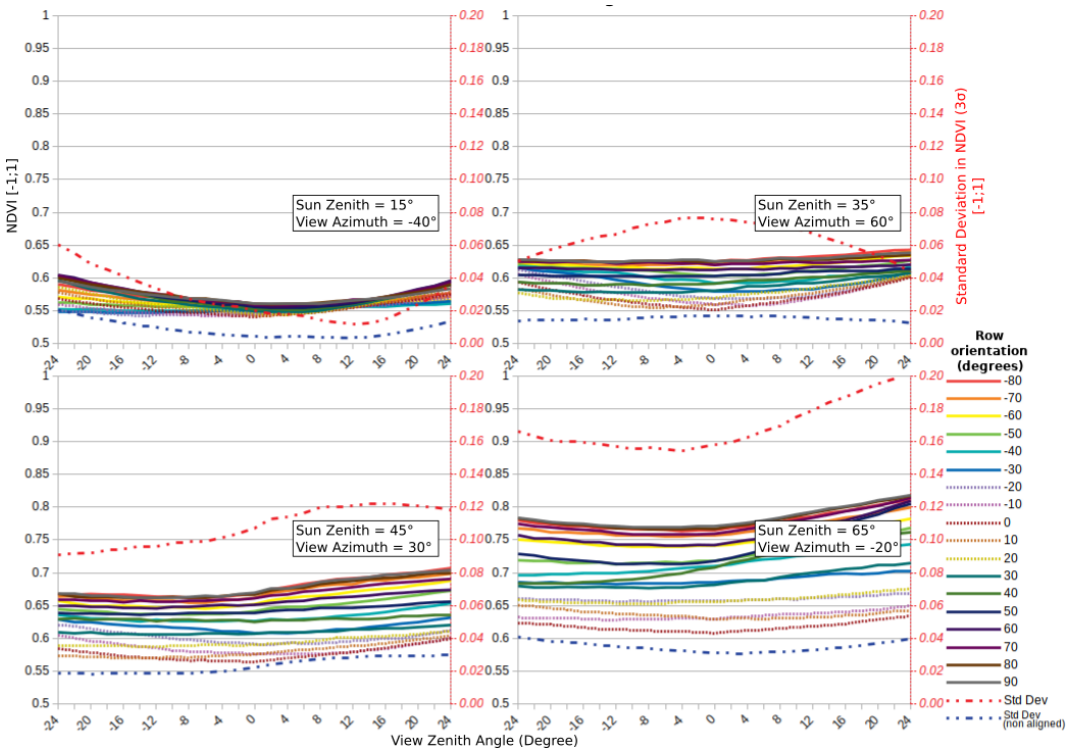

Figure 2.12: NDVI variation for a simulated vineyard (half grass inter-rows) for given sun angles and view zenith angle, for various row orientations (source: CESBIO blog)

(b) Intra-parcel heterogeneity during growing season

Intra-parcel heterogeneity accross the growing season can be a proxy for differences of several phenological indicators, including germination, maturity, senescence and

weeds within the parcel. Heterogeneity is also the result of plant disease or pest damages or prance trails of adventices. Weather events (wind, rain) may also have an impact on parts of a plot that induce a decrease of the yield. Although the revisit of Sentinel-HR might not be sufficient for these phenomena, its fusion with Sentinel-2 data or with other VHR resolution sensors could be useful for these questions.

(c) Bare soil and intermediate culture outside of growing season

Patterns, color and texture of bare parcel soil out of the growing season, as well as vegetation cover, is of interest to monitor agricultural practices and to estimate a lot of agro-environment impacts. It is in particular of great interest to discriminate weeds, regrowth and cover crops which growth is much more variable in space than during the growing season.

2.7.3 Objectives

1. Target indicators and excepted accuracy

   (a) Structural features Objects of interest are similar to use cases 2.8, 2.6 and 2.5.

   (b) Dynamic features

   Dynamic features include :

   - Row orientation (up to a few degrees)
   - Number of rows
   - Intra-parcel phenological state
   - Intra-parcel rugosity
   - intra-parcel soil-moisture
   - Intra-parcel bare soil color
   - Intra-parcel bare soil / vegetation fraction
   - crop damages due to weeds, pests, diseases or weather
   - Abundance of weeds versus regrowth during the crop season and between two crops (intercrop period)

2. Target coverage and update frequency

   Coverage can potentially be large, as crops represent 7% of the total emerged lands (source ourworldindata.org). Update frequency is low for structural indicators (typically yearly update) but some structural elements require a few acquisitions along the growing season for precise mapping. Update frequency would be higher for structural indicators, which would require several images along the growing season.

2.7.4 Methodological insights

Most of techniques have been covered in use cases 2.8, 2.6 and 2.5, apart from the use of textural information that has been explored in [LAL+18] and can be of interest at 2 meters resolution. Rows orientation determination has been studied in [SBF14].

2.7.5 Current readiness level

Structural features for large western countries parcels are well addressed by current techniques and data. Small landscape features and heterogeneous landscapes remain a challenge. Most of dynamic features at intra-parcel level remain a challenge due to the lack of resolution combined with revisiting time.

2.7.6 Benefits expected from the Sentinel-HR data

Access to a few 2m resolution images along the growing season will enable major progress on the structural features, as well as access to some of the dynamic features. It should be stressed that some countries are well equipped with local very high resolution imagery. They are therefore ideal areas to develop method in order to prepare Sentinel-HR applications to their whole country and to less equipped countries.

In agriculture, there are every year a lot of in-field experimentation, to evaluate various inputs (varieties, fertilizers, pesticides, dates of sowing...) and long term cropping systems. But the size of individual plots of factorials experimentation are relatively small : between 3 and 12 meters width in general. Therefore, it is not compatible with Sentinel-2, but the 2 meters resolution of Sentinel-HR will allow a monitoring of these experimentation.

2.7.7 Limitations of Sentinel-HR specifications

Revisit time can be too large for some intra-parcel phenological indicators. Resolution may be too coarse for some row crops. Limited number of spectral bands will impact indicators such as soil color or moisture (no SWIR bands).

2.8 Forest and Trees outside forest

Contributors: David Sheeren, UMR DYNAFOR, Toulouse INP-ENSAT / INRAE, Mathieu Fauvel, UMR CESBIO, INRAE/CNES/IRD/CNRS,

Camille Lelong, UMR TETIS, Cirad/INRAE/AgroParisTech/CNRS

2.8.1 Summary

Forests and trees outside forests provide a wide range of fundamental ecosystem services to humanity. Mapping their extent, composition and structure, and monitoring their dynamic is crucial for both agricultural and forestry management as well as biodiversity conservation. Sentinel-HR can offer a unique combination of multitemporal 2D and 3D images of very high spatial resolution with constant view angle. The sensor characteristics should greatly improve the estimation of the main forest parameters based on the spatial, spectral, temporal and structural information.

2.8.2 Context

Forest ecosystems play a major role in global biodiversity. They deliver several fundamental services to humanity including climate change mitigation (through carbon sequestration), timber production, soil protection, food and water provision, biodiversity and recreation. They also have an impact on human health and well-being. Their protection and sustainable

use are addressed since 1992 through the global framework of the Convention on Biological Diversity (CBD) with an expanded program of work initially defined at the 2002 Conference of the Parties (COP). An incentive mechanism for tropical countries also started in 2008 to reduce carbon dioxide emissions from deforestation and forest degradation (UNFCCC REDD+ program).

Recently, specific attention has been given in Europe to **'primary'** or **'old-growth'** forests (i.e. un-managed forests dominated by natural processes) estimated at about 4.9 million hectares [BBT+21]. Despite the fact that most of them are part of the Natura 2000 network, protection gaps exist with the need for an accurate and up-to-date mapping [SKL+20]. EU is working on the census of this natural heritage hosting a large number of highly specialised species. The location and strict protection of old-growth forests is part of the EU Biodiversity Strategy to 2030, in line with the IUCN 2020 motion 125 ("Strengthening the protection of old-growth forests in Europe and facilitating their restoration where possible") stated during the last World Conservation Congress 2020.

Trees outside forests (TOFs) are another important natural resource existing in many lowland agricultural regions across the world but also in urban and peri-urban landscapes [DFST+13, SKS15]. They also contribute substantially to the global carbon cycle [SASK15] and provide goods and services for human societies with important value for biodiversity. Small and linear woody features in particular, such as hedgerows, are key ecological corridors for wildlife, ensuring movements from one core habitat to another across a landscape [FB84]. This helps to maintain minimum viable populations (through emigration / immigration processes) and favours a genetic mixing. Hedgerows also provide food resources for fauna (mammal and bird species, pollinating insects and other invertebrates) as well as nesting, breeding and hibernation sites [GBvL05]. They ensure various other functions such as physical, chemical and biological fluxes control (water protection, erosion control), windbreak, and barrier [BBB00]. They are recognised as major component in agricultural landscapes and contribute to the "green belt network" (green infrastructures) defined for conservation planning from the local to the global (statewide) scale. Since they promote crop pollination, natural pest control and potentially crop production, such semi-natural habitats are widely integrated in the agri-environmental schemes for ecological intensification [KRS+11, BSV+17]. The woody components (isolated trees and hedgerows) are supported by the Common Agricultural Policy (CAP) in the European Union which conditions its funding to farmers based on how they maintain them, promoting implicitly **agroforestry** practices (woody perennials associated with arable lands and permanent grasslands) [SFRRA+18].

In this context, knowledge on TOFs and forests extent, their composition and dynamics, is crucial for both agricultural and forestry management and biodiversity conservation.

2.8.3 Objectives

1. Target indicators and excepted accuracy

   Key indicators for fine-scale mapping of forests and TOFs are required, some of them being integrated in the Essential Biodiversity Variable (EBVs) framework sustained by the Group on Earth Observation – Biodiversity Observation Network GEO BON [PFW+13].

   (a) Position

- Position and extent of managed and natural forests, tree plantations, hedgerows and isolated trees
  - Planimetric accuracy expected at the individual scale (trees, hedgerows) : ± 1 meter
  - Planimetric accuracy expected at circular plot scale (e.g. r = 15m) : ± 1-2 meters
  - Planimetric accuracy expected at the stand scale : ± 5 meters
- Position and identification of old-growth forest patches
  - Planimetric accuracy expected : ± 5 meters
- Position and identification of agroforestry parcels

(b) Composition

- Identification of tree species at the individual level (for both forests and TOFs)
- Estimation of taxonomic diversity (alpha, beta) at the forest plot/stand level + hedgerows

(c) Structure

- Quantification of vegetation canopy structure, morphology and physiognomy
  - height (at tree level) and mean + variability (at plot / stand level or for hedgerows)
    - Accuracy expected at the individual scale : ± 1-2 meters
  - crown diameter (at tree level)
  - diameter at breast height (dbh ; at tree level)
  - basal area (for stand density ; at plot / stand level)
  - above ground biomass (at tree / plot / stand level)
  - canopy horizontal openness (at plot / stand level)
    - Accuracy expected : ± 10 % (cover)
  - vertical complexity / foliage height diversity (at plot / stand level)
  - existence of under-story vegetation
  - standing deadwood (at tree level), downed logs, woody debris
  - physiognomic and morphological traits (such as LAI, SLA, ...)
  - forest management regime (coppice, high forest, coppice-with-standards) and un-managed forests
  - level of maturity / naturalness (related to dbh, height, deadwood, complexity...)
  - width and length for hedgerows
  - existence of multiple vegetation layers in hedgerows
- Tree density (Nb/ha) in agroforestry parcels (for CAP)

(d) Function

- Quantification of functional traits:
  - plant phenological traits (including flowering)
    - Accuracy expected : ± 5 days for phenological events (start of season...)
  - biochemical traits (pigments content, water content, nitrogen...)

- Estimation of functional diversity (richness, divergence) based on functional traits

(e) Dynamics

- Growth dynamics for natural forests but also for short rotation woody plantations cultivated to produce biomass (used for energy purposes among others)
- Changes in species composition and distribution
- Changes in structural and functional patterns (fragmentation...)
- Changes in extent (forest cover lost / gain) related to :
  - Abrupt changes :
    - Natural disturbances : forest fires, storm-related damage
    - Antropogenic disturbances : harvesting, clear-cut, deforestation, selective logging / thinning, hedgerow removal, new planting, annual cutting of hedgerow with time period (month)
  - Gradual changes :
    - water stress, drought, pests and diseases, invasive species
- Changes in phenology (trend, inter-annual variability)

2. Target coverage and update frequency

   Forests cover approximately 30.6% of the global land area [FAO15]. This represents approximately 4 billions hectares unevenly distributed (more than half of forests are found in only five countries).

   The update frequency of each group of indicators could be:

   - each year for the extent of forest cover and TOF (to detect deforestation and new plantations)
   - every 3 to 5 years for the composition (including invasive species)
   - every 3 to 5 years for the structure
   - each month for some functional traits such as phenological events or to monitor some environmental stress

2.8.4 Methodological insights

Mapping and monitoring forest ecosystems (including managed, natural and forest plantations) is an archetypal application in remote sensing. Significant progress has been achieved in the last two decades with technological advances in sensors design, information extraction techniques, and a better understanding of user requirements [WF03, AH12]. The remote sensing of forests is motivated by a wide variety of applications for forest managers and ecologists but also for policy-makers. This includes, in the most basic way, the mapping of forest extent or global percentage tree cover (e.g. see Copernicus HRL forest products). This also refers to the monitoring of changes and dynamics related to natural or anthropogenic disturbances. Remote sensing is used to map forest types [FLS+16] and taxonomic or functional diversity [SMS+17], or to extract biophysical and biochemical properties. Depending on the sensor, forest canopy structure (with vertical complexity and openness) can be informed, in addition to classical forest structural parameters of tree and tree stands (such as height, basal area or

diameter at breast height). A synthesis of the relevant remote sensing approaches to retrieve the key variables of forests is given in Figure 2.13 [MHH+15]. A comprehensive review can also be found in [WCW+16].

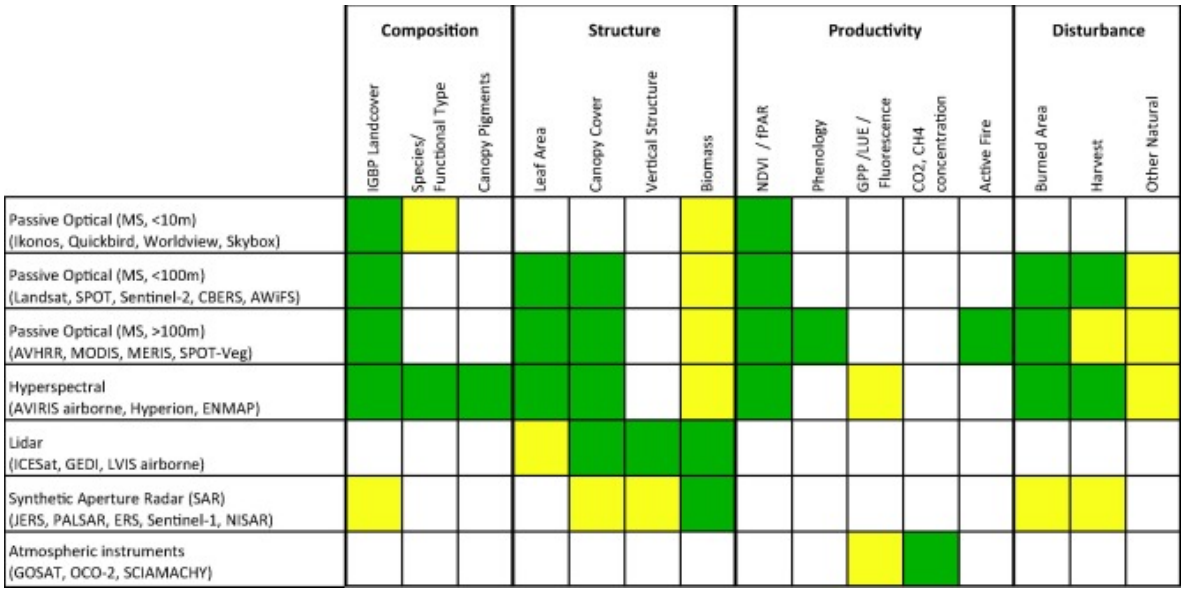

Figure 2.13: Interests and limits of the passive and active remote sensing approaches to retrieve forest parameters. Green : strongly relevant for retrieving variable; Yellow = can support variable retrieval with limitations in accuracy (Source : [MHH+15]).

Optical VHR satellite imagery (< 5m) are currently used to characterise forest structure based on textural information at stand level. Texture analysis is mainly based on Wavelet or Fourier transformation [PCF07, VCVDW07] but also on Grey level Co-occurrence matrix [KHD06]. The performances depend on the studied site, the tree species and the image used (sensor, acquisition date). In [BGBC14], five forest structure variables of maritime pine have been predicted from multi-spectral and panchromatic Quickbird and Pléiades spectral bands. The average prediction error was estimated to 1.1 m on crown diameter, 0.9 m on tree spacing, 3 m on height and 0.06 m on diameter at breast height.

Canopy Height Models (CHM) derived from VHR stereo imagery are also combined with spectral bands to estimate forest metrics. In [PMG+19], a CHM from Pléiades images was used to estimate the maximum height (Hmax), the 95 and 50 height percentiles (Hp95, Hp50), the standard deviation (HStd) of the height distribution, and the canopy gap (Gaps) in the Swiss Alps. They obtained median errors of -0.25 m for Hmax, +0.33 m for Hp95, +0.03 m for HStd, and -5.6% for the Gaps. The authors observed a high variance of forest metrics in forested areas with steep slopes (> 50°). They also noticed the negative effect of shadows on stereo dense image matching which increases in the winter season. They called for additional studies to investigate the effect of tree leaf-off conditions on the quality of extracted CHM, in addition to the possibility of using a VHR time series for tree species classification. Despite some limits related to topography and shadow, CHM obtained via stereo matching have proved to be suitable to map forest metrics in different contexts (St Onge et al. 2008, Persson and Perko 2016, Immitzer et al. 2016).

Recently, the potential of time series of VHR images for predicting and mapping forest

LAI has been investigated [PL19]. A significant seasonal change of forest LAI was observed from a VHR multi-seasonal Pléiades imagery. The texture features from 0.5m Pléiades images were identified as the best predictors of forest LAI using the image acquired in May ($R2 > 0.8$) and outperformed vegetation indices. This was confirmed in other studies (see details in the reference). The interest of VHR imagery is also to map individual trees. A recent study tested the ability of a simple RGB set of images to separate tree and non-tree pixels at 0.5m spatial resolution [FDG17]. They showed a 5% performance gain compared to SPOT-5 tree map with an improved detection of scattered trees. Since the authors used an airborne digital sensor (ADS) imagery with only three visible bands, the increase in accuracy can be partially attributed to the increase in spatial resolution. A simple thresholds-based classification method was defined in this study but more advanced approaches exist to extract the trees automatically [MGG+19, KL21].

A more challenging task is the automatic identification of tree species. Although some works have demonstrated the possible classification of dominant species using a single-date panchromatic or multi-spectral VHR data [MWW10, IAK12]„ it is now recognise that the temporal dimension is required to improve the discrimination [FLS+16]. However, there is no clear answer about the optimal number of dates and the key periods to integrate. The comparison of previous studies is difficult because of different methods, sensors and species and also, because of optimistic bias in the validation process due to spatial auto-correlation [KDF+19].

The extraction of Trees outside forests from VHR imagery has also received attention in the last decade. Several methods have been proposed from pixel-based approaches [GMA08] to object-based [VHM08, TCA+09, AILB13, LTS20] or a combination of both [SBO+09, SMC+12]. The classification process use the spectral information but can also integrate the textural, contextual or shape properties of objects. Additionally, specific detection techniques based on directional morphological filters [FAB+12] or edge detection filters [AAW09] have been proposed. Now, CHM are combined with optical data to improve the extraction [BLML19] and to estimate the annual woody biomass supply [MLE+17]. In general, CHM come from LiDAR data which implies that the data is available but CHM from airborne stereo-images is also used [MRGW21].

2.8.5 Current readiness level

Mapping the forest extent or the percentage tree cover is operational (TRL>6) with a large number of products available from different sensors: Yearly L3 Global 250m MODIS Vegetation Continuous Fields (VCF), Global 30m Landsat Tree Canopy Cover, Pan-European 10m Sentinel-2 Forest High Resolution Layer (HRL). However, the forest definition vary between these products because of the difference in the spatial detail, the threshold on the tree cover density and the canopy cover height. The height of the woody vegetation is often ignored because of the absence of CHM. The update frequency is also variable (yearly or irregular).

Operational product of TOF also exist (see the Copernicus HRL Small Woody Features). This includes linear woody features longer than 50m and not exceeding a width of 30m, in addition of small patches ($200\ m^2 \leq$ area $\leq 5000\ m^2$). There is no available product informing the structure of these objects (as for forests). However, the level of maturity for generating canopy height models from stereo-imagery or LiDAR data is high and allows to consider an operational production if the data is available.

The automatic discrimination of tree species still needs research work to be able to provide

accurate maps including a high number of species. Hyperspectral systems still show higher potential than multi-spectral data [FLS+16]. However, multi-spectral time series have enabled significant progress with high classification accuracy for specific species (e.g. see the recent results for poplar plantations in [HPC+21]). Their potential could be increased by combining them with VHR data and CHM to provide single-tree based information.

Overall, using the most appropriate sensor, the forest parameters (composition, structure and others) can be retrieved accurately (Figure 2.13). However, this requires to combine multiple sources, each with its own limitations (in terms of spatial resolution, spectral continuity, revisit time...).

2.8.6 Benefits expected from the Sentinel-HR data

Sentinel-HR will provide a unique combination of images with a very high spatial resolution, every 20 days, with constant view angle at nadir, and with systematic stereo acquisitions, offering multi-temporal digital surface models (DSM). Currently, no sensor has such a configuration. Multiple sources of data must be used, possibly with significant planimetric and temporal shifts, large differences in spectral bands, calibration, or view angles.

Sentinel-HR will be highly complementary to Sentinel-2 NG. Time-series of DSM and optical images with a high level of spatial detail will be provided by Sentinel-HR, which will be complemented by the very high temporal frequency with a greater diversity of spectral bands provided by Sentinel-2 NG.

1. For Forests

   Very high spatial resolution combined with canopy height model and constant nadir view angle may enable to:

   - **improve the mapping of forest extent taking into account a precise definition** (e.g. FAO-FRA classification framework including canopy cover and height thresholds).
   - **extract individual trees** in forest stands
   - **estimate morphological properties** of trees (crown diameter, height)
   - **model allometric relationships to infer some structure parameters** (e.g. dbh)
   - **estimate canopy horizontal openness / canopy cover** at plot and stand levels
   - **characterize canopy structure** at plot and stand levels
   - **estimate growing stock volume or biomass** at plot and stand levels
   - **possibly identify standing deadwood**
   - possibly **identify a level of maturity** (based on height, canopy structure, deadwood...) or patches of old-growth forests

   Very high temporal frequency combined with canopy height model and constant nadir view angle may enable to:

   - possibly **discriminate tree species** at the individual tree level based on their respective phenology (or groups of species according to their temporal behaviour)

- **estimate taxonomic diversity** (alpha and beta) at the plot or stand levels
- **monitor growth dynamics for short rotation woody plantations**
- **monitor forest expansion, deforestation, clear-cuts and estimate net changes**
- **possibly monitor stand thinning / selective logging and predict timing for silvicultural operations**
- **monitor dieback and diseases, anomalies (stress...)**

2. For TOFs

   Very high spatial resolution combined with canopy height model and constant nadir view angle may enable to:

   - **improve the mapping of TOFs extent taking into account a precise definition** (e.g. FAO-FRA classification framework including canopy cover and height thresholds).
   - **estimate morphological properties** of hedgerows accurately (length, width, height) **including gaps** between two sections
   - **extract individual trees** in hedgerows
   - **classify hedgerows types according to their structure and morphology** (e.g. shrubby hedgerow)
   - **estimate their specific above ground biomass** (for carbon stock) on a single tree basis

   Very high temporal frequency combined with canopy height model and constant nadir view angle may enable to:

   - **monitor the removal of isolated trees or hedgerows and to detect new plantations each year** (useful to develop agro-environmental indicators and monitor the CAP rules)
   - **discriminate tree species** in hedgerows at the individual tree level based on their respective phenology (or groups of species according to their temporal behaviour)
   - **monitor management practices of hedgerows with possibly cutting or trimming frequency** (required to estimate their ecological quality and to ensure that ecosystem services can actually be supplied ; also required to deliver the new "Haie" label in France)

3. For Agroforestry parcels

   • Very high spatial resolution combined with canopy height model and constant nadir view angle may enable to:

   - **improve the mapping of agroforestry parcels**
     - **identify parcels in agroforestry, and more especially discriminate forest stands, woodlots, and mixed tree crops**
     - **characterise the cropping structure inside the agroforestry parcel** (rows/inter-rows, clumping, random distribution...)

• Very high temporal frequency combined with canopy height model and constant nadir view angle may enable to:

- **identify parcels in agroforestry, especially discriminate between forest stands, woodlots, and mixed tree crops**
- distinguish between **agroforestry practices**:
  - silvoarable systems: trees with temporary or permanent agricultural crops
  - silvopastoral systems: pastures with open forest trees or scattered fruit trees
  - orchard intercropping: fruit tree systems on arable land or grassland, possibly mixing different fruit species and forest trees in various proportions.
- **characterise tree diversity inside a given parcel, and identify some major species**

2.8.7 Limitations of Sentinel-HR specifications

The number of spectral bands is limited with no bands in the Red-Edge and Short-Wave Infrared. This could limit the ability of the sensor to discriminate tree species as well as water stress. The temporal dimension of the data will not compensate because short phenological differences between species ($<$ 20 days) will not be detectable accounting for the possible cloud cover. Global phenological patterns could be observed but phenological metrics (e.g. start of growing season, peak, leaf fall, end of season...) will be imprecise. By contrast, the 20-days revisit appear to be well-adapted to distinguish between agroforestry parcels with temporary agricultural crops or grassland (e.g. tree orchards).

The 3-m height accuracy will be inadequate to detect very young tree plantations and shrubby hedgerows. The accuracy of monitoring growth dynamics, especially for short rotation woody plantations, will also be limited but development stages could be estimated qualitatively (e.g. young, intermediate, mature). Canopy height model does not allow to identify the existence of multiple vegetation layers in hedgerows and forests. However, the high spatial resolution combined with the CHM could enable to improve the characterisation of canopy structure with its openness. This is key to detect old-growth forests.

Detecting hedgerow pruning and selective logging in forests is also very challenging. The spatial resolution of Sentinel-HR as well as the height accuracy of CHM may be limiting but the detection of these practices could be potentially improved using the 2D/3D time series.

2.9 Erosion and sediment transport

Contributors: Antoine Lucas (IPG)

2.9.1 Summary

Spatial observation is a major asset for the study of erosion and sediment transport since it allows both the location of sudden events, such as landslides, and the ability to carry out temporal monitoring of the evolution of watersheds, glaciers or dune systems, for example. Hence, this application case concerns gravity driven processes (mass wasting, landslide, granular avalanches...), river transport (suspended load, bed load and solute matter) as well as aeolian transport. In order to assess sediment fluxes, but also to understand the couplings

between the processes at work, high-resolution temporal monitoring becomes essential. This is why Sentinel-HR will help to meet these needs. Indeed, consistent monitoring at one meter of spatial resolution coupled with stereo abilities of areas such as tropical forests, volcanic islands, large deserts and of course mountainous regions will be at reach. Additionally, the revisit time will provide insights on the dynamics and hence on the control factors, such as climate, with a [**Olivier quarterly ?**] monthly accuracy.

2.9.2 Context

The study of erosion is essential in many ways. Firstly, at a fundamental level, we need to better understand how feedback between climate, tectonic, topographic settings and erosion mechanisms occur, and at what spatial and temporal scales. In other words, how do controlling factors such as climate, which are themselves changing, affect sediment transport mechanisms? Secondly, erosion involves important socio-economic issues. This is particularly true for regions with high population growth, for example volcanic islands under tropical climates, such as West Indies. But these issues are just as important in regions with strong topographical features such as the Alps. Storm Alex, which occurred in the autumn of 2020 in south-eastern France, is a remarkable example of this. In addition to the qualitative and quantitative study of the consequences, political decisions must be taken in response to these challenges, which are expected to become increasingly frequent. The contribution of Sentinel HR to these issues is clear. The mission will provide a decision-making tool that we will need to better prepare our societies to anticipate and mitigate the devastating sediment transport aftermaths during extreme events.

2.9.3 Objectives

1. Target indicators and excepted accuracy Indicators include:

    - Individual landslide/mass wasting scarp locations and surfaces with width larger than 1-2m
    - Estimation of scarp depth and deposit's volume with 2-3m vertical accuracy
    - Estimation of exported sediment at river outlet from calibrated radiometry change (water colour)
    - Vegetation recover rate after erosion event such as landslide (quarterly evolution)
    - Dune field quarterly to yearly evolution (migration rate, crest orientation evolution...)
    - Dune height for large structures (2-3m vertical accuracy)

2. Target coverage and update frequency

    Typical targets are watersheds monitored by observatories (i.e., IR-OZCAR in France) for which we have time series of water level/discharge, turbidity and other metrics such as physical and chemical properties. Typical examples are Guadeloupe (ObsEra), Réunion Island, Draix Bléone (ORE) which show strong erosion rate under various geological and climatic conditions. Additionally, large and slow landslides monitored by the OMIV French national service would take advantage of Sentinel-HR as well. Areas for which, indicators should be monitored for changes on a monthly to quarterly basis.

High mountains catchments, also subject to mass wasting due to the permafrost degradation are of great importance. Northern alps catchments such as Arve valley are typical example. While they might be targeted for application use to glaciers themselves, they are also concerned in the hillslope-river sediment transfer mechanisms, hence indicators of watershed erosion that should be monitored for changes on a quarterly basis. Finally, remote areas such desert are of great importance for a better assessment of the aeolian sediment transport through dune systems. Ténéré desert is one great example. As a matter of fact, this area is the source of 2/5 of the world aerosols production. Due to the wind regime, indicators should be monitored for changes on the quarterly to yearly basis.

2.9.4 Methodological insights

Typical methods for assessing landslides locations and associated deposit areas are either based on orthoimage photointerpretation [HZOH$^+$05, ALDD12] or from automatic detection involving machine learning techniques. Volume can be derived from DTM either obtained from LiDAR and/or photogrammetry [HZOH$^+$05, SMA$^+$15, Lac16]. Topographic reconstruction has been also considered [KD05, SCH08, LMMB11]. Regarding the dynamic aspect, in absence of ground measurements such as optical fibre for instance, image correlation from orthoimages (aerial and satellite based) have shown excellent performance [WCDD04, SMD17]. Mixed approach combining ground measurements with spatial observations have shown interesting results as well on the dynamics and mass balance [BLAD13]. More recently and thanks to Sentinel-1 in particular, InSAR measurements are also possible when the flow velocity is sufficiently slow for keeping the structures patterns similar all along the observations in order to have sufficient phase coherence [HHF$^+$19, KLZ$^+$21].

Regarding the river sediment transport, great work has been conducted using remote-sensing and ground imagery. One can take examples of various rivers including La Réunion, the Rhône or the Durance rivers to name a few at national scale [ODA04, OP05, DFC02, GPP05, SADB16, **?**, LGew]. Classification in the sediment plume has been conducted from multi-spectral data [VLDM12, **?**, LFO01]. Nonetheless, due to the highly dynamical behaviour of rivers, especially during flood events, in situ measurements (strongly supported by observatories) remain the most used approach nowadays as opposed to remote sensing. Repeating time and high spatial resolution are critical for this task, and nowadays platforms do not offer both (e.g., Sentinel-2 vs PHR).

On the dune side, photointerpretation has been done for a long time [CA69]. More recently, time series using both aerial and modern satellite imagery have been conducted in various regions [VL12, LNR$^+$15]. High resolution satellite with stereo ability (i.e., PHR) allow to generate DTM that provides critical metrics used to derive sediment fluxes [LNR$^+$15]. Time series of DTM would be a substantial step forward for assessing the morphodynamics of aeolian systems.

2.9.5 Current readiness level

The current performances offer a weekly update over various regions of interest with medium to low spatial resolution (e.g., Sentinel's, LandSat8...). The VHR satellite imagery is offering a much better description and hence a better depiction of features while still offering a good temporal revisit, especially in case of strong event (Figure 2.14). SAR data are being

more and more considered, in both parts, the real for amplitude time series, and phase offer InSAR measurements that may characterise slow motions such as large landslides and creep. Nonetheless spatial resolution is a strong limitation for such data ($\approx$ 13m).

Figure 2.14: Example of sediment plumes after Alex storm (Oct. 2020) in Southeast France as seen from Nasa Worldview.

2.9.6 Benefits expected from the Sentinel-HR data

Repeating observations with a metric accuracy is providing a real improvement in regards to a highly changing landscape. This is critical for identifying the sediment sources from hillslope (mass wasting...) as well as tracking the sediment path through the watershed. On the dune task, this is important to be able to track any change due to wind regime evolution at quarterly basis in order to refine our vision of the dynamic shift that theory predicts.

Time series of DTM would be a substantial step forward for assessing the morphodynamics of sediment transport in the three considered cases. Landslides may occur as multi-event. Being able to track such complex scenario is important for assessing the resulting mass released and better understanding how rivers react from such sediment sources.

Current VHR such as PHR cannot track with sufficient update frequency any evolution on a systematic way. Higher frequency, yet less resolved, cannot offer a metric detection threshold, which happens to be the scale of major interest. Hence, S-HR will offer the best of the two worlds and provide substantial leverage compared to current readiness.

2.9.7 Limitations of Sentinel-HR specifications

Metric spatial resolution is key for most of geomorphic processes. Besides, frequency update allows to track and better constrain the dynamics of these mechanisms. Therefore, the spatial resolution of 1m [**Olivier: peut mettre 1-2m**] is a key parameter that should be considered as critical. Hence the radiometric dynamics is also important as we are interested in steep terrain that usually imply shaded areas during acquisition. Low dynamics can lead to subsequent low detection and characterisation in such places. This is also critical for highly reflected terrain with low features as opposed to glacier scene, such as dune fields.

Finally, the ability of deriving DTM is also very critical for most aspects. Hence the sensor characteristics needs to be carefully performed so as to guarantee a good relative accuracy on the derived topography. Pixel RMS should as low as possible and reach the 3m value. [**Olivier: pareil, on est passé dans les specs de 3m 1 sigma à 4m CE90, il faudrait vérifier que nos utilisateurs ont bien compris qu'on parlait d'écarts types avec 3m**].

2.10 Land-sea topo-bathymetry coastal continuum

Contributors: Rafael Almar (LEGOS)

2.10.1 Summary

Until recently, the main application of optical satellite remote sensing of the coastline was photogrammetry, including shoreline mapping. By analysing stereoscopic pairs of satellite optical images, it is possible to cover large coastal areas with vertical errors of less than 0.5 m. Intertidal areas between spring tides also benefit from the wide range of satellite data available. Satellite-derived bathymetry (SDB) can reach fine resolution thanks to two approaches: methods based on the radiative transfer of light in water, and methods based on the influence of topography on waves. Each method/sensor comes with its own strengths, limitations, and scope of applications. The monitoring of land sea morphology continuum is clearly the way forward for coastal studies.

2.10.2 Context

With a large part of the world's population, coastal regions are largely vulnerable to the dynamics of natural and human-induced changes. A single storm can reshape the coast. But only a small fraction of world coasts are surveyed by hydrographic and geographic national services, and nautical charts and Digital Elevation Models (DEMs) are decades old. This leads to severe uncertainty in forecasting the impact of storms and climate changes. Characterisation of physical properties of the coastal zone is thus needed for natural hazard assessments. Conventional coastal monitoring in-situ measurements are reliable, but limited to the local scale. Alternatively, optical satellites are becoming more and more effective tools for monitoring coastlines, with the ability to reach anywhere in the world with increasing frequency and resolution allowing for capturing seasonal to inter-annual changes (research observatories, program COPERNICUS land/marine services, commercial services).

2.10.3 Objectives

1. Target indicators and excepted accuracy

   - Shoreline: 1-5 m horizontal, daily to monthly
   - Intertidal topography: sub-metric vertical accuracy, daily to monthly
   - Topography: sub-metric vertical accuracy, daily to monthly
   - Bathymetry: metric vertical accuracy, daily to monthly

2. Target coverage and update frequency

   To capture seasonal to inter-annual coastline changes, recommendations to improve the monitoring of the coastal zone morphology with the following settings: 100 km^2 coverage, daily to monthly revisit, meters of resolution and burst of images over tens of seconds.

2.10.4 Methodological insights and current readiness level

1. Shoreline monitoring

   The practical use of satellite optical imagery to obtain and analyse shorelines along sandy coastlines builds upon several decades of well-established research and practice that has traditionally used fixed cameras and video for automated and routine image collection (e.g., [HS07]). As shorelines provide a fundamental measure of coastline variability and change and the optical signature of this land-water feature is relatively distinct [BT05], there is a growing body of work that now reports the use of satellite-derived shorelines (SDS) applied to a range of shoreline mapping and monitoring applications around the world (e.g., [ACSGPP$^+$16, Xu18, HdL$^+$18, CW20, SGPVPP$^+$20, CMS$^+$21]).

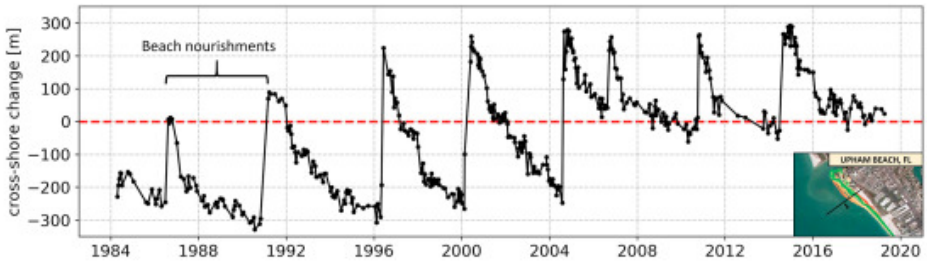

Figure 2.15: Illustration of satellite-derived shorelines (SDS) to monitor and measure 35 years of engineered coastal changes at Upham Beach located on the west coast of Florida USA, the site of multiple beach nourishments (from [THAB21]).

2. Intertidal topography

   Intertidal topography and its variation also benefit from the use of satellite remote sensing [**?**, FRHM21, KAD$^+$19]. The majority of applications involve delineation of the waterline with optical satellites [MGK00], followed by new methods with other sensors [SFA$^+$19] such as interferometric synthetic aperture radar (InSAR) [CK18] and satellite radar altimetry [SFM$^+$18].

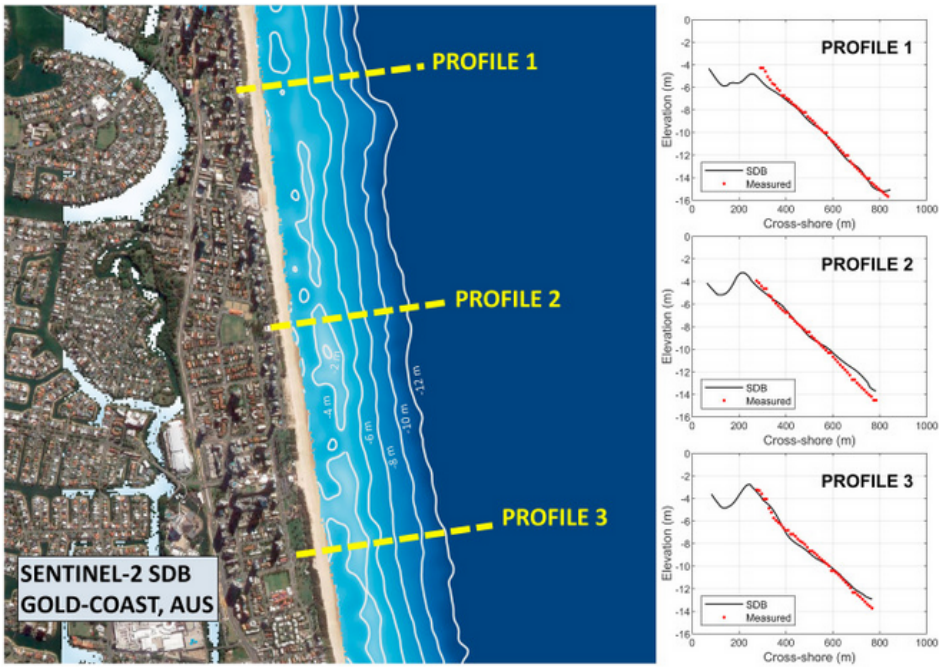

Figure 2.16: Illustration of satellite-derived bathymetry (SDB) applied along approximately 4 km of the highly engineered Gold Coast, located in eastern Australia. For the three representative cross-shore profiles 1-3 where surveyed and SDB cross-sections are compared, vertical RMSE are 0.44 m, 0.53 m and 0.39 m, respectively (from [THAB21]).

3. Bathymetry

   Satellite-derived bathymetry can reach fine resolution thanks to two approaches [SFA+19, MTLC+20] : methods based on the radiative transfer of light in water, and methods based on the influence of topography on waves. Each method/sensor comes with its own strengths, limitations, and scope of applications. Specifically, methods based on the radiative transfer perform better in clear and calm waters, whereas techniques based on water depth inversion requires waves [Abi06, DB13, DF16, PIDMR16, ABMd19, DBB+21, BAM19].

4. Topography

   By analysing stereoscopic pairs of satellite optical images [TA92], it is possible to study large coastal areas with vertical errors of less than 0.5 m. Examples using Pleiades are given in [CHP+18, Alm19, TAB+21]. these techniques offer the novel opportunity to derive topography and bathymetry DEMs during a single pass, with a vertical accuracy and precision for topography that is similar to state-of-the-art survey methodologies for coastal monitoring (GPS and LIDAR airborne surveys).

2.10.5 Benefits expected from the Sentinel-HR data

Coastal morphology changes over a wide range of timescales (from storm events, seasonal and inter-annual variability to longer-term adaptation to changing environmental conditions), in particular in response to changing incoming wave regimes [KHCK+16, BAM19] and human interventions. Despite their high potential, satellite coastal DEMs have only been applied to punctual space and time domains, and efforts remain to be done to map nearshore bathymetry and its time-evolution at larger scale (e.g. [MJA+18, WSA+19, BCV+19]).

[Julien: dans cette partie, ainsi que dans la section limitations, la notion de bursts n'est pas claire: fais tu référence aux modes vidéos de Pléiades ou Planet ? Cette capacité n'est pas prévue sur Sentinel HR (mais n'est pas non plus présente sur Venμs. Est ce que tu pourrais exprimer les contraintes en terme de B/H et de temps d'acquisition entre les deux vues stéréo ?]

It is all a question of compromise in the combination of the acquisition settings. The swath of JILIN is smaller than other missions such as Pleiades and VENUS (and even more different from the 10 000 km² of Sentinel-2) but offers a longer duration of burst at an advantageous frame-rate: short compared with wave period with dt/dx small compared with celerity. Satellite short burst at even high resolution such as WordView and Planet focus even on a smaller area despite proving longer videos.

Lastly the revisit is important, regular 2-day revisits such as VENUS phase 3 [BAR+21] (now daily in phase 5) offers the double possibility of capturing topo-bathy changes, despite lower performances (due to coarser resolution and reduce number of frames). Sentinel-2 mission also offer a 5-day revisit but cannot produce accurate bathymetries and topographies.

Recommendations are given for Sentinel-HR mission to improve the monitoring of the crucial foreshore with the following settings: 100 km² coverage, monthly revisit, meters of resolution and burst of images over tens of seconds.

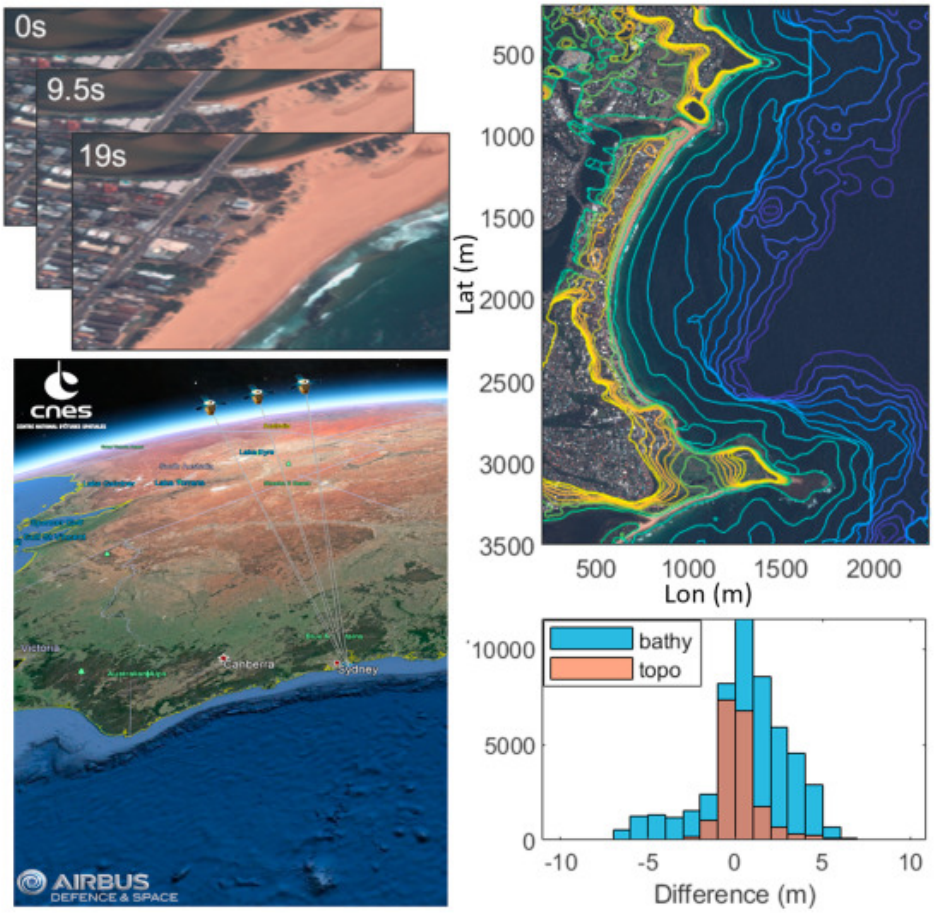

Figure 2.17: Example of a seamless 3D topo-bathy derived from Pleiades-HR tri-stereo imagery obtained at Collaroy-Narrabeen Beach in southeast Australia. The acquisition of 3 images captured 9.5 seconds apart of the same location but from different positions along the satellite orbit enables the topography to be derived using stereoscopy, and simultaneously the bathymetry to be inferred based on the observed wave-kinematics in the nearshore zone. When compared to a combined airborne Lidar and hydrographic survey dataset obtained to coincide with the Pleiades-HR mission at Narrabeen, within the near-coast topographic region (0 – 15 above mean sea level) the satellite-derived RMSE = 0.83 m (r2 = 0.97) and in the nearshore region (0 – -20 m below sea level) RMSE = 1.89 m (r2 = 0.76). Though this figure correctly captures key coastal features such as the elevated headlands and their adjacent rock platforms, sand dunes, a steeper beachface and more gently sloping nearshore region interrupted by several rocky reefs, the present accuracy of this satellite-derived product is variable, and further refinement will be required for it to become a practical tool for Coastal Engineers. The next generation of 'video from space' satellites can be anticipated to significantly improve the accuracy of these and similar methods (from [THAB21]).

2.10.6 Limitations of Sentinel-HR specifications

Regarding Sentinel-HR when applied to the coastal zone, we believe they should consider the following :

Swath In general, the need for high accuracy DEM is local, here a few tens of square kilometres, localised at the shoreline in shallow water where the bed evolves under the action of waves and currents,

Resolution typically, there is no big constraint for the bathymetry retrieval where meters are sufficient but rather for the topography estimation which directly depends on the pixel resolution,

Revisit not necessarily daily to capture event scale but typically monthly and seasonal evolution which represents a reasonable target for coastal studies and management,

Sequence of frames to capture wave kinematic, acquisitions durations of tens of seconds covering 2-3 waves are a minimum to reduce the stochastic influence of the wave field, in order to accurately inverse bathymetry and to allow stereo photogrammetry on land (Large base-over-height ratio give good results for flat areas while small base-over-height ratio are better for steep areas). As in coastal zones, dunes and beach generally present slopes of 0.01 to 0.1 [Kom98]. The temporal resolution is important and should remain a small fraction of wave period which ranges from 5 to 25 s typically. [**Julien: même remarque ici, avec Sentinel-HR, la séquence sera de 2 frames uniquement**]

2.11 Monitoring geo-hazards: volcanoes, landslides, earthquakes

*Contributors: * ForM@Ter / Optical Working Group, Service National d'Observation ISDeform (CNRS-INSU), Group contact : Jean-Philippe Malet (CNRS/EOST)

2.11.1 Summary

Mapping, monitoring and modelling geological hazards such as volcanoes, landslides and earthquakes can be achieved using satellite imaging platforms to obtain broad scale information and synoptic coverage. Multi-temporal and stereoscopic observations are relevant to complement InSAR observations in terms of complementary of viewing angles, sensitivity to other components of the motion, and range of velocities. Monitoring geohazards is critical for disaster risk management, the identification of hazard warning criteria, and a physical understanding of the mechanics of the processes and of their triggering. It implies consistent and systematic observation of the Earth land, high revisit time and high spatial resolution. Further, the relatively high-rate revisit time proposed for Sentinel-HR would also allow tackling a broader scope of geohazards, including geohazard related to fast modification of the landscapes like changes in coastal conditions, sand dunes motion and abrupt erosion and deposition processes (mud-flows), during strong weather episodes.

2.11.2 Context

Monitoring geohazards from space is a key aspect of increasing the resilience of the Society to natural risks and sustainable development in general. Optical space-borne images for civil

applications have been routinely acquired since the 1980s at both high (Landsat and Copernicus Sentinel-2 programmes) and very-high (Spot, Pléiades, Rapideye/Worldview, PlanetLab) spatial resolutions. Among other, the high revisit time of Sentinel-2, the very-high spatial resolution and the stereoscopic capability of Pléiades, and the agility of PlanetLabs data have conducted to a new understanding of the mechanisms controlling volcanoes, landslides and fault ruptures/motion, and in some cases helped during operational crisis situations. Consistent algorithms, processing chains and web-services (ForM@Ter, GEP) are now available to exploit these observations and deliver ground motion measurements in short-time.

To obtain a global picture of the dynamics of these objects, a combination of the high revisit time of Sentinel-2 and the very-high spatial resolution of Pléiades, including stereoscopic acquisitions, will be a critical step forward to propose new products such as 3D motion fields, to better identify transient (in space and time) motion. In this context, Sentinel-HR can provide valuable insight for increasing our anticipation and response capacity to disasters. Of course, the revisit period is too loose to allow the use of Sentinel-HR for emergency action, but the availability of Sentinel-HR provides a recent reference to compare to the satellite acquisitions after the event.

2.11.3 Objectives

1. Target indicators and excepted accuracy

   Domain-oriented indicators are:

   - Landslides:
   - Detection and mapping of landslide of size < 200 m2
   - Quantifying motion of slow-moving landslides (velocity < 1-2 m.yr-1)
   - Increased identification of landslide pre-failures processes
   - Increased sensitivity to detect and measure vertical motion of > 0.5 m
   - Volcanoes
   - Quantification of lava flow volumes of > 100 x 100 m2 area x 10 m thickness = 0.1 Mm3.
   - Mapping of flank motion, lahar and pyroclastic mass movements.
   - Detection of small-scale thermal anomalies with infrared bands (lava lakes, lava flows)
   - Measurement of surface motion associated with rifting.
   - Earthquakes - active faults
   - Measurement of horizontal motion (>30cm) and vertical motion (>50cm) across surface ruptures induced by magnitude > 6.5 earthquakes.
   - Measurement of surface deformation at short distance (<10 km) from surface ruptures induced by magnitude > 7.5 earthquakes.
   - Detection of liquefaction areas by loss of correlation between two acquisitions.
   - Mapping and monitoring of (potentially transient) creep across faults with shallow slip rates faster than 1 cm.yr-1.

   Measurement indicator accuracies are:

- Quantification of ground motion at 1/3th or 1/5th of pixel size (e.g. 0.3 or 0.2 m; for a Sentinel-HR pixel of 1 m) - note that If ground condition are favourable and loss of coherence is small (aside from the effect of the external change), a detection sensitivity threshold for changes down to 1/10th of pixel size might be attained (with the use of hierarchical / pyramidal cross-correlation functions).
- DSM : Accuracy of Z at 1 m, Accuracy of horizontal positioning at 0.5 m
- Accuracy of volume (Z difference from multi-date DSM) : 0.5 m
- Temporal sampling better than 1 acquisition per month.

The acquisition should be sun-synchronised for the revisit time (as for current Sentinel-2), relevant masks of cloud/shadow and consistent accuracy of absolute positioning should be provided for solid Earth applications.

2. Target coverage and update frequency

- All active volcanoes of the Earth : 1413 volcanoes with eruptions during the Holocene period according to GPV database. Roughly 1000 targets with individual area of 100 km2 yields 100,000 km2. These volcanoes are mostly located in the Pacific "ring of fire", Indonesia, East African Rift, Lesser Antilles, Iceland, or scattered around the globe. Most targets are located in the tropical and equatorial region. Systematic acquisitions enhance the chances to obtain cloud-free observations.
- Main tectonic areas of the Earth or main active faults: a first list of the continental faults zones could be established to acquire a general archive. Then, some zones where changes are more frequent (human activities, vegetation changes. . .) should be reacquired on a regular basis. Eventually, active tectonic areas in a broad acceptance should be at least archived once in a while, if not regularly,
- Landslides : mountain regions (e.g. elevation $>$ 500 m) of the Earth and inter-tropical zones affected by typhoons/hurricanes. A monthly revisit time of all these zones would allow to construct consistent landslide catalogues, with both information on newly triggered landslides and information on surface velocity/strain for persistently active landslides.

2.11.4 Methodological insights

- Image correlation / offset tracking methods (e.g. MicMac, Cosi-Corr, Medicis, GeFolki, ..)

Several tools and on-line services to process optical imagery are currently availbes, and used/maintained/developed by the scientific community. The most relevant and frequently used tools are: Stereoscopic image matching methods (e.g. MicMac, CARS, AMES-ASP, ..)

- Enhanced co-registration methods (CO-REGIS, AROCSIS, . . .)
- Change detection methods: ALADIM, SALAD, deep-learning approaches
- Web-services: GDM-OPT-ETQ, GDM-OPT-SLIDE, DSM-OPT.

2.11.5 Current readiness level

As a matter of example, to express the necessity to construct archives of very-high resolution images, for the earthquake of Ridgecrest (USA), which occurred in July 2019, it took about 2 months (thanks to the specific effort of CNES/ForM@Ter) to get a complete set of stereo acquisitions over the rupture (70km) with Pléiades. The very-high resolution archive was quite limited and usually not stereo, so an external DEM has been needed to process images pre-earthquake.

The same holds for the follow-up of the volcano crisis of the La Soufrière de St-Vincent in 2021, or the monitoring of the Barry Arm landslide (possibly triggering a tsunami) in Alaska for which no pre-DEMs were available and needed to be constructed.

2.11.6 Benefits expected from the Sentinel-HR data

Sentinel-HR will provide the necessary coverage, spatial resolution (1 m) [**Olivier: peut on écrire 1-2m**] and revisit (20 days) to propose a 2 months (in the hypothetical guess of no clouds) geohazard monitoring achievable. The spatial resolution will be good enough for increasing the sensibility of motion measurements to lower displacements, and will provide higher details to decipher the spatial variability of motion ...

Note that the Sentinel NG foreseen spatial resolution of 5m will likely be insufficient for this use case, even if the addition of a 2.5m panchromatic band is being discussed. The CO3D imagery would be suitable for the production of the indicators but as of now the tasking of the constellation is not oriented toward systematic global coverage, but rather to on-demand tasking, after a first phase aiming at gathering a complete DTM over France and an area in middle East.

2.12 Crisis and risk recovery mapping

Contributors: Stephen Clandillon, Stéphanie Battiston, Robin Faivre (ICUBE-SERTIT/Université de Strasbourg)

2.12.1 Summary

Rapid mapping (RM) in the context of natural or man-made disasters requires the rapid acquisition and delivery of images at short notice [IAS20]. Hence, the pertinence of Sentinel-HR might seem limited, except that to allow a rapid mapping of the changes due to a catastrophe, reference data are needed, especially in the VHR1 (<1m) and VHR2 categories (<4m), as pre-event basis for the damage assessment. Furthermore, high quality Sentinel-HR derived DEM data would improve the orthorectification of VHR data. A Sentinel-HR X, Y, Z reference could integrate future flood propagation modelling, especially in modelling urban flooding. In summarising damage or during the recovery phase, Sentinel-HR 3D data could help in modelling building damage assessment, maximum flood extent mapping, flood depth analysis and estimate vegetation type and volume loss due to fires and/or storms. This type of mapping is important as often in preparing for the recovery phase wood resources need to be known and damaged tree crops can impact a population's capacity to feed itself. Moreover, Sentinel-HR could contribute to the 3D analysis of earth movements and understanding of landslides, mud-flows, building collapse damage assessments.

2.12.2 Context

Rapid Mapping, through the International Charter 'Space and major disasters' and Copernicus Emergency Management Service (EMS) - Mapping, is a well-established and ever improving field [BCF+19]. Reference, Delineation and Grading products are delivered to a wide user community of civil protection agencies, the UN, humanitarian organisations and local crisis managers and environmental agencies by Rapid Mapping (RM) organisations.

Within Copernicus EMS, RM users would like a better coverage of urban flooding. Having precise DEMs is a prerequisite for this analysis with Sentinel-HR being an improvement on existing systems. Furthermore, within the Risk & Recovery context and thanks to its consistent, systematic acquisitions, Sentinel-HR should enable better 3D analysis of landslides, improvements in flood water depth and maximum flood estimates along with providing systematic VHR2 optical reference imagery. These precise DEMs would be a valuable input to flood forecast models. The systematically available DEM compatible imagery could also be used to estimate the fire/storm damage on vegetation in terms of the height of vegetation burnt or affected by windfall, which can be linked to economic and biodiversity loss, and help estimate tree crop damage and the potential impact on food sources. The above comments hold for storm damage where sometimes whole tree crops (bananas, coconuts...) have been destroyed.

Sentinel-HR would transform the market for 3D products being systematic, precise, ready for use, free and open access.

2.12.3 Objectives

1. Target indicators and excepted accuracy

   There are a number of potential uses for Sentinel-HR data in the Rapid Mapping and Risk & Recovery domains. Some ideas are shown in the list below.

   Up to date background reference imagery Colour composites in standard software packages

   DTM creation photogrammetric restitution to elaborate DTMs, operator validation and modification where necessary. Various software packages are available for this.

   Orthorectification Use of Sentinel-HR derived precise DTMs plus sensor models and possibly Ground Control Points to orthorectify imagery. Various software packages are available for this.

   Ground movement indicators, vertical changes Calculate the difference between before and after DTMs taking into account the 3m Z error margin. Of course this would be linked to major land and/or mudslides

   Maximum flood water extents Model/interpret potential flooded areas from an existing flood map, hydrological models and of course using precise Sentinel-HR DTMs/DEMs as input.

   Flood water depth Use the maximum water extent and the DTMs/DEMs to derive flood water depth classes

   Slope and slope length Derive VHR DTMs and/or DEMs to calculate slope and slope length for input into Revised Universal Soil Loss Equation (RUSLE) and Landslide Susceptibility Index (LSI) model calculations.

LULC Systematic regular VHR optical acquisitions to derive land use and land cover layers in reference and exposure mapping.

Vegetation volume and volume dynamic mapping Map vegetation in X, Y and Z to obtain an idea of vegetation volume. This can help indicate vegetation losses due to fire or storm events.

Building height measurement and change assessment Useful to map buildings and estimate if height variations have occurred due to seismic or other natural hazard events.

Sentinel-HR should provide a valuable resource of precise, 3D enabled, VHR2 reference imagery at low incident angles. This is often needed in rapid mapping and Risk & Recovery. Widely available and accurate DEMs would greatly help in obtaining more precise mapping and advantageously replace the currently used EUDEM and SRTM. These more accurate DEMs should enable a better mapping and modelling of urban flood mapping (X, Y, Z). Moreover, more precise flood extents, maximum flood extents and water depth analyses should be facilitated.

As already stated, the exploitation of 3D dynamics analyses should help indicate vegetation volume loss mostly for forest exploitation and damage analyses. This can be applied no matter the damage cause (storm, fire). Building damage assessment is not easy just after events with satellite data especially in urban areas, but to obtain anything without considering 3D aspects sub-metric acquisitions are necessary. Satellite EO is good for overall indications. It is thought that a benefit 3D analysis could bring is the improved detection of partial collapse or when the lower floors collapse (Kathmandu, Nepal). Sentinel-HR could be used as reference 3D data with other platforms most likely providing the crisis 3D data.

Interestingly, these precise data should help derive more precise slope, slope-length parameters for the Revised Universal Soil Loss Equation, Landslide susceptibility Index, avalanche risk, among other risk indicators [MCP+17a].

2. Target coverage and update frequency

   The availability of a worldwide systematic coverage similar to Sentinel-1 and Sentinel-2 is foreseen to be of great benefit. If the coverage is updated every 20 days that would ensure Landsat-type coverage frequencies (revisit frequencies) with a much higher resolution. Combined together, these aspects are of great value.

2.12.4 Current readiness level

Currently, no optical mission systematically acquires photogrammetric pairs that can be transformed into 3D surfaces. This applies to HR and VHR data. They must be programmed on an ad-hoc basis and are expensive commercial data. The current TRL levels for ad-hoc work are high, the applications are operational even if manual editing is necessary. Work would be needed to create automatic processing chains for the large quantities of data while reducing operator needs to a minimum. Readiness of various indicators are presented in table 2.2.

ICUBE / SERTIT is involved into several operational risks mapping activities:

- FRAMEWORK SERVICE CONTRACT FOR COPERNICUS EMERGENCY MANAGEMENT SERVICE RAPID MAPPING (2019-2023) (JRC/IPR/2018/E.1/0016/OC)

Prime: e-GEOS, ICube-SERTIT is involved in contract management, product evolution (mega-disaster fire and flood product) and 24/7 activation management and 24/7 Production Site

- FRAMEWORK SERVICE CONTRACT FOR COPERNICUS EMERGENCY MANAGEMENT SERVICE RISK AND RECOVERY (2020-2024) (JRC/IPR/2019/OP/1766) Lot 2 Standard Products Prime: e-GEOS, Lot 1 FLEX Products Prime: IABG. ICube-SERTIT is involved in 7/7 activation management and 7/7 Production Site
- Framework contract CNES-SERTIT (rapid mapping) (2004-2024) Support the CNES in its International Charter "Space and Major Disaster" work especially in relation to 24/7 rapid mapping, promotion, Charter PM, demonstration products. Recovery Observatory support for the CNES.

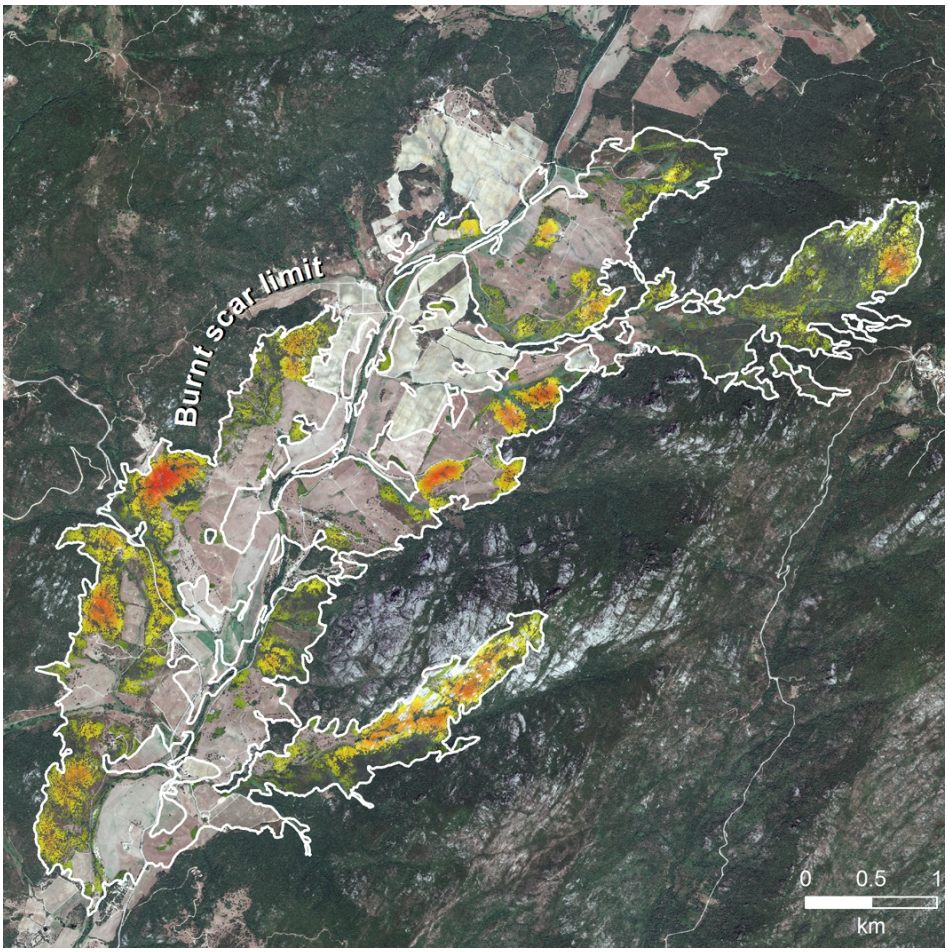

Figure 2.18: 3D fire impact monitoring maps are generated by using burn scar and vegetation recovery products, along with Digital Elevation Models (DEMs) to indicate potential vegetation volume losses. This work was performed during the PREFER (Space-based Information Support for Prevention and REcovery of Forest Fires Emergency in the MediteRranean Area) FP7 EU project. This work has continued in further projects and contracts [BFG+19, MCP+17b, CYS+15]

Target	**Current source**	**TRL**	**Comment**
Maximum flood extent mapping	Combined multiple individual layers, Photo-interpretation	7	Better DEM information would greatly help here
Water depth	Maximum flood extent mapping, DEM	7	Better DEM information would greatly help here
Building and infrastructure damage assessment (earthquakes, cyclones)	Before and after multi-spectral VHR1 (<1m) optical data	7	Both the double angle looks and the before and after building heights could be a valuable addition to building damage assessment
Vegetation loss	Vegetation map, burn scar	5	Systematic DEM information would help to indicate the vegetation height loss and whether they were mature stands, scrub or low-lying vegetation
Slope and slope length	Available DEMs often EUDEM or SRTM	7	Precise systematic DEMs would help in accessing source data and creating these important relief parameters for the RUSLE and other indexes
LULC	Multi-temporal, multi-spectral data and ancillary data	9	Could be improved through the systematic access to LULC height and perhaps height texture parameters
Ground movement indicators	Before and after DEMs	7	More precise systematic DEMs could help better describe mass movements (surface and volume)

Table 2.2: Curent readiness level of various rapid mapping indicators

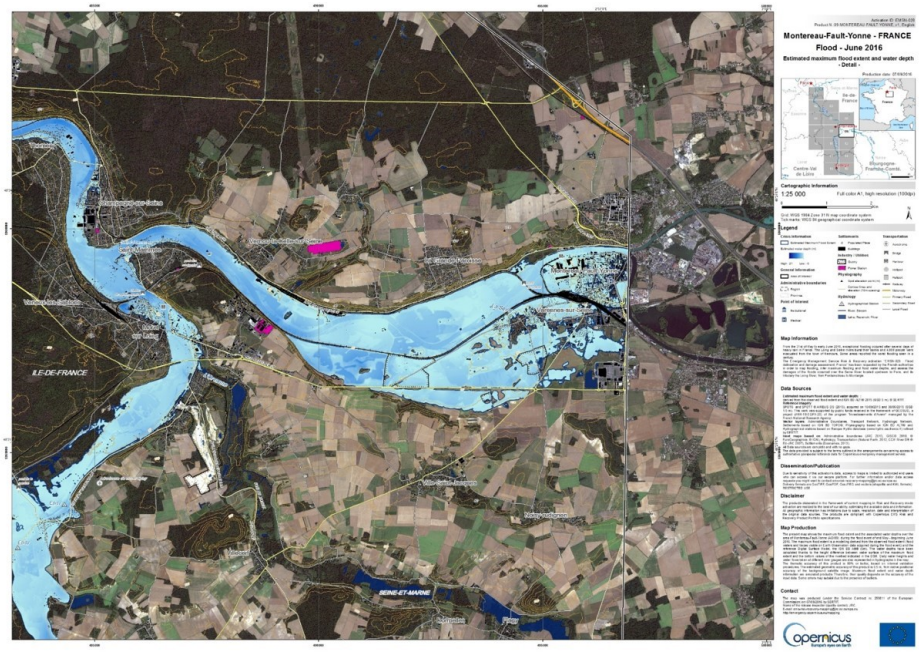

Figure 2.19: Estimated maximum flood extent and water depth, Copernicus Emergency Management Service (© 2016 European Union), [EMSN028] 09MONTEREAU-FAULT-YONNE

2.12.5 Benefits expected from the Sentinel-HR data

Sentinel-HR data will provide access to up-to-date terrain and land use / land cover (LULC) information useful in a wide range of activities linked to basic LULC mapping and many product needs from highly precise DEMs for accurate ortho-rectification to terrain linked analysis such as mass movement, landslide or soil erosion susceptibility, helping through models to analyse urban flooding, post-fire vegetation loss, and a better understanding of building damage assessment with side looks and building height measurements (see table above).

2.12.6 Limitations of Sentinel-HR specifications

With respect to Rapid Mapping applications the 20 day revisit interval is quite long. Furthermore, the it is considered that a maximum of VHR2 resolution needs to be kept to facilitate the data's use as a reference data. Nevertheless, for urban applications VHR1 would be preferable and it is important to keep to preferably sub-metric resolutions to enable the best possible urban analysis. The DEMs will of course have more relaxed resolutions, being adapted to each application.

For many applications including water extent mapping a SWIR channel is very interesting to have.

Chapter 3

Mission design

In this chapter, we present two possible configurations to implement the Sentinel-HR mission. The first configuration consists in designing a set of ad-hoc satellites, while the second configuration consists in an extension of the CO3D constellation with dedicated small satellites.

3.1 Solution based on ad-hoc satellites

3.1.1 Hypotheses

As the phase 0 did not include dedicated resources for a complete mission study for the ad-hoc solution, we assumed some hypotheses in order to narrow the possibilities, so as to demonstrate at least one possible configuration. Optimisation of this configuration has not been addressed. The main specifications hypotheses are presented in table 1.1.

In addition, the main starting hypotheses for the instrumental and mission study were:

- Number of satellites is limited to two, in order to stay in line with the costs of current Sentinel2 constellation.
- 3D restitution will be achieved by stereo-restitution of two similar channels with a baseline angle difference, on board of each satellite.
- Orbit is heliosynchronous with an altitude comprised between 600 km and 800 km
- No night acquisitions
- Ascending Node Local Time is approximately 10h30
- 5 km of overlap between traces are required at equator, in order to allow for cloud shadow tracking

3.1.2 Orbital configuration

1. Orbit selection

   Based on the hypothesis of 2 satellites, the following orbits have been considered:

   Orbit (14,7,20) at 769 km altitude This orbit has a revisit of 20 days. Longitude of both satellites are adjusted so that each satellite is responsible for half of the

field, with an overlap of 5 kilometers at equator. Note that with this orbit, a single satellite only acquires half of the target surface, with 20 days revisit.

Orbit (14,11,40), at 794 km altitude This orbit has a revisit of 40 days, and both satellites are on the same track with a phase shift so as to ensure a global revisit of 20 days at equator. Note that with this orbit, a single satellite acquires the total target surface, but with a revisit of 40 days.

Orbit (14,19,60) at 780 km This orbit has a revisit of 60 days, but a sub-cycle of 19 days, meaning that each satellite will fly over the next or previous node 19 days later. This would allow to better distribute revisit at medium (European) latitude, but needs to be further investigated.

Among those orbits, (14,11,40) seems to be the most reasonable choice, as it ensures the full coverage with a revisit of 40 days with a single satellite. This leads to a half Field Of View of $\approx 2.5°$ and a corresponding swath width of ≈ 67 kilometers.

2. Field Of View adjustment

   As earth is not perfectly spherical, it is necessary to simulate local revisit time in order to ensure that there are no gaps, and optimize field of view accordingly. Figure 3.1 presents the maximum revisit map of the first simulation ran with a half Field Of View of 2.505°. We can observe gaps in the map, which means that some position on earth never enter the Field Of View. In order to fill those gaps, it is necessary to increase slightly the half Field Of View to 2.62°, as shown in the map of maximum revisit time presented figure 3.2. Figure 3.3 present the map of mean revisit time for the same value, and figures 3.4 and 3.5 present statistics of maximum and mean revisit time depending on the latitude. This new Field Of View value leads to a wider required swath of 70.42 kilometers. Note that dues to iterations on orbit selection, this adjustment has been made on orbit (14,7,20), and that required swath for selected orbit might be slightly different (but not much).

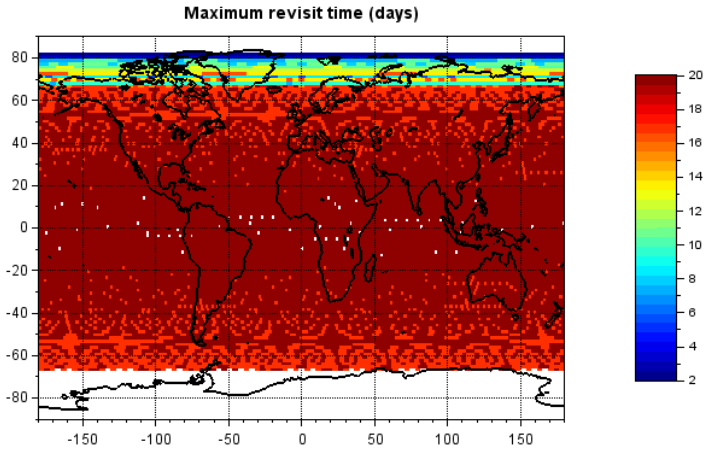

Figure 3.1: Simulated local maximum revisit time with a half Field Of View of 2.505°

3. Optimisation of local revisit time at medium latitude

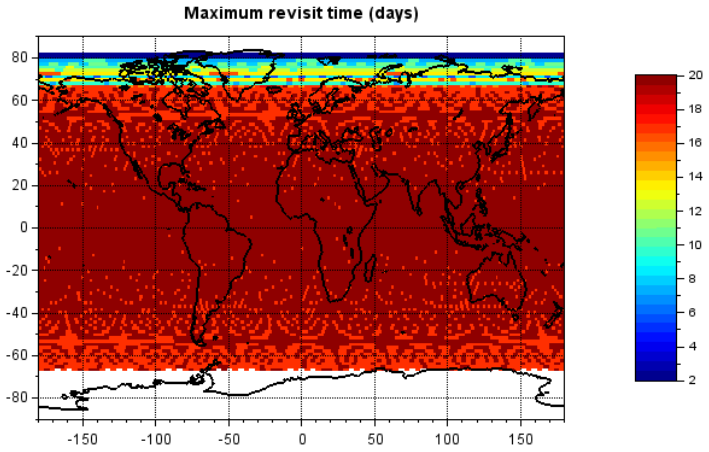

Figure 3.2: Simulated local maximum revisit time with a half Field Of View of 2.62°

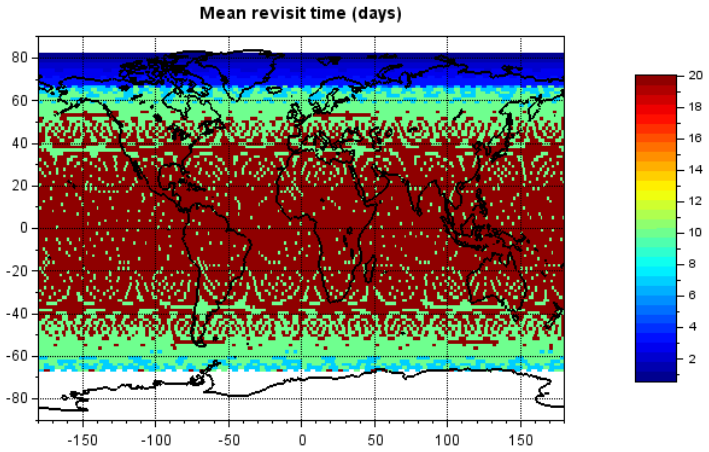

Figure 3.3: Simulated local mean revisit time with a half Field Of View of 2.62°

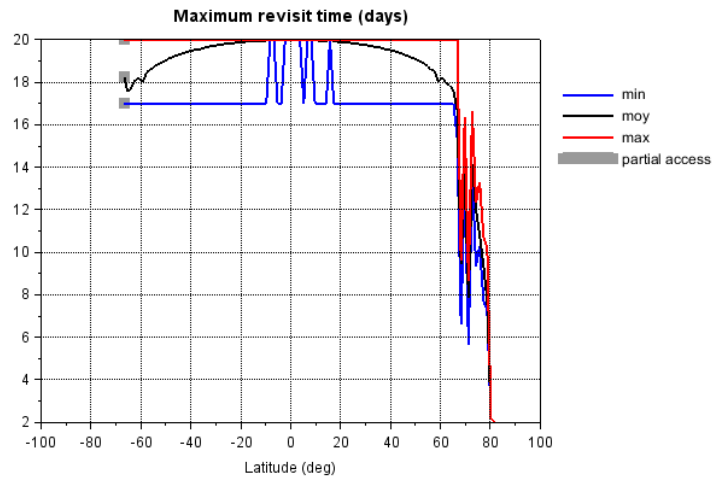

Figure 3.4: Maximum revisit time statistics by lattitude with a half Field Of View of 2.62°

If we compare figures 3.5 and 3.6 which show the mean revisit time statistics as a function of latitude for orbit (14,7,20) and (14, 19,60) in latitude range 40° to 60°, we can observe that the maximum revisit time is 20 days for orbit (7,14,20) but lower than 15 days for orbit (14, 19, 60).

What are the drawbacks of this alternative orbit ? For the 20 days revisit orbit (7, 14, 20), at medium latitude revisit can be better than 20 days because of swath overlap of nearby orbits. For a given ground location this means observation at constant, most nadir viewing angles every 20 days, plus observations from nearby swaths at different viewing angles, depending on the location: some locations will get only 20 days, while other will get regular in between images. In the case of the 60 days revisit orbit (14, 19, 60), it is more likely for a given location to get more frequent observations, but the most nadir observation will only occur every 60 days, and observations in-between will have more diverse viewing angles. Another drawback is that the minimum revisit time at medium latitude increases likewise : as shown in figure 3.6, it is 12 days for most latitude between 40° and 60° for orbit (14, 19, 60), but only 10 days for all latitude between 40° and 60° for orbit (7,14,20).

This kind of orbit configuration as been selected for the Trishna mission for instance, as the more diverse viewing angles allows to reach observation out of hotspot configuration. It has also been suggested for Sentinel2 NG. It remains an interesting option for Sentinel-HR that would require further investigations.

4. Acquired surface

With the (7,14,20) orbit, we estimated the following acquired surfaces :

- 118.838 Mkm² of emerged land per cycle with solar illumination constraints
- 5.94192 Mkm² of emerged land per day with solar illumination constraints

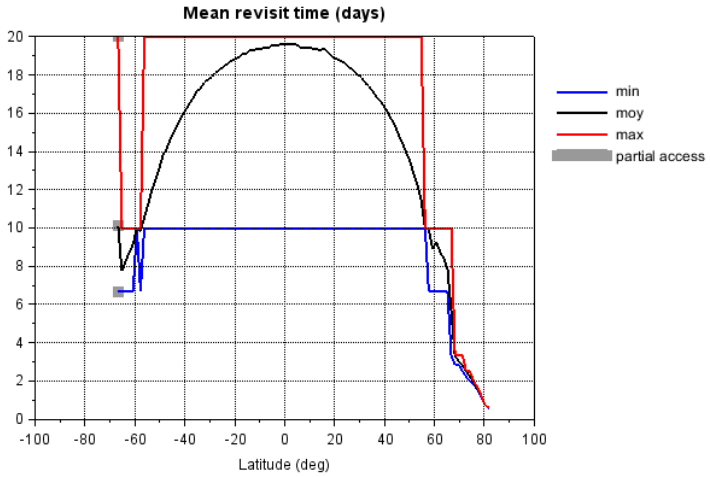

Figure 3.5: Mean revisit time statistics by lattitude with a half Field Of View of 2.62°

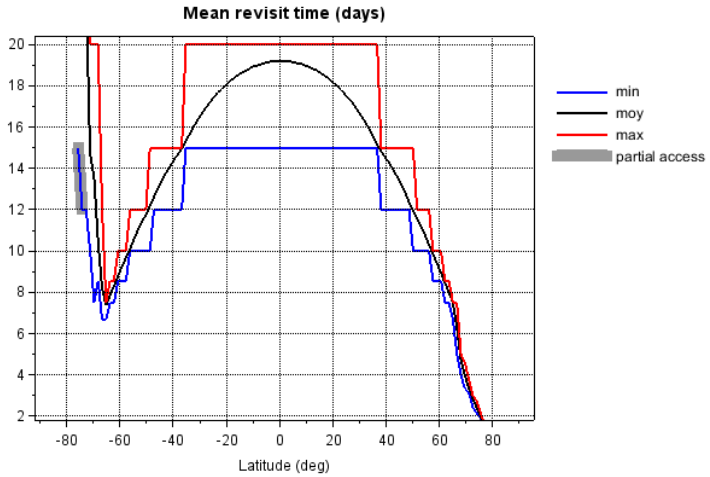

Figure 3.6: Simulated local mean revisit time for orbit (14,19,60)

3.1.3 Telemetry

Using the estimation of 5.94 Mkm² acquired daily for each satellite, we can estimate the daily acquired volume and the required telemetry bandwidth. We can see in table 3.1 that even with the coarsest resolution and best compression rate, each satellite will have to transfer several TB of data each day, which amount to a required bandwidth of 2.8 Gbps if considering a single station visible 100 minutes a day. If the resolution is 2m, this number increases to 4.3 Gbps. Note that latest fixed quality compression algorithms might be able to reach compression rate bellow 3.5 bpp.

State of the art telemetry solutions at CNES can reach an average rate of around 2 Gbps using two X band transmitters in two different polarisation modes and using the full X band bandwidth (375 MHz). This requires a high-gain, pointed antenna on board, and large antennas on ground (5m to 11m) compatible with CORMORAN CNES or MiniMUM networks. Using more complex waveform, a few additional hundreds of Mbps may be reachable, with low readiness level.

Reaching 5 Gbps per satellite will require to leverage other technical solutions, such as:

- Use another frequency range, either Ka band (25.5 GHz to 27 GHz) or optical. In both cases, readiness level is lower than X band. CNES network is currently not compatible with Ka band, but ESA has a Ka network used for Sentinels, which could probably be used for Sentinel-HR. Reaching the target rate of 5 Gbps will probably require 4 different transmitters for each satellite.

- Keep X band transmission and increase the number of on-board memory flush per day of at least a factor 2.

- Use an hybrid solution combining X band and Ka or optical link to a geostationary satellite. This would of course increase costs and constraints as it would imply embedding two different kind of terminals onboard.

  In terms of telemetry, the solution based on two ad-hoc satellites is therefore very demanding and would require additional development to meet the specifications.

3.1.4 Instrumental design

This section presents a very preliminary instrumental design which aims at demonstrating the feasibility of the mission in the configuration with a pair of ad hoc satellites, and highlights challenging aspects of the design. Should this configuration be studied further, a complete design study with in-depth trade-offs needs to be conducted.

In order to work on the instrumental design, we had to chose key specification values, that are detailed in table 3.2. While some of these values directly are deducted from the mission goals, other have been set arbitrarily in order to proceed with the design, and can therefore be modified in further studies.

The global coverage requirements imposes a system without motion compensation and drives towards a TDI pushbroom or pushframe with images summation system.

Given the target Nyquist MTF of 0.1 at 770 km, the pupil size mainly depends on spectral bands and ground sampling distance. Mirror size constraints are given by table 3.3 table for a push-broom instrument, while table 3.4 gives the values for a push-frame instrument, where a 20% margin is needed to compensate for motion blur of approximately 1 pixel.

GSD (m)	compression (bits/pixel/band)	Daily acquisition (TB)	Bandwidth (Gbps)
1	12	44.5	59.3
1	5	18.6	24.8
1	3.5	13.0	17.3
2	12	11.1	14.8
2	5	4.6	6.1
2	3.5	3.2	4.3
2.5	12	7.1	9.5
2.5	5	3.0	4.0
2.5	3.5	2.1	2.8

Table 3.1: Daily data acquisition and required bandwidth in the ad hoc pair of satellite configuration for transmitting to a single station with 10 minutes of ground visibility 10 times a day. Compression is 12 bits / value (no compression) or 5 bits / value (similar to S2) or 3.5 bits / value (average compression rate foreseen on CO3D with the fixed quality compression algorithm).

Coverage	All emerged lands
Field of view	70.4 km
Altitude	770 km
Ground Sampling Distance	1m - 2.5m
MTF at Nyquist frequency	≤ 0.1 for all bands (low aliasing)
B/H between stereo detectors	≤ 0.1, the higher the better
Signal to noise ratio (SNR)	50 - 70 at L_{min}
L_{sat}	320 W/m²/sr/µm for all bands
B2 (blue)	492 nm, (bw=66 nm), L_{min} = 50 W/m²/sr/µm
B3 (green)	560 nm, (bw=36 nm), L_{min} = 30 W/m²/sr/µm
B4 (red)	665 nm, (bw=31nm), L_{min} = 20 W/m²/sr/µm
B8 (Near Infra-Red)	832 nm, (bw=106 nm), L_{min} = 30 W/m²/sr/µm

Table 3.2: Recap of specifications used for the instrumental design.

Resolution (m)	Size for B1 (cm)	Size for B1 (cm)	Size for B3 (cm)	Size for B4 (cm)
1	27.5	31.9	37.4	47.3
2	12.5	15	17.5	21.25
2.5	10	12	14	17

Table 3.3: Pupil size imposed by the different spectral bands and ground sampling distance hypotheses for a push-broom instrument.

GSD (m)	Size for B1 (cm)	Size for B2 (cm)	Size for B3 (cm)	Size for B4 (cm)
1	34.1	38.5	46.2	57.2
2	16.25	17.5	21.25	26.25
2.5	13	14	17	21

Table 3.4: Pupil size imposed by the different spectral bands and ground sampling distance hypotheses for a push-frame instrument.

Table 3.5 gives the number of electrons to store in a single pixel in order to achieve the target signal to noise ratio. In the push-broom case, those numbers impose a minimal pixel size of 7 to 8 µm. Because there is no transfer of electrons between views in the push-frame case, we can adjust the signal to noise ratio by the number of views, which allows for smaller pixels of 3.5 µm.

SNR	B1 (ke)	B2 (ke)	B3 (ke)	B4 (ke)
50	17	28	42	28
70	32	54	80	54

Table 3.5: Number of electrons required to achieve the target SNR

By considering a BSI Teledyne quantum efficiency and an optical transmission of 85%, we can derive the number of TDI stages (in the push-broom case) or the number of views (in the push-frame case) required to achieve the target SNR at different resolutions, as presented in table 3.6.

In push-broom configuration, multi-TDI detectors are not available off the shelf, but a 4 bands detector with 16 to 64 stages, 12 000 pixels of around 7 µm should not present feasibility issues.

In push-frame configuration, we therefore have to ensure a minimum of about 5x9 readings of images during matrix overpass. We therefore need a matrix detector that is fast enough. Possible options (with limitations) are:

- Sony IMX411 (10 000 x 15 000 pixels, 6 fps - CO3D), not fast enough
- IMX253 (3 000 x 4 000, 60 fps, certified by CNES in 3D PLUS project), will not allow a GSD better than 2m for a SNR of 50.

GSD (m)	SNR	B1		B2		B3		B4	
		stages	views	stages	views	stages	views	stages	views
1	50	9	6	21	14	32	22	8	6
1	70	16	11	41	28	63	43	16	11
2	50	5	4	12	8	18	12	6	4
2	70	10	7	26	15	34	23	10	7
2.5	50	4	3	9	6	13	9	4	3
2.5	70	7	5	17	11	26	17	7	5

Table 3.6: Estimated number of TDI stages (in push-broom case) or views (in push-frame case) for target SNR and resolutions

Regarding optical design two solutions have been considered: a single camera to cover the whole field of view (6.5°) or two cameras covering half of the field of view each (3.3°). Main optical parameters are presented in table 3.7 for push-broom case and 3.8 for push-frame case. In all cases, focal length and mirror diameter are large and will require a combination of mirrors. In the push-broom case, Image field is high with respect to the pupil diameter, which can make the optics more complex.

Stereo-acquisition can be implemented either within a single instrument field, or with two separate instruments pointing in different directions. In the case of a single instrument field, there are two different cases:

FoV	GSD (m)	Focal length (m)	Diameter (m)	Image field (m)	aperture
6.5	1	4.9	0.43	0.56	11.4
	2.5	1.96	0.17	0.22	
3.3	1	4.9	0.43	0.28	11.4
	2.5	1.96	0.17	0.11	

Table 3.7: Optical parameters of the push-broom configuration, with a single camera or two camera spanning the field of view.

FoV	GSD (m)	Focal length (m)	Diameter (m)	Image field (m)	aperture
6.5	1	2.45	0.52	0.28	4.7
	2.5	0.98	0.21	0.11	
3.3	1	2.45	0.52	0.14	4.7
	2.5	0.98	0.21	0.055	

Table 3.8: Optical parameters of the push-frame configuration, with a single camera or two camera spanning the field of view.

- If field of view is equivalent to B/H, the instrument field needs to be a square, with same constraints across-track and along-track. That would mean a B/H of 0.057 for swath of 40 kilometers and 0.114 for a swath of 80 kilometers. This imposes heavy optical constraints.
- If B/H is smaller than the field of view, then the instrument will be rectangular and oriented across-track. A ratio of 1/3 seems reachable, which means a maximal B/H of 0.019 for a field of view of 40 kilometers and 0.038 for 80 kilometers.

Table 3.9 presents the total field of view (diameter of a circular field of view including across track and along track constraints) required by the single instrument configuration depending on field of view (half or full field of view) and target B/H values. Those values heavily limit the possible optical configurations. The double instrument configuration is less constrained and enable higher B/H, at the expense of instrument volume and cost. It should be noted that in terms of stereo-restitution performances, and for such small B/H values, higher values will be preferred.

	B/H = 0.025	B/H = 0.035	B/H = 0.1
Swath = 40 km	3.6°	3.8°	6.6°
Swath = 80 km	6.7°	6.8°	8.6°

Table 3.9: Total field of view needed with respect to B/H and swath. The total field of view corresponds to the diameter of a circular field of view including across track and along track constraints.

With those figures in mind we were able to derive 4 instrumental design for Sentinel-HR, depending on push-broom or push-frame configuration on one hand, and stereoscopic or monoscopic instrument on the other hand. Those designs are presented in table 3.10.

Design **(stereo-pb)** requires 2 or 3 cameras to build the full swath. It is noteworthy that a single detector of 12 000 pixels is sufficient for each camera at 2.5m resolution. This design

is strongly limited in B/H values, which will be small. Design **(stereo-pf)** is the only one that requires a single camera. It also allows for slightly higher B/H values. Designs **(mono-pb)** and **(mono-pf)** both require two cameras for stereoscopy. They are less limited than the stereoscopic designs in terms of resolution and imposes no constraints on B/H value, which is implemented by the angle between both cameras. This comes at the expanse of a larger volume of each camera. In any design, bringing resolution down to 2 meters would imply increasing camera dimensions by roughly 30% in each dimension. It is also important to add that these different optical concepts have very different telecentricities (the TMA being the best choice) which is important for spectral response uniformity.

Design	(stereo-pb)	(stereo-pf)	(mono-pb)	(mono-pf)
	Stereoscopic Push-broom	Sterescopic Push-frame	Monoscopic Push-broom	Monoscopic Push-frame
Telescope	Korsh	Newton	TMA	TMA
Resolution (m)	>2.5	>2.5	< 2.5	< 2.5
Detectors size (µm)	7	3.5	7	3.5
Swath (km)	30	> 60	80	80
B/H	<0.03	>0.03	No constraints	No constraints
Volume per inst. (mm^3)	300x500x800	350xx500x1200	500x600x1500	500x700x1000
Estimated mass per inst. (kg)	21	37	80	62
Number of cameras	2 to 3 (field)	1	2 (stereo)	2 (stereo)

Table 3.10: Overview of possible instrumental designs for Sentinel-HR. Mass is roughly estimated by extrapolating density of CO3D instrument (610x900x850 mm^3 for 83 kg).

3.1.5 Estimation of 3D restitution accuracy

1. Origins of the Sentinel-HR stereo capability

   The idea of giving Sentinel-HR native stereo-capabilities originally comes from the Venµs experience [FCD+10, DHK+18]. Venµs is a franco-israeli earth observation mission that provides very high revisit of 2 to 3 days, at 5 meters resolution, over a selection of 123 sites around the world with a constant viewing angle. Swath is approximately 26 km and detectors are composed of 5200 pixels. It includes 11 spectral bands ranging from visible to near infra-red (420 nm to 910 nm). In addition, the 600 nm - 650 nm spectral band is doubled by a 12th detector, forming a stereo baseline of 0.025. While originally designed to ease cloud detection by estimating their apparent movement between the two redundant band, [ARN19] demonstrated that Digital Surface Model could be generated by stereo-restitution using the redundant detector, after careful correction of the satellite attitude jitter. They demonstrated that Venµs could be used to generate 100 meters resolution DSM with an accuracy of 8 meters RMSE (measured with respect to SRTM), despite of the very narrow stereo angle. When the Sentinel-HR concept emerged, it has been proposed to apply the same design in order to give Sentinel-HR the same capabilities. With the same stereo angle, and assuming that attitude jitter can be managed in a similar way, we could foresee an accuracy of 3.2 meters RMSE for a DSM resolution of 40 meters. Moreover, in this study, DSM was obtained by striding the correlation process, and not by averaging a full resolution DSM obtained with a stride

of 1 pixel. We can therefore infer that those figures would still be valid to some extent for higher, closer to native resolution.

2. Assessing performances of the low-baseline Sentinel-HR configuration

   As we can see in section 3.1.4, and particularly in table 3.10, among the proposed designs, only the native stereoscopic instruments **(stereo-pb)** and **(stereo-pf)** are limited in terms of stereoscopic baseline ratio. The other designs imply two separate instruments for which the angle can be chosen without any heavy constraints. In the case of stereoscopic instruments, the stereo baseline ratio has been estimated to not exceed 0.035.

   In order to consolidate the DSM accuracy estimates in that configuration (resolution and baseline ratio), we used an in-house image simulation tools that can generate aliasing-free satellite views from geo-referenced textured 3D meshes. Simulations were made from three different off-the-shelf meshes, for 3 sites in France: Nanterre, with a dense urban landscape, Canari (in Corsica) a semi-natural landscape with shore and cliffs, and Argentière glacier, a glacier landscape. Acquisition parameters (see table 3.11) were close to the one presented in this chapter, with some small discrepancies due to the concurrent work (refined orbital and detectors parameters were not fully available at beginning of the study). From this raw simulation quantified on 12 bits, images were further processed with MTF blurring and realistic noise in order to recreate the effects of the image acquisition chain of Sentinel-HR. In order to separate the effects of the very narrow stereoscopic angle, the exact same simulations were then generated with a baseline ratio of 0.2, which is typical of single-track stereoscopic acquisitions with VHR satellites. Finally, the simulation tool also allows to generate a perfect DSM ground-truth.

   From the simulated images, stereo-reconstruction was achieved using CARS [SAM+16], the open-source processing chain developed by CNES in the frame of the CO3D mission. In CARS, disparity estimation is achieved using Pandora, an open-source disparity estimation library also developped by CNES in the frame of C03D mission [CSD+20]. As SGM with census cost, the default disparity estimation method used by CARS, is not well suited for very small baseline ratios, Pandora has been further configured to use Zero-Mean Normalized Cross Correlation instead, similar to what has been used form Venμs DSM. Subpixel disparity was achieved by using subpixel steps of 1/4th of pixels, with quadratic refinements of the correlation peak. The size of the correlation windows has been set to 11 pixels (TODO: check with Jonathan). Quality of generated DSMs was then assessed using CNES open-source tool DEMCompare, allowing to derive a large range of quality metrics using the simulated ground-truth as reference.

Altitude	700 km
Resolution	2 meters
Pixel size	10 µm
Pixel acquisition duration	2.95762e-4 s
B/H north to south	[-0.0175, 0.0175]

Table 3.11: Parameters for simulation of Sentinel-HR stereoscopic acquisition from 3D textured meshes

Note that the baseline ratio of 0.035 leads to a conversion coefficient of 59 meters between disparity and elevation (1 pixel of disparity corresponds to 59 meters). Therefore, in order to achieve 4m CE90 absolute accuracy, the collocation error, including geometric accuracy and disparity estimation process, should not exceed 0.068 pixels, or 0.14 meters. It is needless to say that this is very challenging, both in terms of of geometric accuracy and disparity map estimation algorithms.

3. Experiments on Nanterre site

   First simulation is the Nanterre site, an urban area located near Paris in France. Simulated DSM are presented in figure 3.7. We can see that the narrower baseline yields a noisier DSM, whith a lot of missing data. Important larger buildings and urban fabric can still be distinguished, but with very distorted shapes.

   Performances metrics are displayed in table 3.12 (for 0.035 baseline ratio) and 3.13 (for 0.2 baseline ratio). One can observe that the smaller baseline ratio achieves an absolute reconstruction error of 5.38 meters for 90% of values, all slopes considered. Meanwhile, the 0.2 baseline ratio configuration achieves 2.98 meters absolute accuracy for 90% of values.

Slope	Max	Min	Mean	Std	RMSE	Median	NMAD	CE90
All	12.79	-11.04	0.96	3.19	3.33	0.92	2.84	5.38
0% - 5%	12.75	-11.02	0.98	3.12	3.27	0.88	2.82	5.17
5% - 10%	12.78	-11.02	1.03	2.92	3.09	0.97	2.66	4.79
10% - 25%	12.78	-11.03	1.07	2.89	3.08	1.01	2.62	4.72
25% - 45%	12.77	-11.03	0.96	2.97	3.13	0.92	2.69	4.91
45% - inf	12.79	-11.04	0.80	3.71	3.79	0.81	3.30	6.80

Table 3.12: Performances of stereo-reconstruction of Nanterre site with radiometric simulation, with a B/H of 0.035

Slope	Max	Min	Mean	Std	RMSE	Median	NMAD	CE90
All	9.79	-10.51	-0.23	1.86	1.88	-0.16	1.10	2.98
0% - 5%	9.78	-10.51	-0.23	1.25	1.27	-0.17	0.81	1.76
5% - 10%	9.76	-10.50	-0.28	1.25	1.28	-0.21	0.80	1.73
10% - 25%	9.79	-10.49	-0.26	1.43	1.45	-0.19	0.94	2.09
25% - 45%	9.76	-10.51	-0.17	1.72	1.73	-0.10	1.23	2.62
45% - inf	9.79	-10.51	-0.22	2.77	2.78	-0.08	2.05	5.42

Table 3.13: Performances of stereo-reconstruction of Nanterre site with radiometric simulation, with a B/H of 0.2

4. Experiments on Canari quary site

   The second simulation is on a quary site near Canari, in Corsica, France. This site has a semi-natural shoreline landscape, with a quary in its center. Simulated DSM are presented in figure 3.8. We can see that while the 0.2 baseline ratio still allow to dinstiguish the quary site as well as the building near the shoreline, this is no longer true for the 0.035 baseline ratio, because of higher noise and missing values. The general structure of the landscape remains visible though.

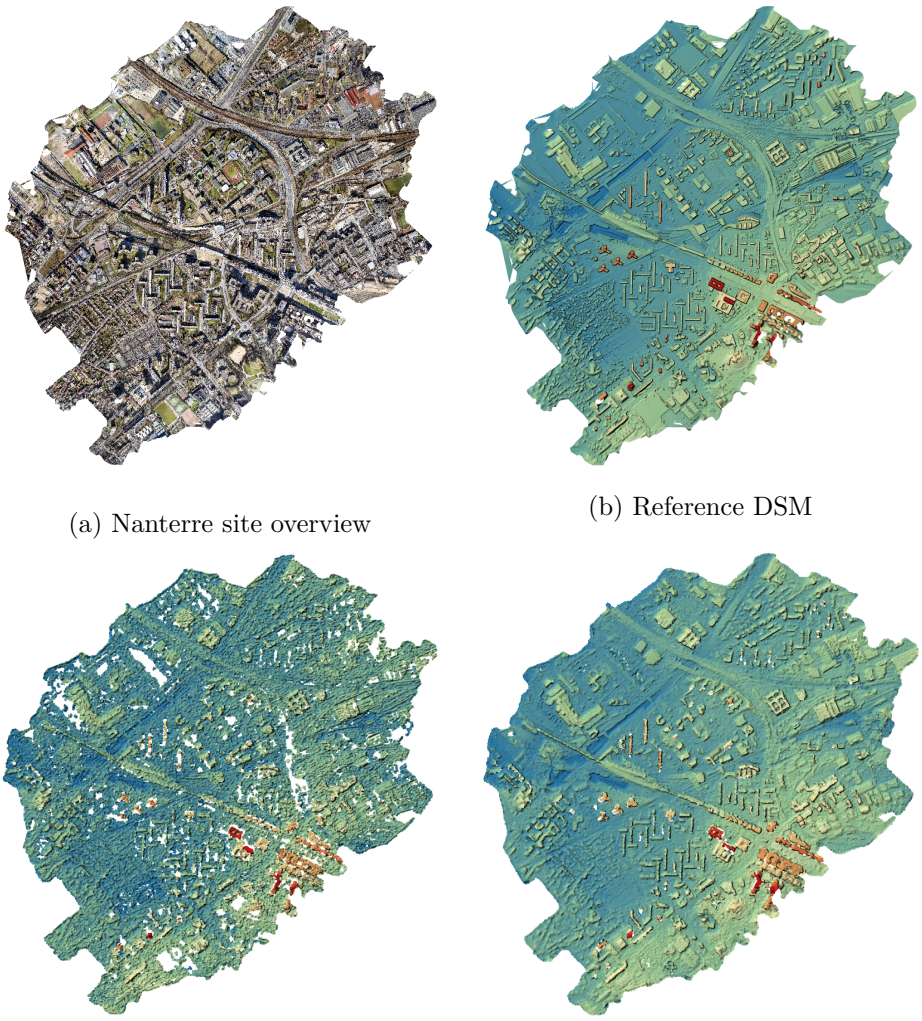

(a) Nanterre site overview

(b) Reference DSM

(c) b/h=0.035

(d) b/h=0.2

Figure 3.7: DSM reconstructed by CARS for the different configuration of baseline ratio for Nanterre site

Performances metrics are displayed in table 3.14 (for 0.035 baseline ratio) and 3.15 (for 0.2 baseline ratio). Conclusions are similar to those of the Nanterre site, with a CE90 performance of 4.6 meters for the 0.035 baseline ratio, and 2.17 meters for the 0.2 ratio.

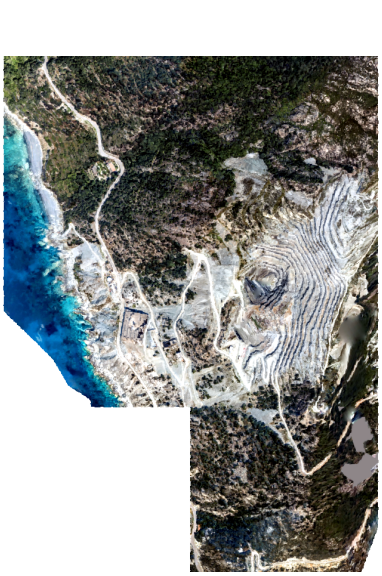

(a) Reference DSM

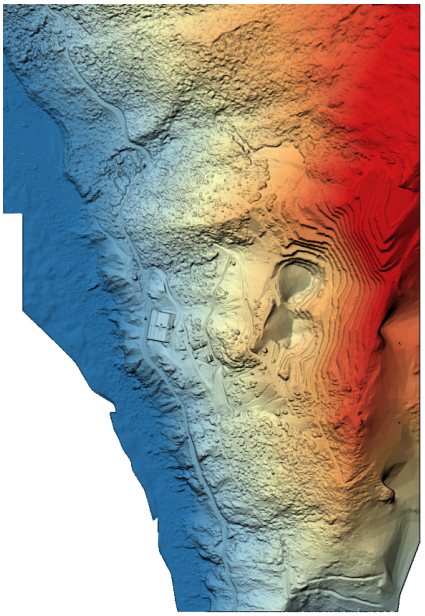

(b) Reference DSM

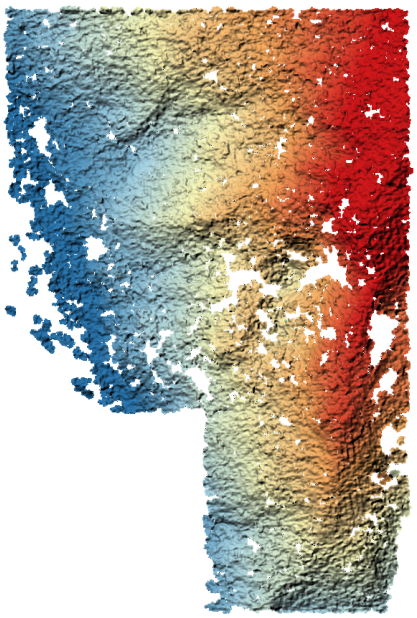

(c) b/h=0.035

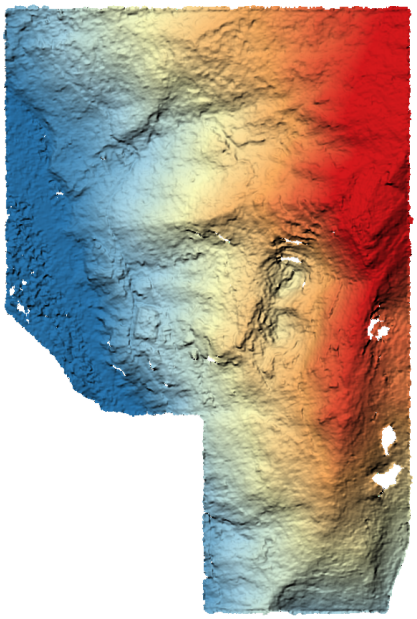

(d) b/h=0.2

Figure 3.8: DSM reconstructed by CARS for the different configuration of baseline ratio for Canari quary site

5. Experiments on Canari village site

   The third simulation is on a village near Canari, in Corsica, France. This site has a

Slope	Max	Min	Mean	Std	RMSE	Median	NMAD	CE90
All	10.87	-11.45	-0.16	2.79	2.79	-0.12	2.54	4.60
0% - 5%	10.52	-11.20	-1.08	3.23	3.40	-0.94	2.98	5.37
5% - 10%	10.64	-11.41	-1.10	3.26	3.44	-0.97	3.00	5.47
10% - 25%	10.58	-11.37	-0.43	3.02	3.05	-0.33	2.73	5.05
25% - 45%	10.85	-11.45	0.02	2.71	2.71	0.07	2.52	4.43
45% - inf	10.87	-11.45	-0.08	2.71	2.72	-0.07	2.48	4.48

Table 3.14: Performances of stereo-reconstruction of Canari quary site with radiometric simulation, with a B/H of 0.035

Slope	Max	Min	Mean	Std	RMSE	Median	NMAD	CE90
All	5.28	-5.05	0.17	1.29	1.30	0.14	1.03	2.17
0% - 5%	5.22	-5.03	0.14	1.20	1.21	0.12	0.93	2.01
5% - 10%	5.26	-5.00	0.17	1.29	1.30	0.14	1.00	2.20
10% - 25%	5.27	-5.05	0.18	1.29	1.30	0.20	1.03	2.17
25% - 45%	5.25	-5.04	0.22	1.13	1.15	0.19	0.93	1.83
45% - inf	5.28	-5.05	0.16	1.33	1.34	0.12	1.07	2.27

Table 3.15: Performances of stereo-reconstruction of Canari quary site with radiometric simulation, with a B/H of 0.2

semi-natural urban landscape, with buildings loosely spread across the scene. Simulated DSM are presented in figure 3.9. We can see that buildings can still be distinguished with the 0.2 baseline ratio, which is no longer true for the 0.035 baseline ratio. Only the general structure of the landscape remains visible.

Performances metrics are displayed in table 3.16 (for 0.035 baseline ratio) and 3.17 (for 0.2 baseline ratio). Conclusions are similar to those of the two other sites, with a CE90 performance of 4.53 meters for the 0.035 baseline ratio, and 3.22 meters for the 0.2 ratio.

Slope	Max	Min	Mean	Std	RMSE	Median	NMAD	CE90
All	9.00	-8.28	0.34	2.67	2.70	0.23	2.53	4.53
0% - 5%	8.61	-8.27	-0.65	2.48	2.56	-0.61	2.38	4.23
5% - 10%	8.85	-8.19	-0.35	2.43	2.45	-0.35	2.25	4.06
10% - 25%	8.96	-8.28	-0.20	2.41	2.42	-0.23	2.26	4.02
25% - 45%	9.00	-8.28	0.04	2.49	2.49	-0.03	2.33	4.16
45% - inf	9.00	-8.28	0.75	2.80	2.90	0.65	2.69	4.78

Table 3.16: Performances of stereo-reconstruction of Canari village site with radiometric simulation, with a B/H of 0.035

6. Conclusions and limitations

   If the performances for the 0.035 ratio are higher, but quite close to the specification of 4 meters absolute accuracy CE90, we must stress that those performances are obtained with a perfect known geometry: line of sights are perfectly known, without noise or distortion. In [ARN19], we can see that noise in attitude restitution impaired greatly

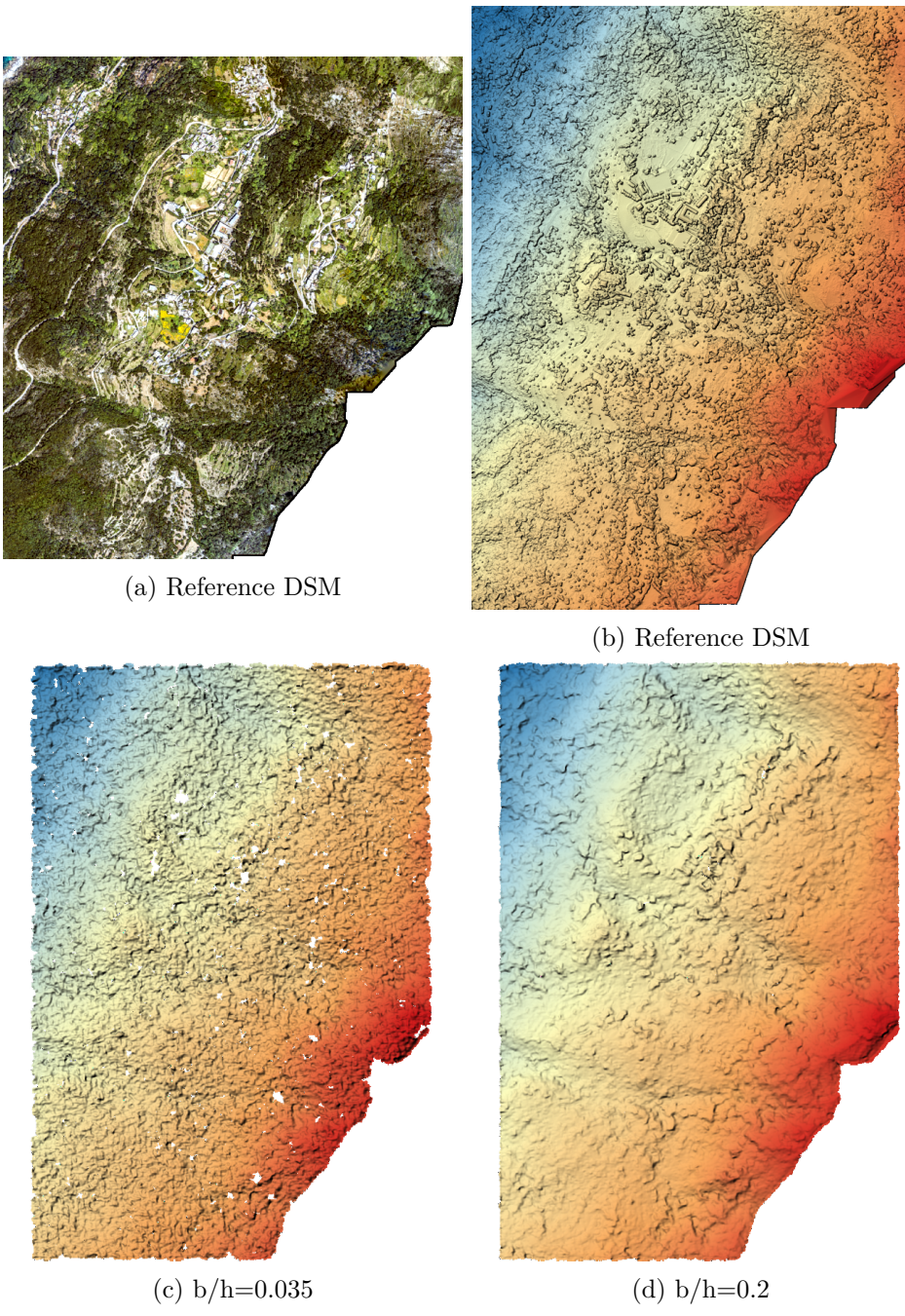

(a) Reference DSM

(b) Reference DSM

(c) b/h=0.035

(d) b/h=0.2

Figure 3.9: DSM reconstructed by CARS for the different configuration of baseline ratio for Canari village site.

Slope	Max	Min	Mean	Std	RMSE	Median	NMAD	CE90
All	6.97	-5.27	0.79	1.81	1.98	0.54	1.44	3.22
0% - 5%	6.78	-5.03	0.20	1.20	1.22	0.16	0.94	1.90
5% - 10%	6.94	-5.25	0.25	1.23	1.26	0.19	0.92	1.88
10% - 25%	6.97	-5.23	0.33	1.33	1.37	0.22	1.00	2.08
25% - 45%	6.97	-5.27	0.53	1.52	1.61	0.37	1.18	2.52
45% - inf	6.97	-5.26	1.12	2.04	2.33	0.90	1.83	3.71

Table 3.17: Performances of stereo-reconstruction of Canari village site with radiometric simulation, with a B/H of 0.2

the reconstruction capabilities for Venμs, and that complex registration and correction strategies had to be designed in order to be able to reach acceptable performances. The CO3D team estimates that geometric errors (which are not modelled in this study) account for up to 2/3 of the total DSM error budget.

3.1.6 Conclusions

We can conclude that the 0.035 baseline configuration will not allow to reach the 4 meters CE90 accuracy, and that this target will be missed by a large amount. This most probably eliminates configurations **(stereo-pf)** and **(stereo-pb)** from the possible designs. Among those two configurations, there is an off the shelf matrix of detectors that has been certified by CNES, which leans toward the **(stereo-pf)** configuration. The parameters of this final design are shown in table 3.18.

	Monoscopic Push-frame
Telescope	TMA
Altitude	794 km
Aperture	10.7
Pupil diameter	26 cm
Focal length	1.39 m
Resolution	2m
Detector size	3.5 μm
Field of view	70 km, 5°, 35e3 pixels
B/H	No constraints
Volume	650x1170x1300 mm^3 ×2
Mass	≈ 150 kg ×2
Number of cameras	2 (stereo)

Table 3.18: Main parameters for final design choice. Mass is roughly estimated by extrapolating density of CO3D instrument (610x900x850 mm^3 for 83 kg).

3.2 Solution based on CO3D constellation extension

After discussions with the CO3D development team, it appears that Sentinel-HR mission can be implemented by extending the CO3D constellation with some modifications on the satellite, leading to a cost effective alternative solution to the design and build of ad-hoc satellites and ground segment.

3.2.1 Required modifications

First modification consist in selecting an orbit with a 40 days revisit cycle with (N,P,Q)=(14,3,40) at an altitude of 845 kilometers (this implies to have 2 pairs of satellites to reach the 20 days revisit). With target resolution of 2 meters, the focal length of the instrument needs to be reduced from 3.77 meters to 1.58 meters, which leads to a footprint of 28.5x21.3 km² (lxh). In order to have a constant along track viewing angle as required by Sentinel-HR specification, the satellite will need to perform a maneuver between each step, which can be achieved in 2.7 seconds and can be achieved with current CO3D specifications (currently 1 second).

2 pairs of CO3D satellites flying in this configuration will provide a swath of 28.5 km and a revisit of 20 days, with the along track stereo acquisition capability and a wide range of possible B/H (which will be mainly limited by the maximum along track viewing angle that can be tolerated). This will generate an inter-swath of 71 kilometers at equator, which can be filled by using 4 extra pairs of CO3D satellites.

For storage, transmission and resources limitation, it is likely that a single pair will not be able to acquire the full orbit. Therefore, it might be necessary to double the number of satellites in order to acquire the full orbit. This lead to a maximum number of 24 CO3D adapted satellites to implement Sentinel-HR mission.

However, a 12 satellites solution may still be reachable, with the following optimisations:

- Relax the focal plane stability constraint after 30 minutes of activity. This would lead to extra errors on relative altimetry performances (order of magnitudes tenth of centimeters) but could be manageable for a target accuracy of 3 meters
- Take into account emerged lands and meteorological predictions to avoid acquisition of cloudy images.

Additionally, we could further reduce the number of satellites by increasing the revisit time for 3D reconstruction to 40 days, while keeping revisit time for 2D to 20 days. In that case we could maybe get down to 9 satellites.

It should be noted that:

- 3D performances are expected to be far better with this configuration than with the ad-hoc configuration because traditional B/H can be achieved (typically 0.1 - 0.3) instead of native low B/H of the ad-hoc solution. By extrapolating CO3D performances and with all errors included, the system would be able to reach 4m CE90 relative accuracy.
- Radiometric performances will be poorer with the current bayer-based CO3D matrix than with an ad-hoc satellite. Expected performances have not been studied, but standard RGB filters suffer from rejection and NIR filter can exhibit variations of up to 2.5 nm accross the field of view. In the frame of an evolution of the CO3D satellite, it might be possible to replace the Bayer matrix by ad-hoc filters on separated matrix (push-frame).

3.2.2 Telemetry

With respect to the daily acquired data estimated in section 3.1.3, The daily amount of data for the CO3D based configuration is presented in table 3.19. We can see that with the CO3D compression algorithm, expected bandwidth is similar to what is achieved on current CO3D with 2 transmitters using 2 different X band polarisation (1.1Gbps). No modifications of telemetry equipment will therefore be required.

GSD (m)	compression (bits/pixel)	Daily acquisition (TB)	Bandwidth (Gbps)
2	5.5	0.3	0.4

Table 3.19: Daily data acquisition and required bandwidth in the CO3D configuration for transmitting to a single station with 10 minutes of ground visibility 10 times a day. Compression rate of 5.5 bbp for all bands is current CO3D rate.

Chapter 4

Hybrid products methodology

This chapter studies how users might benefit from the availability of Sentinel-HR and Sentinel2 to get frequent time series at a very high resolution. It compares different spatio-temporal fusion methods using a benchmark based on VENµS data.

4.1 Problem statement

Accounting for occurrences of clouds in acquisitions, clear pixel availability for Sentinel-HR will be lower than the 20 days theoretical revisit time. In [STAL20], an analysis is performed for the full Sentinel2 archive over year 2017. Figure 4.1 shows a map of the average Sentinel2 cloud cover estimated from product metadata derived by the authors. One can see that a vast amount of the Sentinel-HR target landmass exhibit an average cloud cover higher than 60%. Figure 4.2 presents the percentage of scenes that are contaminated by clouds (cloud coverage higher than 10%). Again, one can see that a large part of the landmass has more than 70% of Sentinel2 scenes contaminated by clouds. With a revisit time of 20 days, their would be around 18 Sentinel-HR acquisition dates over a year for a given location (note that this number may increase with latitude). If 70% of them are contaminated by clouds, this leaves only 5 clear dates a year. Regions of the globe with stable high cloud coverage, such as Himalayas, tropical regions of Africa or South America will have even lower occurrences of cloud free scenes. Moreover, cloud cover is bound to seasonal effects and are therefore not independent, which means that the clear dates will probably not be well distributed across the year. Note that the 10% cloud threshold used to mark Sentinel2 scenes as cloudy is very conservative, which means that most of those cloudy images will still have a large amount of clear pixels that can be used.

It should also be noted that some of the Sentinel-HR use cases presented in chapter 2 require a better revisit time that the 20 days that the mission will offer, while still requiring the High Resolution that lacks in Sentinel2 data.

The classical approach to filling cloud gaps as well as re-sampling time series on a regular grid relies on temporal interpolation of spectral profiles [LAC17]. On the other hand, the continuity of services guaranteed by ESA on the Sentinel programs ensures that during the Sentinel-HR lifetime, Sentinel2 data (5 days revisit time, max. 10 meters resolution) or Sentinel2 NG data (foreseen 3 days revisit time, 5 meter resolution) will be continuously and consistently available. This means that in-between Sentinel-HR clear dates, there might be one or several lower resolution clear dates of similar spectral bands, with a resolution

5 times coarser at most. We can therefore investigate whether those coarser, more frequent observations can be used in order to better interpolate gaps between Sentinel-HR observations, whether caused by clouds or limited revisit time.

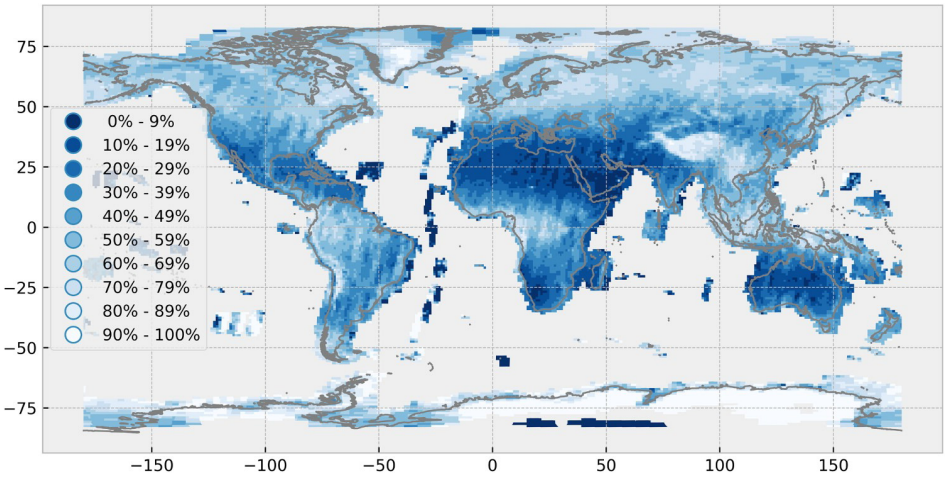

Figure 4.1: Global spatial distribution of the average cloud cover of Sentinel-2A and Sentinel-2B Level-1C scenes acquired in the year 2017 (from [STAL20])

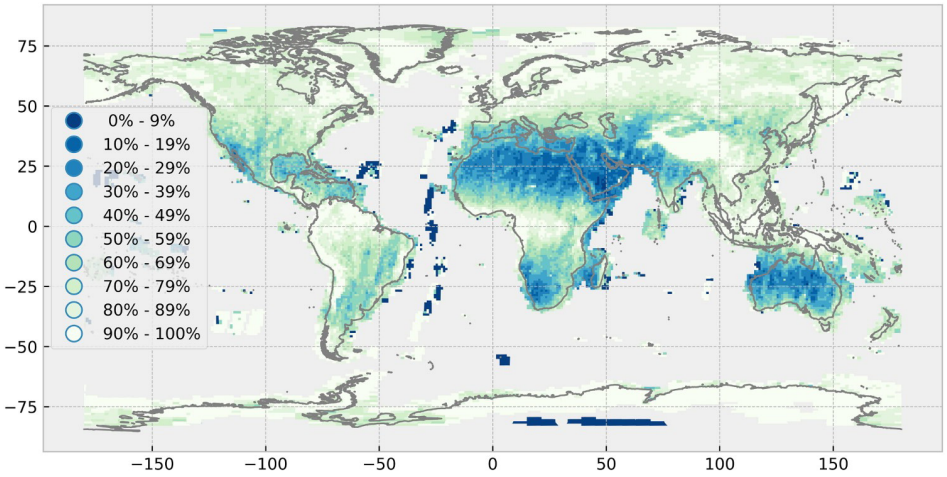

Figure 4.2: Global cloudiness for 2017. Percentages indicate the fraction of cloud-contaminated Sentinel-2A and 2B Level-1C scenes. 0% means that all scenes are cloud-free and 100% means that all scenes are cloud-contaminated. It does not refer to the amount of clouds within the scenes (cloudiness threshold is 10%) (from [STAL20])

In this chapter, we will try to assess whether hybrid surface reflectance products can be derived from the combination of envisioned Sentinel-HR data and available Sentinel2 (NG) data, in order to (a) lower the revisit time below 20 days for applications where both revisit time and spatial resolution are critical and (b) mitigate gaps caused by the occurrence of clouds in Sentinel-HR acquisitions. Higher order information fusion, e.g. indicators derived separately on the two time series and fused later, is out of the scope of the study since it requires domain-specific knowledge. Nonetheless, it must be stressed that such approaches

might be more pertinent than pursuing estimation of surface reflectances.

4.2 Available data

In order to assess our ability to produce synthetic time-series providing the spatial resolution of Sentinel-HR with the revisit of Sentinel2 (NG), we need to gather time-series with:

- Near nadir 2 meter resolution images every approx. 20 days,
- Intermediate Sentinel2 images at 10 meters
- For each intermediate Sentinel2 image, a nadir image at 2 meters of the same day to serve as the reference for quantitative evaluation.

Those time-series would have to be available over various landscapes and regions of the earth. We looked into commercial VHR data to fulfill these specifications at the desired resolution, but we did not find reasonably long time series that could provide both the 20 days revisit and the additional reference dates. Moreover, series we looked into had various viewing angle and lacked of atmospheric parameters for a proper surface reflectance estimation.

Band	Sentinel2	Venus
Blue	B2 (492 ± 33 nm)	B3 (490 ± 20 nm)
Green	B3 (560 ± 18 nm)	B4 (555 ± 20 nm)
Red	B4 (665 ± 15 nm)	B7 (772 ± 16 nm)
NIR	B8 (833 ± 53 nm)	B11 (865 ± 20 nm)

Table 4.1: Corresponding spectral bands between SentineL2 and Venμs

We therefore looked into the Venμs mission [FCD+10, DHK+18], that provides a spatial resolution of only 5 meters, and a very small swath covering a selection of around 100 sites around the world, but has several advantages for our study:

- Venμs has a nominal revisit of 2 to 3 days with constant viewing angles (though not necessarily nadir), with a mission overlap of several years with Sentinel2.
- Venμs has almost the same Red, Green and Blue spectral bands than Sentinel2 as shown in table 4.1 (The NIR band is a bit more narrow on Venμs)
- Venμs and Sentinel2 L2A products distributed by Theia are processed by the exact same L2A processor [LDH+16]. They both benefit from excellent cloud masking and atmospheric corrections, and are therfore very coherent.

  We therefore chose to gather joint Venμs and Sentinel2 time-series from Theia archive according to the following methodology.

4.2.1 Data selection

In order to collect the time-series, we performed the following search on Theia archive, for each Venμs site:

1. Find all Venμs subseries with a revisit time between 15 and 30 days and more than 7 dates, without any cloud coverage threshold. We call this series the **guide images** (this is necessary because the VENμS misison has sometimes suffered from interruptions due to technical reasons),

2. For each subseries from previous step, find all intermediate Sentinel2 images from the tile and relative orbit with highest coverage of the Venμs site, without any cloud coverage threshold,

3. For each selected Sentinel2 image, look for a corresponding Venμs image acquired within 1 day. Discard Sentinel2 images for which no Venμs image could be found. We call the Sentinel2 series the **target images** and the corresponding Venμs series the **reference images**.

From the retrieved time series, we made a selection based on landscape variety, viewing angle, and length of the time-series, and kept the 5 series presented in table 4.2. An overview of the time sampling and clear pixel coverage of all series is given in figure 4.3.

Site Name	Location	Landscape	Guide	Target	Time range
MAD-AMBO	Madagascar	Desert	17	39	2018.11 - 2020.01
FR-LQ1	France	Mixed	9	27	2020.04 - 2020.10
FR-BIL	France	Agri., urban	12	16	2020.03 - 2020.11
ARM	USA	Agri.	16	23	2019.03 - 2020.01
ESGISB-2	France	Agri., urban	10	14	2018.11 - 2019.05

Table 4.2: Main parameters for selected time series

4.2.2 Data pre-processing

With the images from the selected time-series, we applied the following pre-processing:

1. Extract the corresponding spectral bands for Venμs and Sentinel2 according to table 4.1, on a region of interest of 2000x2000 Venμs 5 meters pixels

2. For each image, extract a global missing data mask, including not acquired, cloudy, and saturated pixels,

3. Perform linear-regression to further align Sentinel2 bands to Venμs bands and reduce the slight discrepancies that may occur dues to differences in spectral bandwidths and atmospheric corrections [MI21]

4. While Venμs time-series are rather well registered, localisation errors of up to 2 pixels can occur with Sentinel2 time-series. In order to correct those shifts, a registration based on SIFT points similar to what is done in the pre-processing of CARS [CSD+20] is performed on each Sentinel2 image to register it to its Venμs reference image

5. Because our highest resolution is 5 meters instead of the 2 meters foreseen for Sentinel-HR, we further downscale the Sentinel2 image to 25 meters in order to get a resolution ratio of 5 (Sentinel2 case) and to 12.5 meters in order to get a resolution ratio of 2.5

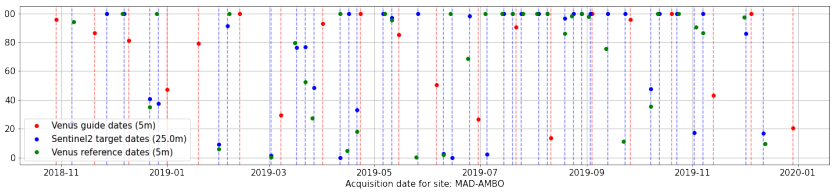

(a) MAD-AMBO time series

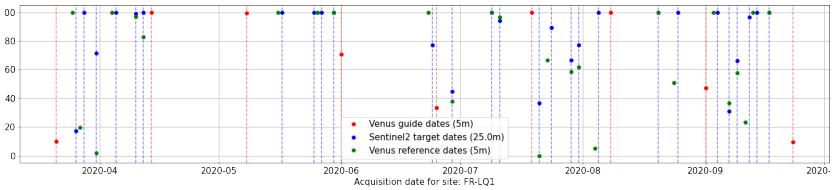

(b) FR-LQ1 time series

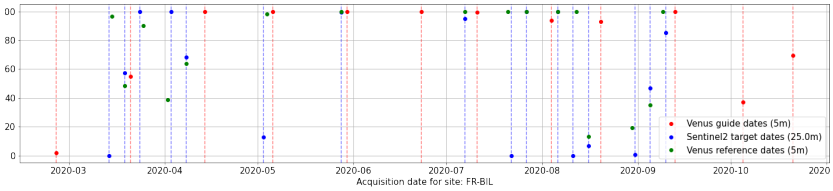

(c) FR-BIL time series

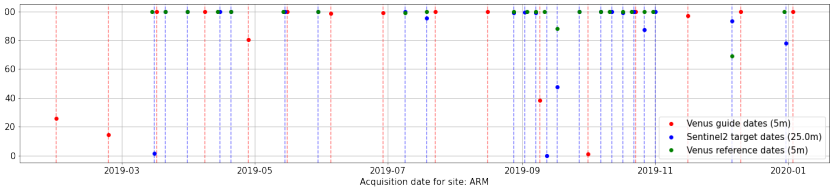

(d) ARM time series

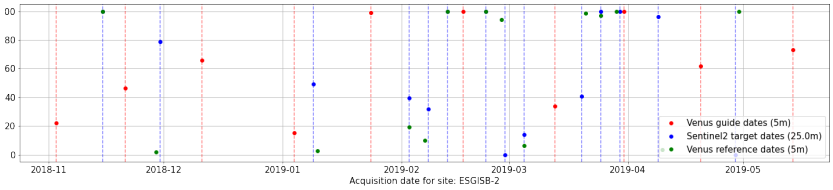

Figure 4.3: ESGISB-2 time series

Figure 4.4: Temporal sampling and respective clear pixels coverage of guide, target, and reference time-series for each selected site.

(Sentinel2 NG case). Down-sampling is made by convolving the image with a gaussian kernel corresponding to a MTF cut-off of 0.1, and then re-sampling to nearest neighbors.

This process yields ready to use tensors for guide, target and reference images time-series, along with their missing values masks. Figures **??** to 5.5, pages **??** to 160 of the Appendices section shows an overview of the final time-series.

4.3 Methods

Our problem can be reformulated as follows: given our guide high resolution time-series and intermediate target coarse resolution time-series, make the best possible prediction of the high resolution that would have been observed at the coarse resolution dates. Performances will be evaluated with respect to the reference time-series.

In this study, we decided to take a step back from the Spatio-Temporal fusion literature, which is mostly focused on Landsat and Modis combination, and also include other methods such as naive solutions, Single Image Super-Resolution or Guided Super-Resolution.

4.3.1 Naive solutions

We have two natural naive solutions that we can immediately think of:

Temporal interpolation of high resolution guide series If we ignore completely the coarse resolution target series, we can simply temporally interpolate the guide series at the target dates, with a linear or cubic interpolation.

Spatial interpolation of coarse resolution target series If we ignore completely the high resolution guide series, we can simply spatially zoom the target series at high resolution, using for instance cubic interpolation.

We think that it is important to include those naive solutions to the Sentinel-HR benchmark, as its purpose is to demonstrate the benefits of using more advanced fusion methods. We should therefore measure these benefits with respect to baseline naive solutions.

4.3.2 Spatio-Temporal Image Fusion

In remote sensing, the mixing of high revisit, coarse resolution time series with low revisit, high resolution time series in order to derive high revisit, high resolution time series is formally known as spatio-temporal fusion. Seminal work is known as the STARFM algorithm [GMSH06] which has been primarily designed for the fusion of Landsat and MODIS imagery. Many more method have followed [BS19, ZCTW18], most of which extend STARFM or try to overcome its limitations by using more complex models. It should be noted that most of spatio-temporal fusion methods mix data pre-processing such as radiometric normalisation, spatial registration and gap-filling with fusion rules. Also note that almost all those papers are heavily biased toward the fusion of Landast (30m) and Modis (500m), and as such are not really tailored for the Sentinel-HR case, where the ratio between high and low resolution will be a lot smaller.

1. An analysis of the STARFM Algorithm

   The STARFM theoretical basis [GMSH06] is that, for an **homogeneous** pixel at location (x_i, y_i) observed at time t_k from coarse image C, and for a corresponding higher resolution pixel F within the coarse pixel cell, we should observe:

   $$F(x_i, y_j, t_k) = C(x_i, y_j, t_k) + \epsilon_k \tag{4.1}$$

   Where ϵ_k stands for differences between the observed reflectances that are sensor related. Note that though being of different resolution, F and C are addressed through the same spatial coordinates, which implies a ressampling of the coarse image C to the high resolution grid of image F. Though many spatio-temporal fusion will use nearest-neighbor interpolation to preserve the observed coarse radiometry, better spatial interpolation methods can be considered. Here homogeneous means that higher resolution pixels with the coarse pixel cell exhibit little or no variations. If we assume that for a given pixel this difference is constant through time, we can write:

   $$F(x_i, y_j, t_0) = F(x_i, y_j, t_k) + C(x_i, y_j, t_0) - C(x_i, y_j, t_k) \tag{4.2}$$

   Which essentially states that changes are driven by the coarse resolution image if the coarse pixel is homogeneous enough and system performances (noise, BRDF effects ...) are stable.

   However, many of those assumptions hardly hold for most of the pixels:

   - True coarse homogeneous pixels are very rare,
   - Changes may occur through time, at high resolution

   In STARFM, equation 4.2 is therefore relaxed so as to express the desired high resolution pixel as a linear combination of known high resolution and coarse images from a spatio-temporal windows of radius r in the spatial domain and among the K known high resolution dates F and corresponding coarse resolution dates C. For a given spatial location (x_0, y_0) and prediction date t_0:

   $$F^*(x_0, y_0, t_0) = \sum_{i=-r}^{r} \sum_{j=-r}^{r} \sum_{k=1}^{K} W_{ijk} \Big(\underbrace{C(x_i, y_j, t_0)}_{\text{Coarse image at } t_0} + \underbrace{F(x_i, y_j, t_k) - C(x_i, y_j, t_k)}_{\text{High res. details at } t_k} \Big) \tag{4.3}$$

   After reordering terms, another possible interpretation of the STARFM linear combination equation is given by:

   $$F^*(x_0, y_0, t_0) = \sum_{i=-r}^{r} \sum_{j=-r}^{r} \sum_{k=1}^{K} W_{ijk} \Big(\underbrace{F(x_i, y_j, t_k)}_{\text{High res. at } t_k} + \underbrace{C(x_i, y_j, t_0) - C(x_i, y_j, t_k)}_{\text{Coarse changes from } t_k \text{ to } t_0} \Big) \tag{4.4}$$

   Note that for the sake of simplicity, spectral bands are not represented in those equation, but that those equations hold independently for each spectral band. W_ijk determines

how much each pixel from the spatial neigborhood and at each date contributes to the final reflecance of the center pixel (x_0, y_0) at date t_0.

W_ijk is derived from 3 different criterions: spectral difference, temporal difference and spatial distance. Spectral difference is given by equation 4.5, temporal difference is given by equation 4.6, and spatial distance is given by equation 4.7.

$$S_{ijk} = |F(x_i, y_j, t_k) - C(x_i, y_j, t_k)| \tag{4.5}$$

$$T_{ijk} = |C(x_i, y_j, t_0) - C(x_i, y_j, t_k)| \tag{4.6}$$

$$D_{ij} = 1 + \frac{\sqrt{(x_i - x_0)^2 + (y_j - y_0)^2}}{A} \tag{4.7}$$

With those notations, in the original paper weights W_{ijk} are given by equation 4.9

$$B_{ijk} = \frac{1}{(S_{ijk} \cdot T_{ijk} \cdot D_{ik})} \tag{4.8}$$

$$W_{ijk} = \frac{B_{ijk}}{\sum_{i=-r}^{r} \sum_{j=-r}^{r} \sum_{k=1}^{K} B_{ijk}} \tag{4.9}$$

In the original paper, pixels participating in weights are further limited to spectrally similar pixels (to the center pixel), by means of an external classification, or by setting an upper threshold on N_{ijk}, the absolute difference between high resolution center pixel and its neighbors, as presented in equation 4.10. There is also an additional pixels filtering that depends on the radiometric uncertainty of both sensors, computed by means of thresholding S_{ijk} and T_{ijk}.

$$N_{ijk} = |F(x_0, y_0, t_k) - F(x_i, y_j, t_k)| \tag{4.10}$$

2. Adaptations of the STARFM algorithm for the study

   In this study, we modified the above STARFM algorithm in the following ways. First, a combined clear pixel mask is used in order to set the weight of unclear pixels to 0 for each date and location in equation 4.9. This is shown in equation 4.11, where M_{ijk} is 1 for a clear pixel and 0 elsewhere.

$$B_{ijk} = \frac{M_{ijk}}{(S_{ijk} \cdot T_{ijk} \cdot D_{ik})} \tag{4.11}$$

   Second, instead of performing the classification or thresholding scheme in order to discard pixels that are not similar to central pixel, we chose to directly add N_{ijk} as a factor in the computation of B_{ijk}, as presented in equation 4.12. The rationale for this is to avoid artifacts linked to an external discrete classification maps at transitions between classes, and to avoid corner cases where no pixels are available for the estimation.

Adding N_{ijk} at denominator of B_{ijk} will anyway favor more similar pixels in a smooth way. Likewise, we do not perform the sample quality filtering.

$$B_{ijk} = \frac{M_{ijk}}{(S_{ijk} \cdot T_{ijk} \cdot N_{ijk} \cdot D_{ik})} \tag{4.12}$$

One last adaptation regards the necessity to get both high resolution and coarse resolution images on the same day. If we have a high resolution image, we can indeed filter it with a gaussian kernel related to the coarse resolution image Modulation Transfer Function and derive the coarse image from the high resolution image. This relaxes greatly the constraints on gathering adequates time-series, since we only need the high resolution series and intermediate coarse resolution series at prediction date.

Lets decompose $F(x_i, y_j, t_k)$ into a sum of its coarse version and high resolution residuals:

$$F(x_i, y_j, t_k) = F_C(x_i, y_j, t_k) + F_{HR}(x_i, y_j, t_k) \tag{4.13}$$

If we use $F_C(x_i, y_j, t_k)$ in place of $C(x_i, y_j, t_k)$, we get a new insight on what information is captured by S_{ijk} and T_{ijk}:

$$S_{ijk} = | \underbrace{F_{HR}(x_i, y_j, t_k)}_{\text{High res. details at } t_k} | \tag{4.14}$$

$$T_{ijk} = | \underbrace{C(x_i, y_j, t_0) - F_C(x_i, y_j, t_k)}_{\text{Low res. changes from } t_0 \text{ to } t_k} | \tag{4.15}$$

This gives us a good insight on how pixels are weighted in the STARFM linear combination:

- Pixels with strong high frequency contents will have lesser weights
- Pixels that exhibit strong coarse resolution change wrt. the target date will have lesser weights
- Pixels that are dissimilar from the high resolution center pixel will have lesser weights
- Pixels spatially further from the center pixel will have lesser weights

  Formulated like this, STARFM is a very clever algorithm:
  - It naturally supports multiple high-resoluiont dates, without any requirements on those dates with respect to the target date,
  - It naturally handles the cloud and other quality masks,
  - I weights pixels contribution according to a balance between multiple criterions.

3. The STAIR algorithm

   One alternative (out of many) to STARFM is the STAIR algorithm [LGP18]. STAIR is advertised by its authors as an approach suitable for large scale operation, that does not rely on exogenous data such as land-cover maps, that may not be available globally.

STAIR has some specifics aiming at addressing Landsat7 TM scan-line data gaps. Generic part include the separate linear gap-filling of high resolution and coarse resolution time-series.

Once this gap-filling is achieved, STAIR uses the following homogeneous pixel model between high resolution observations F and up-sampled coarse resolution image C:

$$F(x_i, y_j, t_k) = C(x_i, y_j, t_k) + \epsilon(x_i, y_j, t_k) \tag{4.16}$$

Where $\epsilon(x_i, y_j, t_k)$ stands for all residuals between high and coarse resolution synchronous observations, which can be computed from those observations:

$$\epsilon(x_i, y_j, t_k) = F(x_i, y_j, t_k) - C(x_i, y_j, t_k) \tag{4.17}$$

Note that since F and C have been gap-filled, ϵ is available at all time and locations.

If at given time t, C is observed, this model still holds:

$$F^\star(x_i, y_j, t) = C(x_i, y_j, t) + \epsilon^\star(x_i, y_j, t) \tag{4.18}$$

In order to estimate $F^\star$ it suffices to estimate $\epsilon^\star(x_i, y_j, t)$, which is done by linear temporal interpolation of the $\epsilon(x_i, y_j, t_k)$.

4. Adaptations of the STAIR algorithm

   In the time-series gathered for the study, we do not have simultaneous high resolution and coarse observations. As in section 2, we will therefore use the MTF filtered version of $F(x_i, y_j, t_k)$ in place of $C(x_i, y_j, t_k)$ when the high resolution image is clear. With this formulation, STAIR essentially amounts to linearly interpolate high resolution details at prediction date, and add those details to the available coarse image at prediction date.

   A second adaptation reside in the gap-filling of the coarse time-series, for which we will use also the coarsened high resolution observation, in order to densify the time sampling and obtain a more accurate interpolation of missing values in coarse target date.

4.3.3 Single Image Super Resolution

Single Image Super Resolution is a field of the computer vision domain which consist in predicting a higher resolution version of a single image without any additional input. Prior to the Deep-Learning era, Single Image Super-Resolution was mostly known as deconvolution, a process that tries to reverse the effect of the instrument Modulation Transfer Function, at the expense of increasing the level of noise [LWDF11]. More advanced techniques have been developed to solve this ill-posed problem if several aliased low resolution images were available, by exploiting the small offsets between the different views generating different aliasing pattern that could guide the inversion, and spatial regularization [KZAB20].

Convolutional Neural Networks and Generative Adversial Networks changed the game entirely, and a wide range of network architectures have been proposed to tackle the Single Image Super Resolution problem [AKB20, LYD+20], as shown in figure 4.5.

1. Network selection

   In order to select a network architecture, we established the following criterion:

   - First, we rule out Generative Adversial Network architectures. GANs are known to render very realistic images, at the expense of hallucinating details that may not correspond to any ground truth. This has a simple explanation: physic tells us that optics and detectors will cut off spatial frequencies higher than an instrument-related threshold. Consequently, images signal will not contain any information on those high frequencies, which imposes limits on what traditional Single Image Super-Resolution can do. GANs overcome this limitation by learning the statistical distribution of those unobserved details conditioned to the observed frequencies that can be observed in a signal. During inference, GANs will use one realisation of this statistical distribution, and thus generate details that are statistically plausible but with a weaker link to the observed signal. As Sentinel-HR primarily aim at scientific applications for which local surface reflectance values correctness is important, we decided to eliminate this family of method.
   - Second, since we are preparing for a mission with global and regular coverage, it is of great importance that both the training and the inference process are as cheap as possible in terms of complexity and algorithmic cost. Fortunately, the authors of [AKB20] did some very informative graph showing the achieved PSNR with respect to both model size (see figure 4.6) and computational complexity related to architectures complexity (see 4.7) to guide our choice.

     From those graphs, we can see that the CAscading Residual Network [AKS18] offers the best trade-off between complexity and PSNR in both model size and number of operations. Consequently, we selected this network for the study.

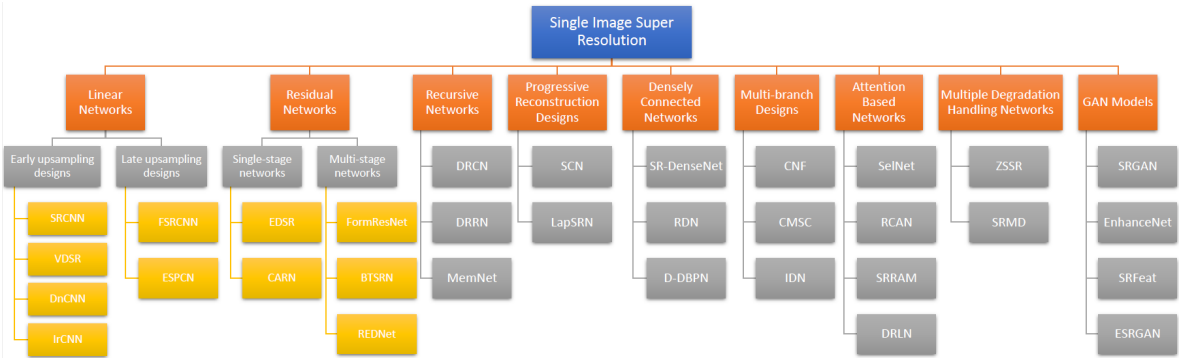

Figure 4.5: Taxonomy of Deep-Learning based Single Image Super-Resolution networks (from [AKB20])

2. Anatomy of CARN

   CARN [AKS18] belongs to the family of residual, late up-sampling networks. It is made of a series of cascading residual blocks with intermediate skip connections, followed by a final Pixel-Shuffle operation, as shown in figure 4.8. Each residual block is made of two grouped convolutions followed by ReLU activation, with local skip connections as shown in figure 4.9. For additional computational efficiency, residual blocks weights

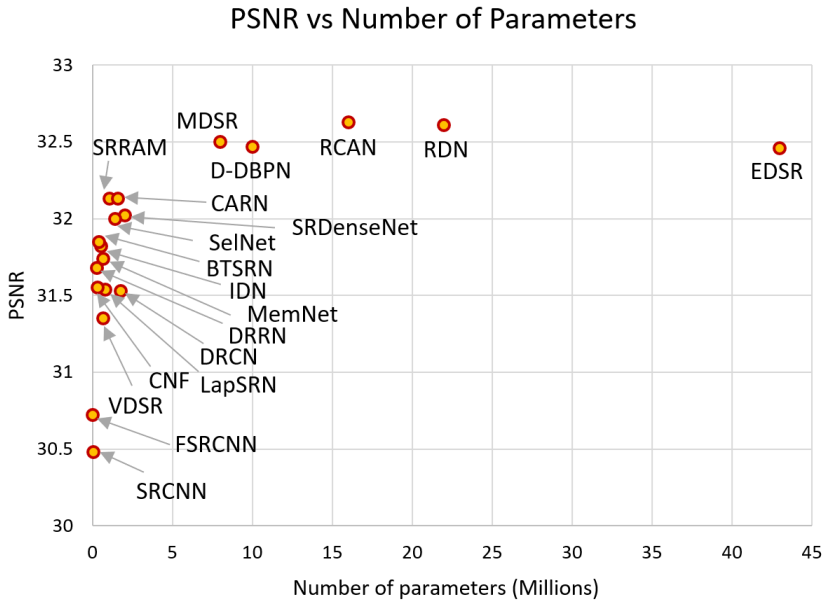

Figure 4.6: PSNR vs. number of parameters for SISR deep-learning architectures (from [AKB20])

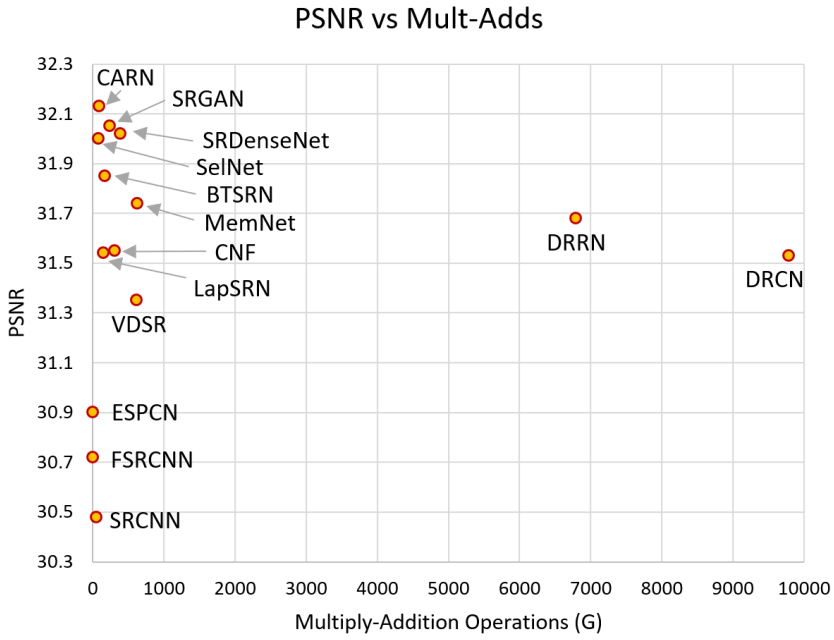

Figure 4.7: PSNR vs. number of multiplications and additions for SISR deep-learning architectures (from [AKB20])

are shared (which in fact means that a single residual block is used with a certain amount of looping). Pixel shuffle is a way of unfolding the features dimension to the spatial dimensions, as shown in figure 4.10. Note that in our study, we use the single output version of CARN, with a single PixelShuffle up-sampling operation to the target resolution.

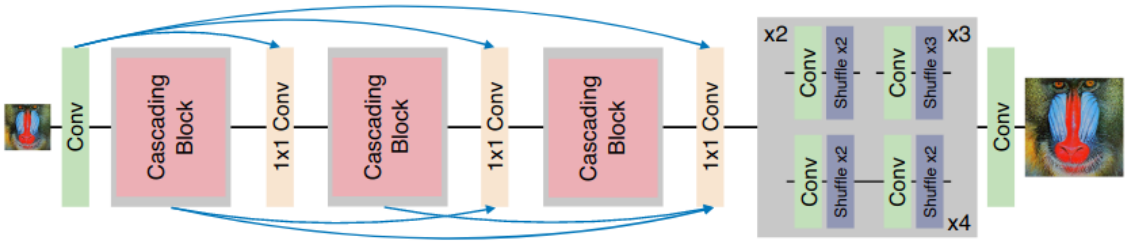

Figure 4.8: Overview of CARN architecture (from [AKS18])

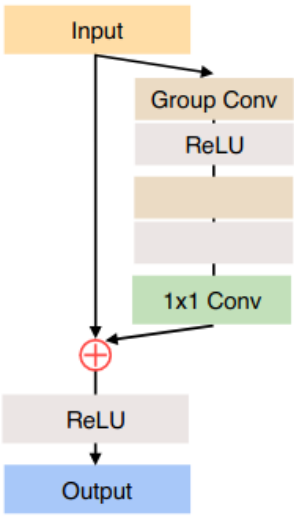

Figure 4.9: CARN residual blocks with local skip connections (from [AKS18])

3. Implementation and offline training

   In our implementation, we use 3 residual blocks with a kernel size of 3 pixels. The number of features is directly related to the up-sampling factor, e.g. 32 features for each high-resolution pixels within the low-resolution pixels. This means that the number of features is 800 for a ratio of 5, and 288 for a ratio of 2.5. In the latter case, in order to accommodate non-integer up-sampling factor, we use the closest integer up-sampling factor and then down-sample to the target resolution (here a factor of 3 then down-sampled to obtain a factor of 2.5). Grouping is set to 2 in residual convolution layers. One last important modification is that our implementation process the 4 selected bands at once (both for input and outputs).

   CARN needs to be trained offline with a large number of samples variety, including different landscapes and times of the year. In order to achieve this, we performed a similar

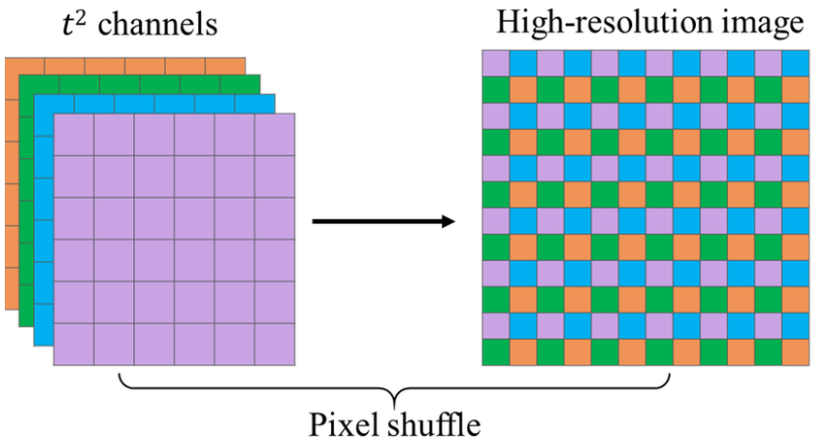

Figure 4.10: Understanding the PixelShuffle operation (from [QMH+20])

cross-search between Venμs and Sentinel2 L2A archive as presented in section 4.2, and looked for all joint acquisition between Sentinel2 and Venμs which are less than 1 day apart. We gathered 116 image pairs over 5 different sites, yielding a total of 11505 cloud-free venμs 5 meters patches of 160x160 pixels along with their corresponding 10 meters 80x80 pixels Sentinel2 patches, both in the 4 bands selected in table 4.1. Available pairs and patches by site are shown in table 4.3. As for the time-series dataset generation, images were registered with the SIFT method and surface reflectances were harmonized by least-square linear regression. However in this case, Venμs reflectances were mapped to Sentinel2 reflectances, in order to ensure an unbiased training of CARN. Note that during training, Sentinel2 patches are further down-sampled to match the target resolution ratio if needed. Prior to training, input data and target data are standardized (thus loss is computed on standardized outputs). During inference, networks performs an additional un-standardization. During training, this set of data is further separated into 6840 training samples, 760 testing samples to measure learning progression and 3905 samples to evaluate network performances. Those last samples are chosen in separate images, that are not used for training.

Our loss is a simple Hinge Loss, i.e. it is quadratic when close to zero to favor convergence and linear far from zero to reduce the effect of potential outliers. For the training, we use stochastic gradient descent with the ADAM optimizer is used, with an initial learning rate of 1e-3, which is further decreased by a factor of 0.5 every time it stagnates for more than 4 epochs. The batch size is set to 25, and the entire training set is reshuffled between each epoch.

(a) Performances of the x5 model

The 25m to 5m instance of the network has 14 116 356 free parameters and has been trained for 150 epochs. The training and testing loss are shown in figure 4.11 while the best testing loss curve is shown in figure 4.12. We can see that after epoch 50, the testing loss does not improve anymore, while the training loss continues to fall, showing a clear sign of over-fitting. The best model is therefore selected before the over-fitting phase. In figures 4.13 and 4.14, we can see the performances

Venμs site	Number of pairs	Number of patches
FGMANAUS	6	505
FR-LQ1	26	2600
KRATIE	26	2600
MAD-AMBO	30	3000
NARYN	28	2800
Total	116	11505

Table 4.3: Number of Venμs and Sentinel2 pairs available to train CARN model

metrics (briefly introduced in section 4.4.1) measured on the validation set at each epoch. Indeed, PSNR reaches a maximum of 42 to 45.5 dB in visible bands and 32 dB in the NIR band near epoch 50. Other metrics show a similar trend. It is noteworthy that the NIR band is more difficult to reconstruct because its bandwidth differs more between Sentinel2 and Venμs. Figure 4.15 shows the results of some predicted patches from the validation set in natural colors, while figure 4.16 shows the prediction from the same patches, for NDVI (NDVI is computed afterward). In both cases we compare with the original image at 25m, zoomed at 5m by means of bicubic interpolation. We can see that the algorithm succeeds in retrieving shapes of objects such as hedgerows or pathways that can not be seen on the 25m image, even though it fails to retrieve textures and still has a blurry feel.

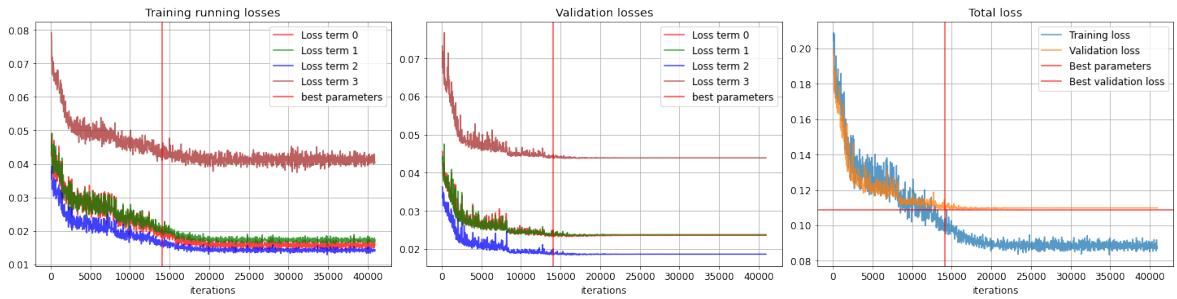

Figure 4.11: Training and testing loss evolution for x5 CARN training (from 25m to 5m)

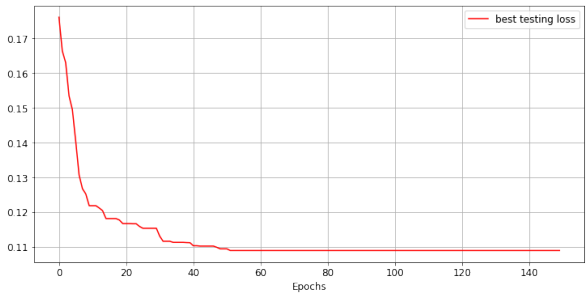

Figure 4.12: Best model loss evolution for x5 CARN training (from 25m to 5m)

(b) Performances of the x2.5 model

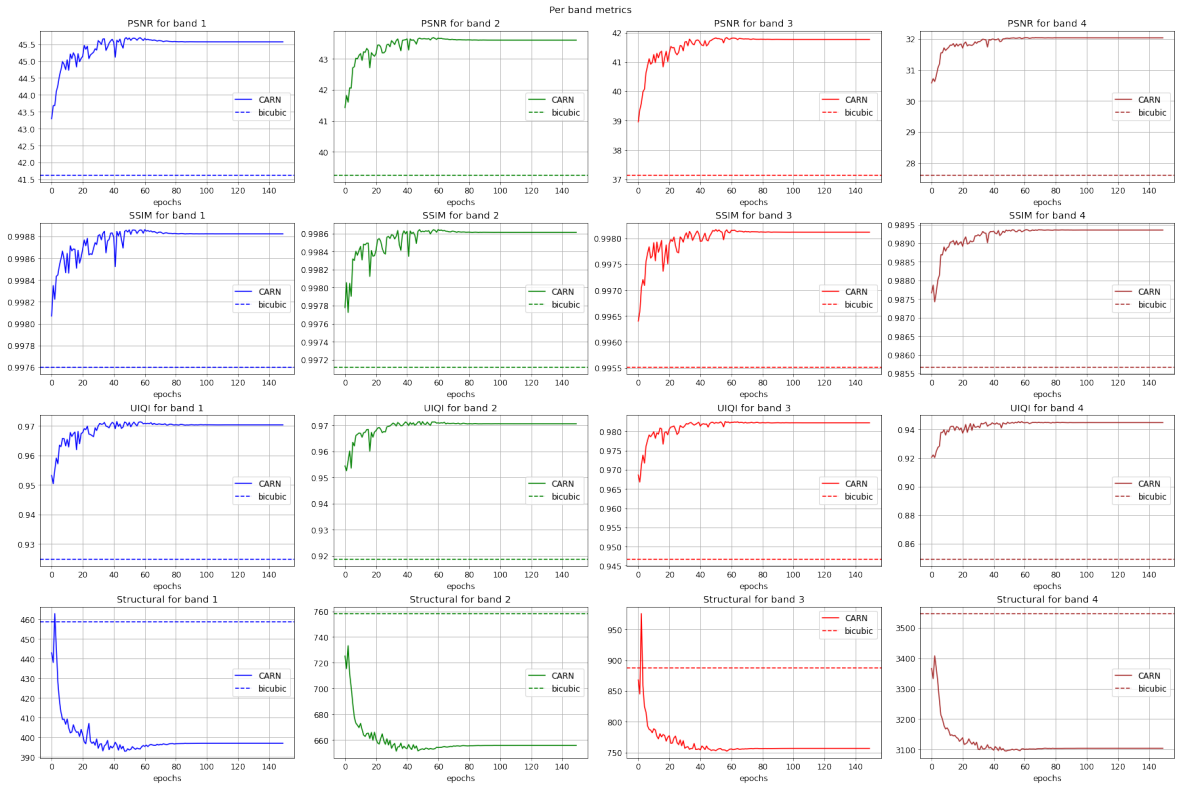

Figure 4.13: Per band metrics evolution during the training of the x5 CARN network. Dashed horizontal line correspond to performance of bicubic zoom.

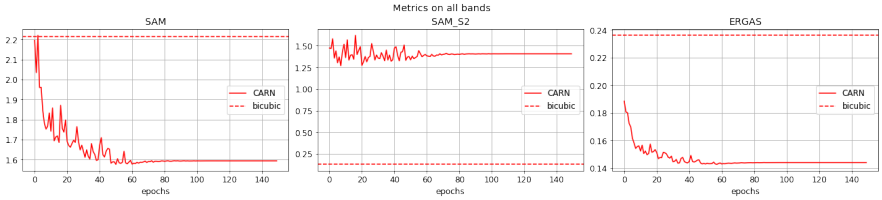

Figure 4.14: Global metrics evolution during the training of the x5 CARN network

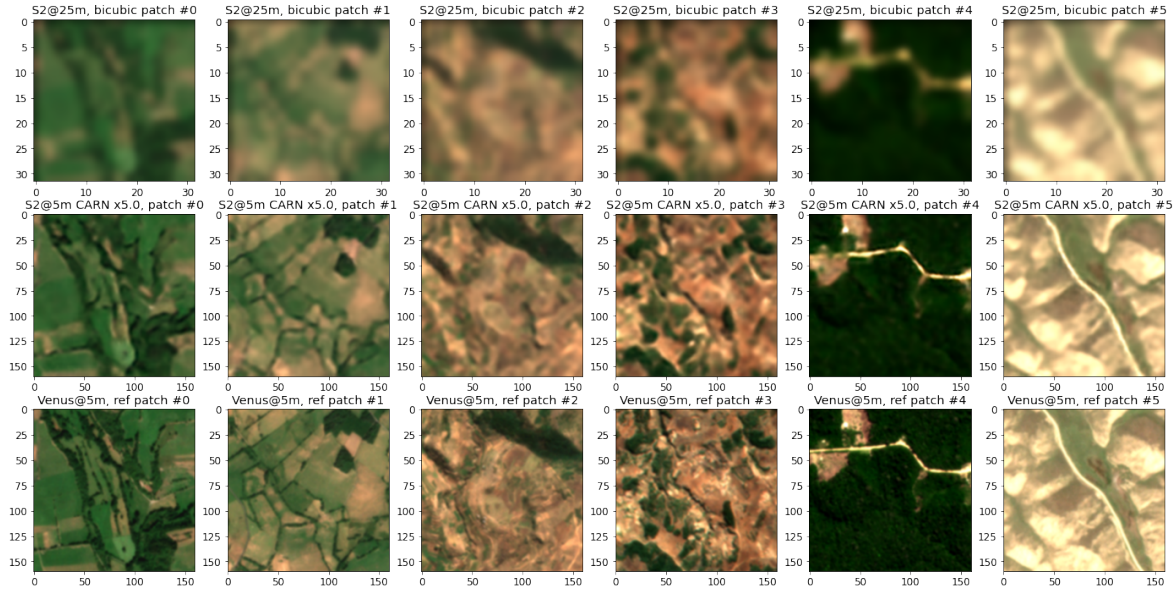

Figure 4.15: Examples of predictions in natural colors (Red, Green, Blue) from validation set for x5 CARN (from 25m to 5m). First line is S2 25m with bicubic zoom to 5m, second line is x5 CARN predictions at 5m, and third line is Venμs reference image at 5m.

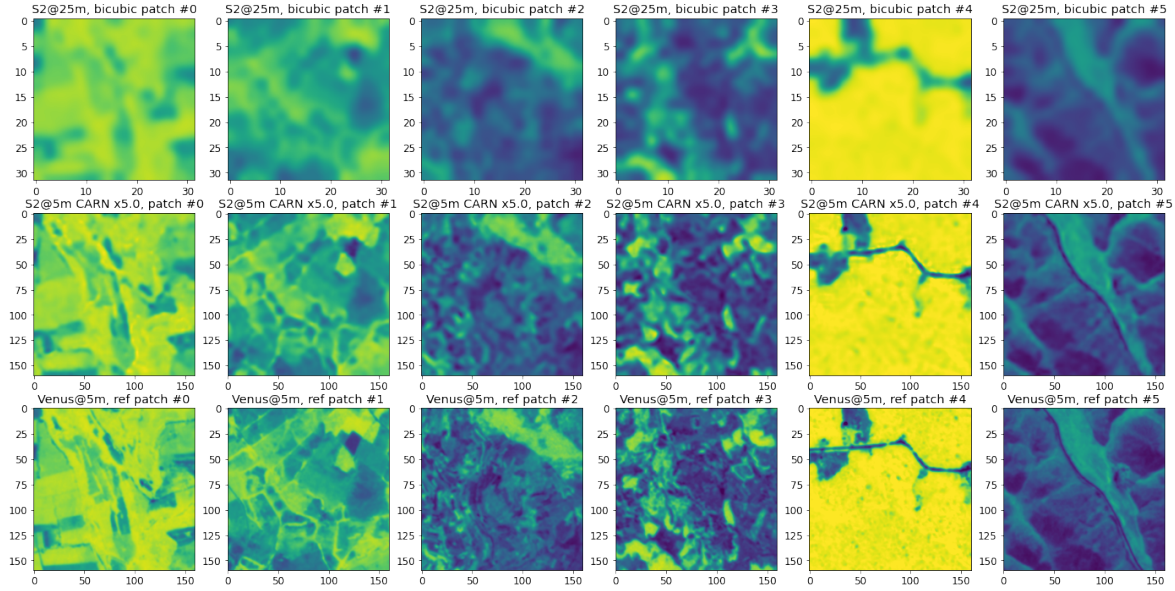

Figure 4.16: Examples of predictions on NDVI from validation set for x5 CARN (from 25m to 5m). First line is S2 25m with bicubic zoom to 5m, second line is x5 CARN predictions at 5m, and third line is Venμs reference image at 5m.

The 12.5m to 5m instance of the network has 1 838 596 free parameters and has been trained for 105 epochs. The training and testing loss are shown in figure 4.17 while the best testing loss curve is shown in figure 4.18. We can see that the testing loss improves almost until the final epoch, even if the comparison with the training loss shows clear signs of start of over-fitting. In figures 4.19 and 4.20, we can see the performances metrics (briefly introduced in section 4.4.1) measured on the validation set at each epoch. We can observe a consistent increase of PSNR until the very last epoch, with values ranging from 35.5 dB for NIR band to almost 47.5 dB for the red band. This is better than the PSNR values of the 25m to 5m model presented in section 3a. Other metrics show similar trends. Figure 4.15 shows the results of some predicted patches from the validation set in natural colors, while figure 4.16 shows the prediction from the same patches, for NDVI (NDVI is computed afterward). The performance gap with the previous model is clearly visible, the predicted image being very close to the reference image, with an additional slight blur.

It should be noted that we also trained the CARN network with a ratio of 2 in resolution from 10m (original Sentinel2 resolution) to 5 meters, and that the performances are even better.

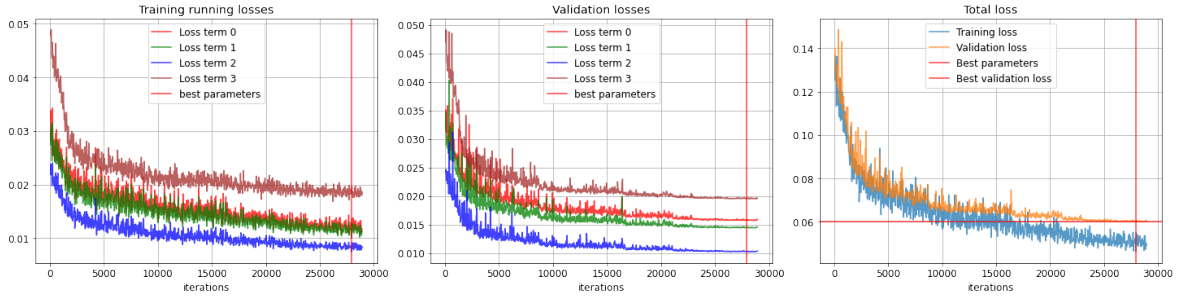

Figure 4.17: Training and testing loss evolution for x2.5 CARN training (from 12.5m to 5m)

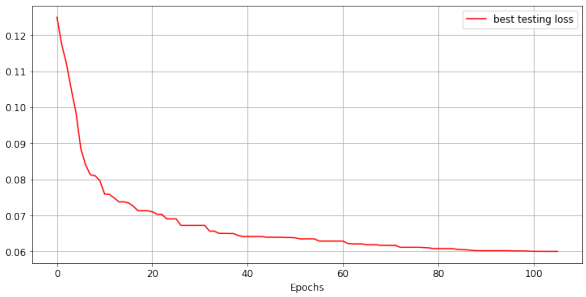

Figure 4.18: Best model loss evolution for x2.5 CARN training (from 12.5m to 5m)

4.3.4 Data-driven interpolation

1. Rationale

   Data-driven Interpolation is an alternative method that has been developed at CESBIO during the phase-0 study. This method results from the combination of the work from

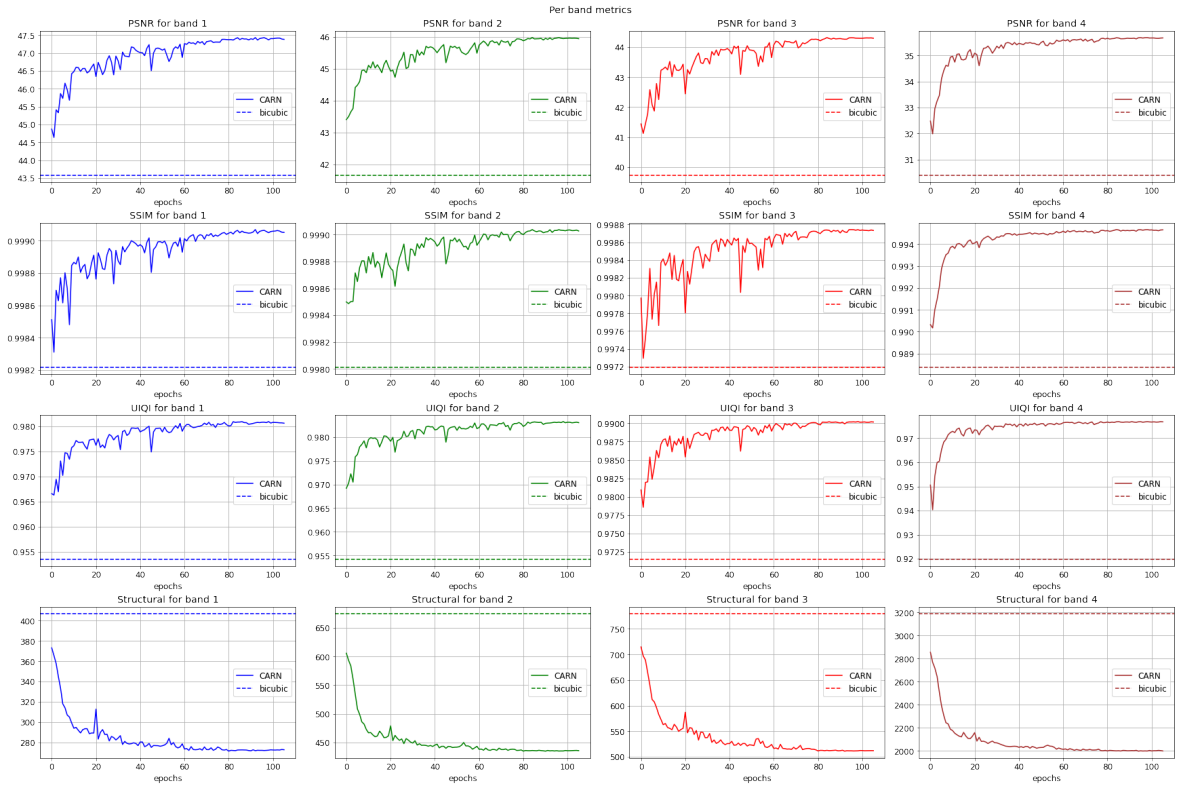

Figure 4.19: Per band metrics evolution during the training of the x2.5 CARN network. Dashed horizontal line correspond to performance of bicubic zoom.

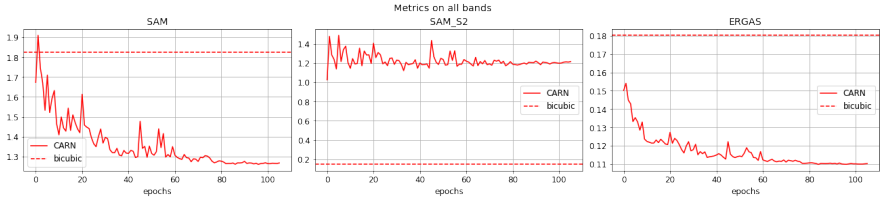

Figure 4.20: Global metrics evolution during the training of the x2.5 CARN network

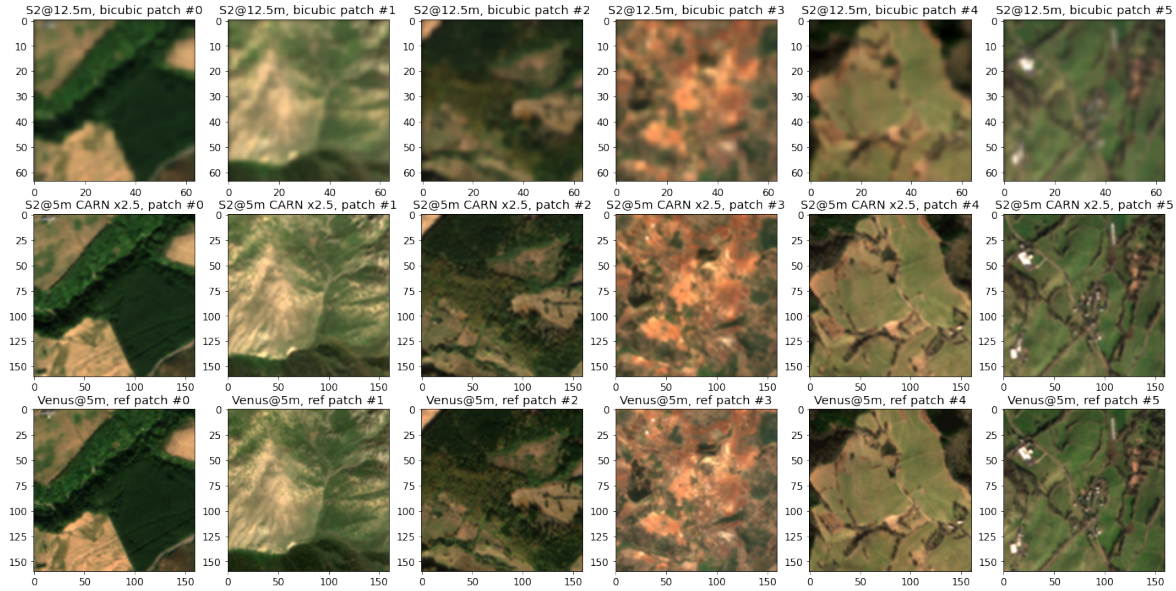

Figure 4.21: Examples of predictions in natural colors (Red, Green, Blue) from validation set for x2.5 CARN (from 12.5m to 5m). First line is S2 12.5m with bicubic zoom to 5m, second line is x2.5 CARN predictions at 5m, and third line is Venμs reference image at 5m.

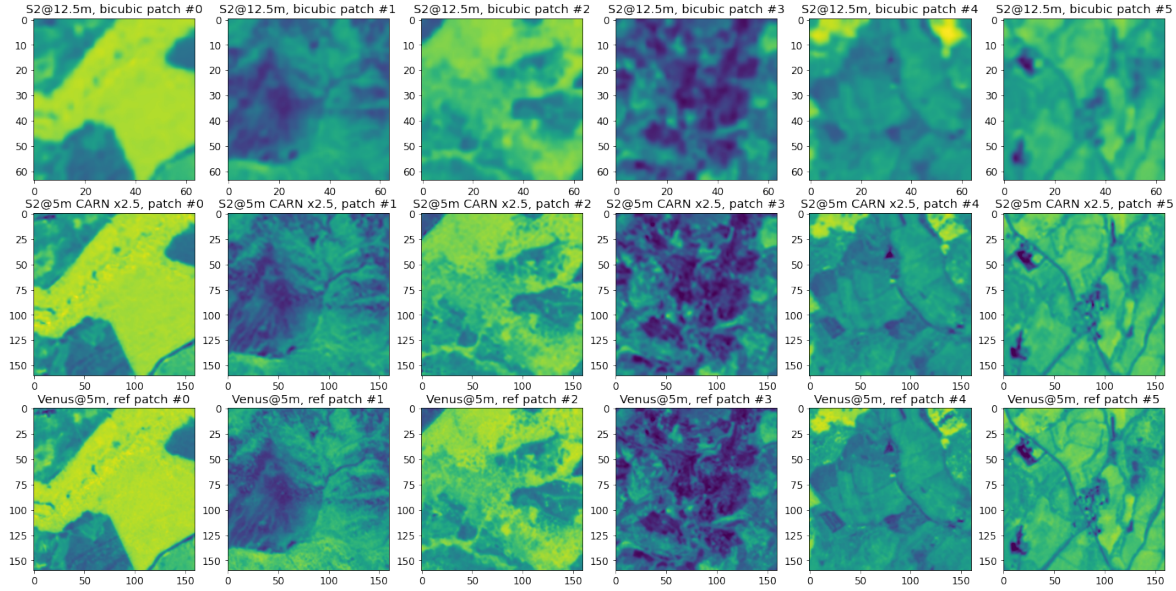

Figure 4.22: Examples of predictions on NDVI from validation set for x2.5 CARN (from 25m to 5m). First line is S2 12.5m with bicubic zoom to 5m, second line is x2.5 CARN predictions at 5m, and third line is Venμs reference image at 5m.

[LDWS19], where a Multi-Layer Perceptron is used to learn the non-linear mapping between an high-resolution guide image and a coarse image that might be of different modality, in order to achieve super-resolution of this coarse image. The neural network weights are learned for each pair of images to process, though some generalisation might be achievable here. The coarse image serves as a reference and the loss function is computed on the down-sampled high resolution prediction, with some regularisation (by means of weight decay) in order to constrain the ill-posed problem towards smoother mapping. At inference stage, the high resolution prediction only depends on the high resolution guide pixel, which allows for very sharp and detailed reconstructions, without any blurring effect.

This is somehow similar to approaches in the Thermal Infra-Red domain [GKA12], where the non-linear mapping between higher resolution shortwave spectral reflectances and coarser resolution Land Surface Temperature is learned at coarse resolution by regression trees. Those regression trees are then applied to the high resolution in order to predict a high resolution LST.

Those approaches however rely on an unformulated hypothesis : similar guide observations should correspond to similar target low-resolution observations, throughout the observed pair of images. This assumption can be breached when changes of the intrinsic properties of the surface can only be observed in the target modality while yielding similar observations in the guide modality. If the guide and target observations are synchronous, this will essentially be caused by spatial heterogeneity of the scene, and in [GKA12] they run local instance of the model in a sliding window in order to account for it.

In a Sentinel-HR configuration however, high resolution and coarse resolution observations are of the same modality, but distant in time. Therefore, temporal changes of surface intrinsic properties will breach the assumption. Crops for instance might exhibit the same surface reflectances at high resolution observation time, but show very different reflectances on the next coarse resolution observation due to differences in culture phenology. In order to introduce more discriminative power in guide observations, we can therefore leverage multi-temporal high resolution observations, i.e. use all the guide dates we have instead of a single one.

2. Proposed Data-Driven Interpolation general architecture

   In order to achieve prediction of M target dates with L spectral bands by using N guide dates with the same L spectral bands, we propose to use the network architecture in figure 4.23. In the absence of the coarse resolution time-series, in order to predict a date that is not observed, we would resort to temporal interpolation (linear, or spline-based, with or without smoothing). If we have coarse resolution observations at the prediction date, we can try to learn the interpolation weights from the data.

   We will therefore pose:

$$F(x_i, y_j, b_k, t_m) = \sum_{n=1}^{N} \sum_{l=0}^{L} W^{\star}_{ijkmnl} \times F(x_i, y_j, t_n, b_l) \tag{4.19}$$

   Where W_{kl} is an interpolation matrix that is learned from the data themselves, using a backbone Multi-Layer Perceptron from the standardized, zero-inputted guide time-

series. For each multi-temporal guide pixel, a different set of weights is predicted, and weights corresponding to missing pixel dates at this location are set to 0. Weights are then normalized along the guide time dimension. Before being used to linearly combine guide observations to form the predicted time-series. The backbone Multi-Layer Perceptron is trained through stochastic gradient descent from the smooth L1 loss with respect to the target time-series (the loss is set-up to ignore missing reference pixels). Since each set of learned weights correspond to a specific time sampling and location, the model is trained separately for each prediction, without seeking for generalization.

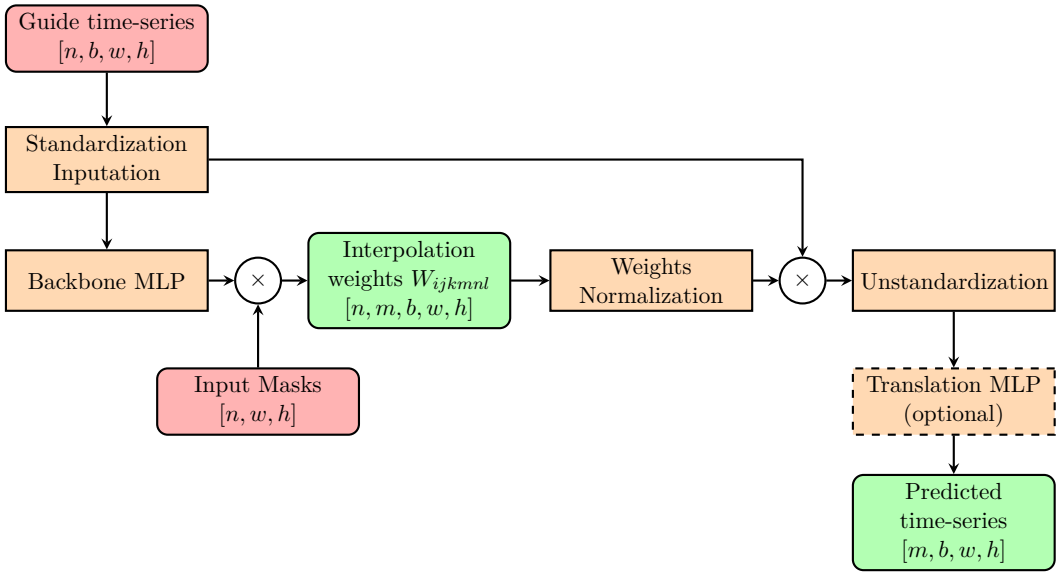

Figure 4.23: Workflow of Data Driven Interpolation. From input images with n dates and b bands, DDI predicts m new dates with b bands. Each band from each pixel of each date is linearly interpolated by a (n, m) matrix predicted by the MLP backbone. Weights corresponding to masked pixels are set to 0, and weights are renormalized. An optional translation MLP can be used if guide and target time-series are of different modalities.

3. Usages of Data-Driven Interpolation

   There are different ways in which the general architecture presented in figure 4.23 can be used:

   Gap-filling without temporal re-sampling If guide and target series are the same time-series with partially missing data caused by clouds or variety in satellites track, DDI can be trained to perform gap-filling of all missing data without any temporal re-sampling. In order to achieve this, The training set should be extended in order to contain sample for each target date where the corresponding date has been excluded from the guide series.

   Guided super-resolution If guide and target time-series have different time sampling, guide has a better resolution than target and modalities are optionally different, DDI can be trained from down-sampled guide time-series in order to reconstruct target coarse time-series. DDI can then be inferred at guide time-series high resolution, achieving super-resolution of the target series.

In any case, even if the model is able to handle the prediction of several dates at once, in practice we found it more stable to learn each target date separately.

4. Samples Stratification

   In order to ensure that the training set is not biased toward the most frequent radiometric trends, we perform an optional stratification of the training set. Target radiometries are clustered into 5 classes using the KMeans algorithm, and samples are selected so that each class has the same amount of samples. Note that this may drastically limit the number of samples if one of the classes is very small with respect to the others.

5. Low-resolution residuals compensation

   Inspired by [GKA12], we also introduced a strategy for the compensation of low resolution residuals that may occur between the prediction and the target low resolution image. We first down-sample the prediction to the target low resolution image, with a gaussian kernel corresponding to a MTF of 0.1. We compute the difference between the down-sampled prediction and the target image for each band, and set the difference to 0 for all masked pixels. We then up-sample the difference image and add it to the prediction image.

6. Training and inference

   Default backbone has two layers of 64 features, with intermediate ReLU activation. Training is performed with the ADAM optimizer, using a learning rate of 0.001 and a batch size of 100. We observed that 10 epochs usually suffice for convergence. The target number of samples is 100 000, among which 10% is kept for testing, though this can be limited by missing data mask or stratification. Hinge loss is used, and is only computed on clear pixels in the target images.

   DDI is used in guided super-resolution mode, which means that Venμs images are down-sampled to the Sentinel2 resolution by means of gaussian kernel smoothing followed by decimation, with a target MTF of 0.1.

   The model is then applied at full Venμs resolution for inference. it should be noted that the model is specific to the data time-sampling and target date. It should be trained again for different time-series or target dates.

   Figure 4.24 shows an example of weights predicted by DDI for different target dates. One can observe that cloud masking in nearest Venμs date makes the algorithm use information in dates that are further in time. One can also observe that the algorithm will use different dates set to interpolate different land-cover types. Finally, one can observe the ability of the algorithm to reconstruct parts of the target images that are covered by clouds.

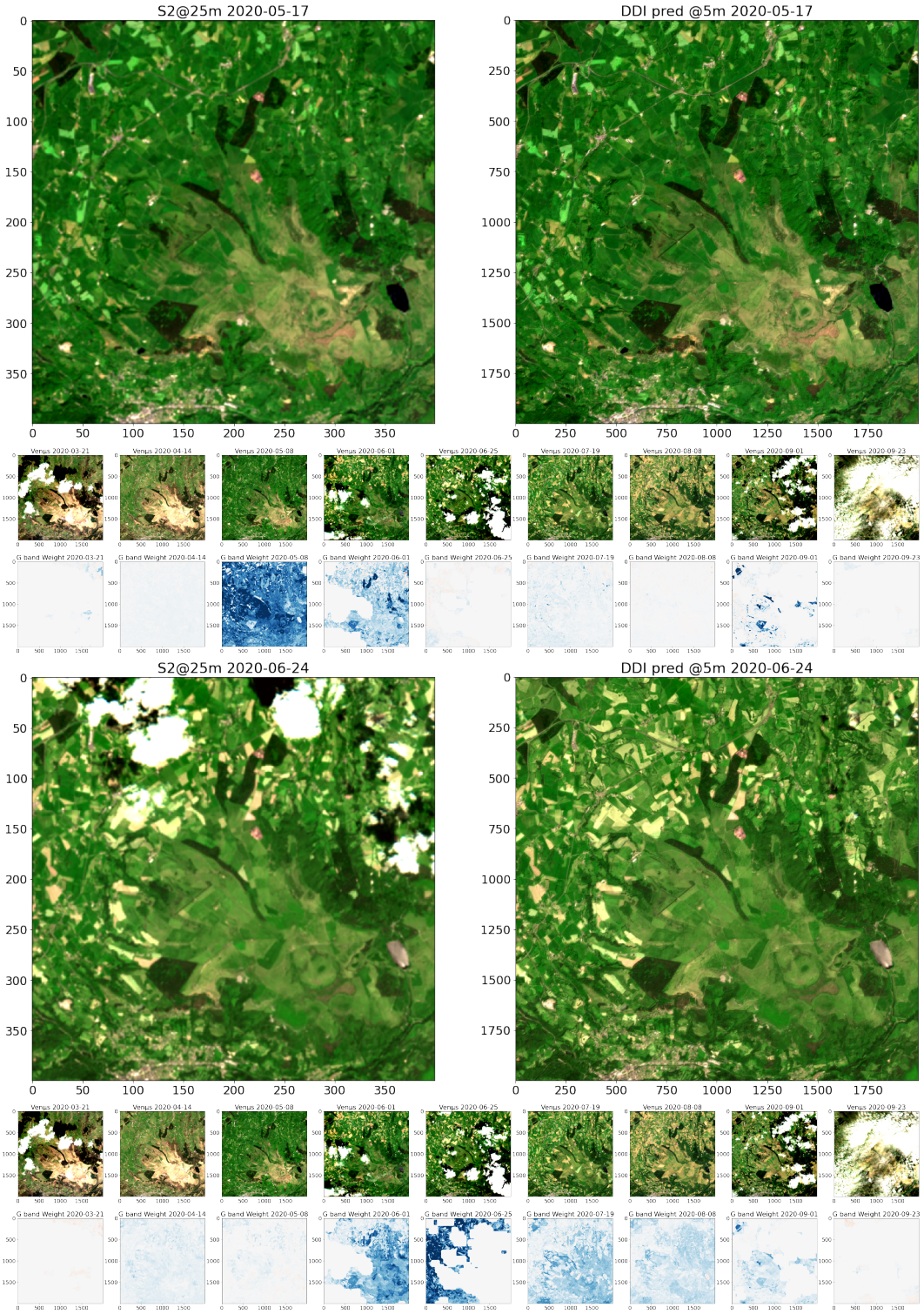

Figure 4.24: DDI applied to the reconstruction of Sentinel2 image of 2020.05.17 (upper part) and 2020.06.04 (lower part). For each part, first row: left, input Sentinel2 image, right, DDI prediction at 5 meters, second row: Venμs guide series at 5m, third row: weight of green band from every Venμs guide image in target green band prediction.

4.4 Benchmark

4.4.1 Methodology

Given the data presented in section 4.2 and the methods described in section 4.3, we set-up a benchmark aiming at reconstructing each target date corresponding to Sentinel2 acquisitions at 5 meters resolution given the guide dates (Venμs acting as Sentinel-HR acquisitions), and compare the reconstruction performances of the different methods, by using the reference 5 meters dates (Extra Venμs images simultaneous to Sentinel2 target date).

Table 4.4 summarize the different bench-marked methods and their characteristics. Those methods can be grouped into 3 sub-categories. The first category is spatial interpolation methods, which regroup traditional zooming as well as Single Image Super-Resolution. Those methods do not make use of the guide dates during inference and can not interpolate missing data at target date. The second category is temporal interpolation, regrouping traditional temporal interpolation (e.g. linear or splines-based), as well as DDI. Given that DDI only uses the target date for training, we can put it in this category. Both methods will be able to perform interpolation of missing data at target date (provided that clear pixels are also available for the training of DDI). The last category regroups spatio-temporal fusion methods, with STARFM and STAIR. Note that neither can perform interpolation of missing data at target date. Since DDI with residual correction also uses target date for inference (in the residual correction), we include it in this category, with the additional benefit of missing data interpolation at target date.

Methods	Uses target date	Uses guide dates	Interpolates missing data
Spatial interpolation			
Spatial zoom	Yes	No	No
SISR (CARN)	Yes	For offline training	No
Temporal interpolation			
Temporal interpolation	No	Yes	Yes
DDI	For training	Yes	Yes[1]
Spatio-temporal fusion			
STARFM	Yes	Yes	No
STAIR	Yes	Yes	No
DDI + residual correction	Yes	Yes	Yes[1]

Table 4.4: Methods compared in the benchmark

In order to assess the performances of the method, we compute a set of reference-based image quality summarized in table 4.5. Those metrics are computed on clear reference pixels only. As we saw in table 4.4, some methods cannot interpolate missing data at target date. In order to perform a fair assessment of performances, we therefore only compute metrics on pixels that are clear in the target image.

Our interest in this benchmark is twofold:

- Assess the ability of different methods to reconstruct high-resolution (thus high spatial frequency) details

[1]Provided that clear pixels are available at target date for the training of DDI

Metric	Computed on	Measures	Reference
Root Mean Square Error	R, G, B, NIR, NDVI	Radiometry	[JH15]
Mean Average Error	"	"	"
Mean Relative Error	"	"	"
CE90 Absolute Error	"	"	"
CE99 Absolute Error	"	"	"
Peak Signal to Noise Ratio	"	"	"
Structural Similarity	R, G, B, NIR, NDVI	Geometry	"
Structural Error	"	"	[GMG+19]
UIQI	"	"	[JH15]
ERGAS	All bands at once	"	"
Spectral Angle Mapper	All bands at once	Spectral signature	[JH15]

Table 4.5: Image quality metrics used in the benchmark

- Assess the ability of the different methods to preserve radiometry and spectral signatures

In order to be able to measure those two goals separately, we performed a stratification of pixels for each site, to separate pixels with high gradients from pixels with low gradients. First, the map of average pixel gradient magnitude over the full reference series is computed for each site. We then define two classes : the 50% pixels with the lowest average gradient magnitude (e.g. flat, low textured areas) and the 25% pixels with the highest gradient magnitude (e.g. edges and strong landscape features). All metrics are then computed on all pixels, 50% lowest gradient and 25% highest gradient. Figure 4.25 shows an example of the masks applied for both stratas, on two different study sites.

4.4.2 Quantitative Analysis

In this section we present the global results for all selected sites. For each site, metrics are computed for each target date. We discard the target dates for which target Sentinel2 image or Venμs reference image is completely cloudy, as well target dates for which the reference date is not on the same day. All sites considered, this leaves 54 target dates, as shown in table 4.6.

Note that STAIR is not included in the figures because it exhibits very poor performances. It has therefore been removed to improve figures readability.

Site	Number of target dates considered
ARM	14
FR-LQ1	13
ESGISB-2	6
MAD-AMBO	13
FR-BIL	8
Total	54

Table 4.6: Number of images per site considered in global metrics evaluation

Figure 4.27 shows box plots of main metrics, for 50% lowest gradients and 25% highest gradient, as well as the SSIM and structural error metric, for all bands and NDVI, for a

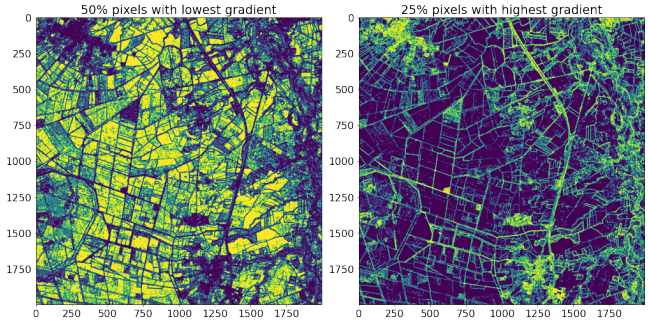

(a) Average gradients stratas for ARM site

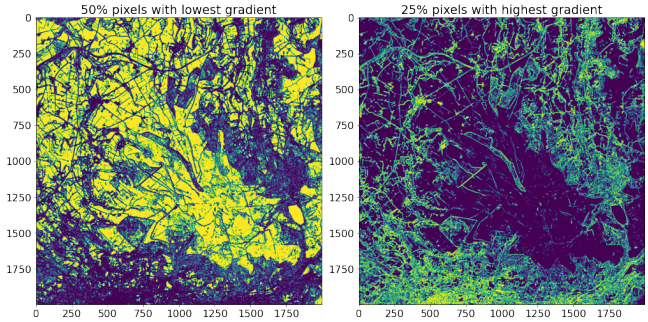

(b) Average gradients stratas for FR-LQ1 site

Figure 4.25: Examples of average gradient magnitude stratas for 2 different sites

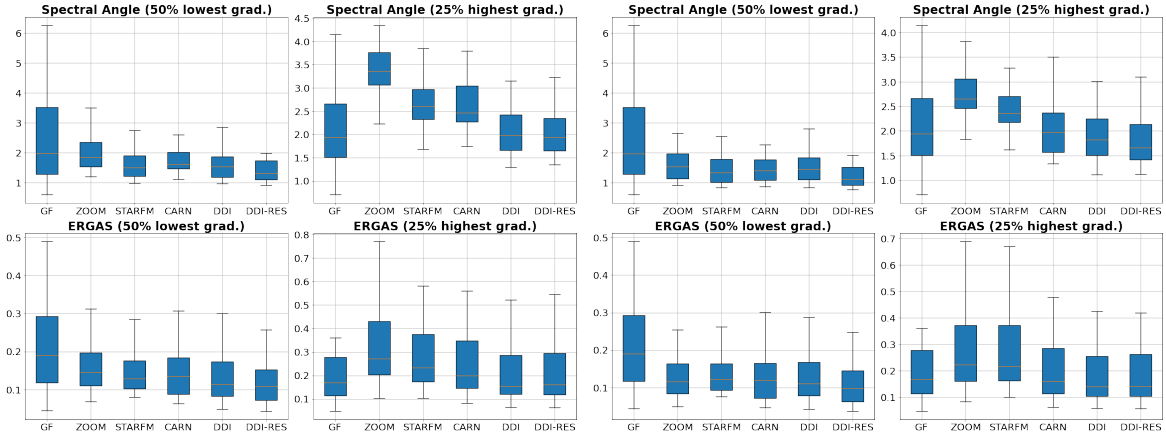

(a) Resolution ratio of 5 (25m → 5m)

(b) Resolution ratio of 2.5 (12.5m → 5m)

Figure 4.26: Spectral Angle and ERGAS metrics for the 50% lowest and 25% highest gradients, for both resolution ratios.

resolution ratio of 5 (25m → 5m), whereas figure 4.28 shows the same metrics for a resolution ratio of 2.5.

For a resolution ratio of 5, looking at metrics on the 50% pixels with lowest gradient, one can observe a clear ordering of performances in most metrics and in all spectral bands, linear gap-filling being the method with the highest variability of performances by far. All methods except linear gap-filling and cubic zoom achieve RMSE surface reflectance accuracy better

than 0.01 in red, green and blue channels and 0.03 in near infra-red for 75% of the dates. Also all methods except linear gap-filling and cubic zoom achieve CE99 surface reflectance accuracy better than 0.05 in red, green and blue channels and 0.1 in near infra-red for 75% of the dates . DDI with or without residuals compensation seems to show the best performances for this ratio and those low gradient pixels, though it should be noted that if residual compensation does not always improve DDI performances. Interestingly, ordering of methods according to performances for low gradients pixel at this resolution ratio does not always hold for NDVI. CE99 error remains quite high for all method (0.2 for 75% of the dates). Those conclusions do not change drastically when looking at resolution ratio of 2.5, with a slight increase in CE99 error without drastically modifying the ordering of methods. However, we can observe that CARN performs better, especially on NDVI, where it often yields the best or one of the best performances. It is also interesting to observe that DDI with residual compensation for 50% of lowest gradient has better or similar performances than DDI without residual compensation in red and NIR bands, but worst performances on NDVI, with a huge increase in variability. Explaining this performance drop requires further investigations.

We can now look at the 25% highest gradients, corresponding to small linear features and textured areas, which should benefit more from improved resolution. For a resolution of 5, we can see that linear temporal interpolation achieves the best performances, though still with a larger dispersion than other methods. This can be easily explained by the fact that temporal interpolation only relies on high resolution observation, without any mixing with the low resolution observation. As a result, and provided that there is little or no registration noise in Venμs time series, it achieves the best sharpness and therefore the best accuracy for pixels with highest gradients. We can also note that difference in performances are larger than for low gradients pixels, with a clear gradation from cubic zoom (worst) to DDI (best). If for low gradient pixels, CARN and DDI performs equally, for high gradient pixels and a ratio of 5, DDI clearly outperforms CARN. Both CARN and DDI achieves a RMSE of 0.15 in red, blue and green channels and 0.05 in near infra-red channel, as well as a CE99 error of 0.06 in red, blue and green channel, and 0.15 in near infra-red channel, for 75% of images. On NDVI, CE99 error is large: 0.25 for 75% of the images for both CARN and DDI.

If we look at the 25% highest gradient pixels for a resolution ration of 2.5, the most obvious change is CARN performing as well, or sometimes slightly better, than DDI, which means that for this resolution ratio, a properly trained super-resolution algorithm is able to extract the high frequency details from the low resolution, without any additional information.

We can turn to SSIM and structural error which are the two last lines of figures 4.27 and 4.28, which consolidate the observations made so far: a clear ordering of metrics for overall radiometric quality, linear temporal interpolation being the worst method and DDI being the best one, and a clear advantage to linear temporal interpolation and DDI regarding geometric quality for resolution ratio of 5. For a resolution ratio of 2.5, CARN offers geometric performances similar to DDI.

If we look at figure 4.26, which presents the box plots for Spectral Angle and ERGAS (which are global values across spectral bands), we can see that DDI is the best method regarding spectral signature faithfulness, on low and high gradient pixels. ERGAS shows trends similar to the metrics analysed above.

It should be noted that individual sites might exhibit different trends. For instance, FR-BIL has most of its landscape evolving very linearly with time, making linear temporal interpolation very effective in most place (but very wrong locally). MAD-AMBO is a desert site with scarce changes, and again favor linear temporal interpolation.

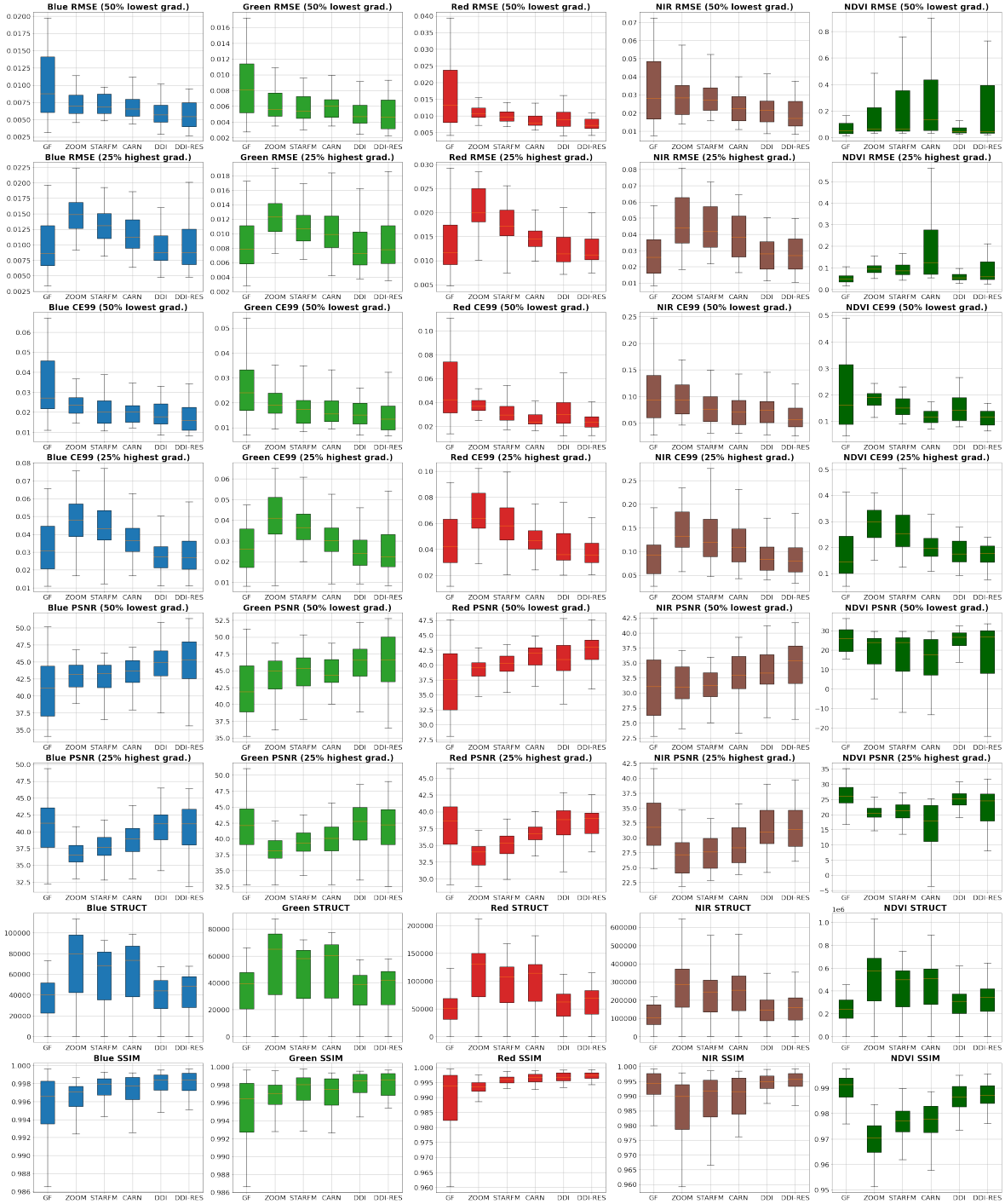

Figure 4.27: Box-plots of RMSE, CE99 absolute error and PSNR for 50% lowest gradients and 25% highest gradients, as well as SSIM and structural error, for Red, Green, Blue, Near Infra-Red and NDVI, on all sites, for methods linear interpolation (GF), cubic zoom (ZOOM), Single Image Super-Resolution (CARN), STARFM (STARFM), Data-Driven Interpolation (DDI) and Data-Driven Interpolation with residuals compensation (DDI-R), with a resolution ratio of 5 (25m $\rightarrow$ 5m).

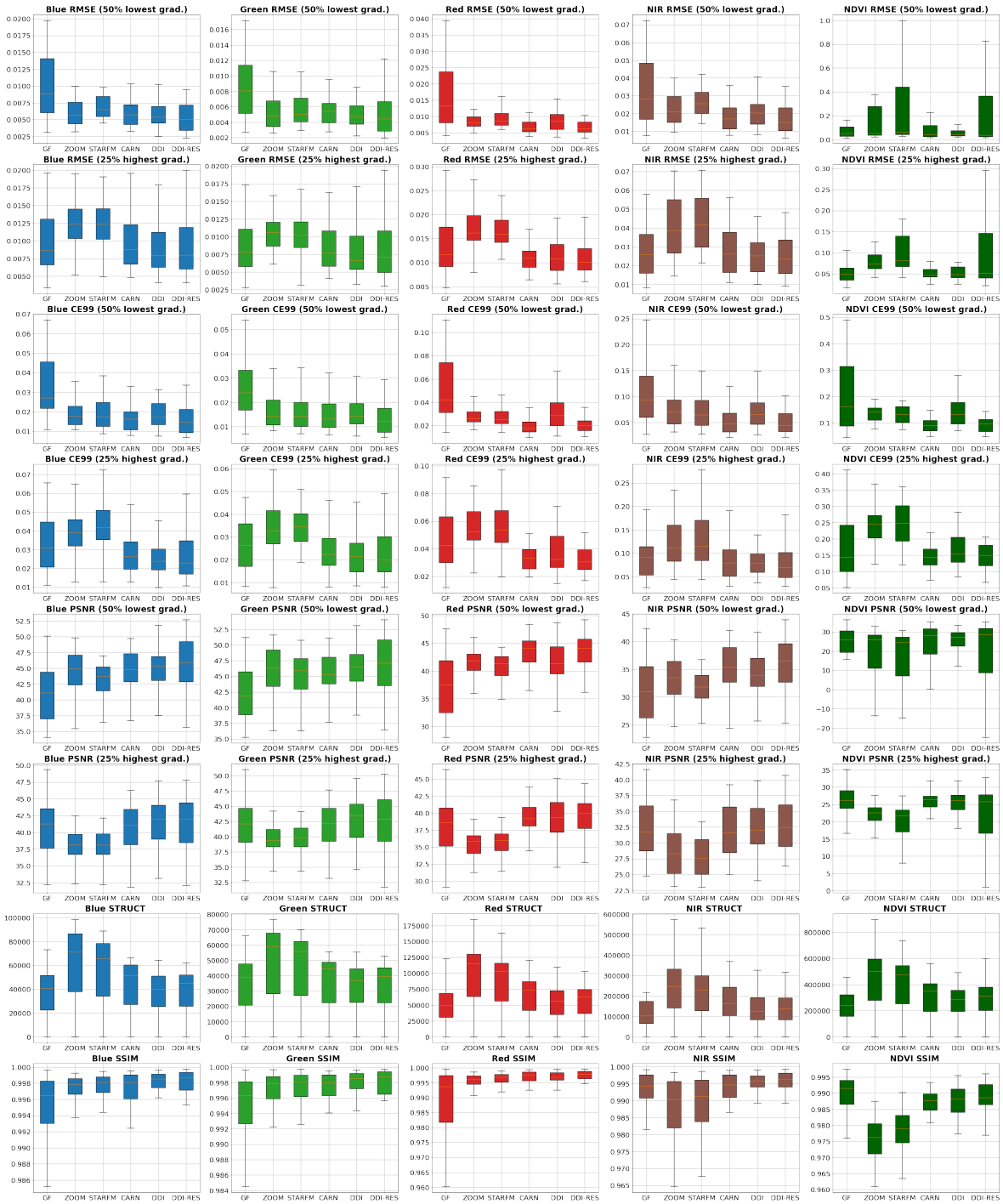

Figure 4.28: Box-plots of RMSE, CE99 absolute error and PSNR for 50% lowest gradients and 25% highest gradients, as well as SSIM and structural error, for Red, Green, Blue, Near Infra-Red and NDVI, on all sites, for methods linear interpolation (GF), cubic zoom (ZOOM), Single Image Super-Resolution (CARN), STARFM (STARFM), Data-Driven Interpolation (DDI) and Data-Driven Interpolation with residuals compensation (DDI-R), with a resolution ratio of 2.5 (12.5m $\rightarrow$ 5m).

4.4.3 Qualitative Analysis

Figures 4.29 to 4.31 show sample predictions for all sites and methods. The conclusions from the quantitative analysis in section 4.4.2 are confirmed by the visual inspection of those samples.

Linear gap-filling has the best high-frequency content. This can be seen in the difference between prediction and Venμs reference image, which does not exhibit the typical gradient patterns occurring when high frequency content is different. However, linear gap-filling is also the method with the largest local errors. It completely misses some landscape changes. This is especially salient in figures 4.29a, 4.29b and 4.31, where phenology of some crops is completely missed by the algorithm.

If we look at CARN predictions, we can see that for a resolution ratio of 5, they exhibit good radiometric fidelity but strong ringing artifacts along edges.Predictions look smoother than the reference image. Those effects (ringing and smoothness) partly disappear for a resolution ratio of 2.5, for which CARN provide sharp predictions that competes with DDI-R.

Regarding the STARFM method, it never reaches the sharpness of DDI-R or CARN, for both resolution ratios. It also exhibits a loss of textures. Nevertheless it provides good radiometric fidelity and consistent results for a fair price, being less computationally intensive than those two methods.

For a resolution ratio of 5, DDI with residuals compensation offers both sharp images and radiometric fidelity, and is therefore the best method. If the resolution ratio is 2.5, it offers performances similar to CARN, or even slightly worse sometimes. Nevertheless, the ringing artifacts of CARN are still present at this resolution ratio and is absent from DDI predictions. In addition, lets remind that DDI is able to interpolate cloudy areas (if there are enough clear pixels for the target date), something CARN is not able to do.

Finally, let's focus on figure 4.31, to highlight the fact that none of the investigated achieve satisfactory results here. Circular crops exhibit spatial heterogeneity, which are not captured accurately by any of the methods. Linear temporal interpolation completely misses those heterogeneous areas, while the other methods tend to miss the sharp transitions and offer only blurry edges.

4.4.4 Sensitivity to mis-registration

In order to assess the sensitivity of methods to mis-registration, we added registration noise of 1-pixel magnitude to the guide series on ARM site and computed the metrics again, for a resolution ratio of 2.5 (12.5m $\rightarrow$ 5m). Metrics are presented in figure 4.32. We can see that registration noise has a very high impact on DDI without residual compensation, which aligns with the worst method for almost all metrics and bands. Adding residual compensation brings DDI back to the top group, but still worse than CARN anyway. This is expected since DDI is the method that uses the full extent of the time-series, and as such will suffer the most from spatial mis-registration across series. We must also stress that CARN is by design tolerant to registration noise in guide series at inference time, but would probably be sensitive to mis-registration between high-resolution and low-resolution patches during offline training.

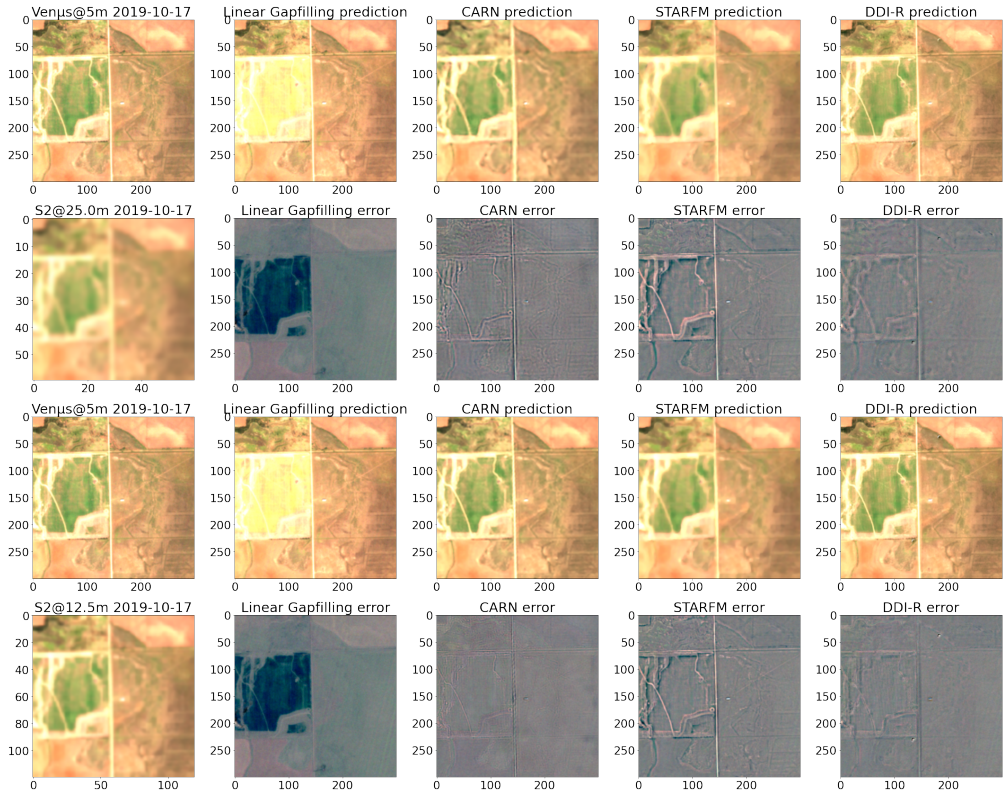

(a) ARM site, resolution ratio of 5 (top) and 2.5 (bottom)

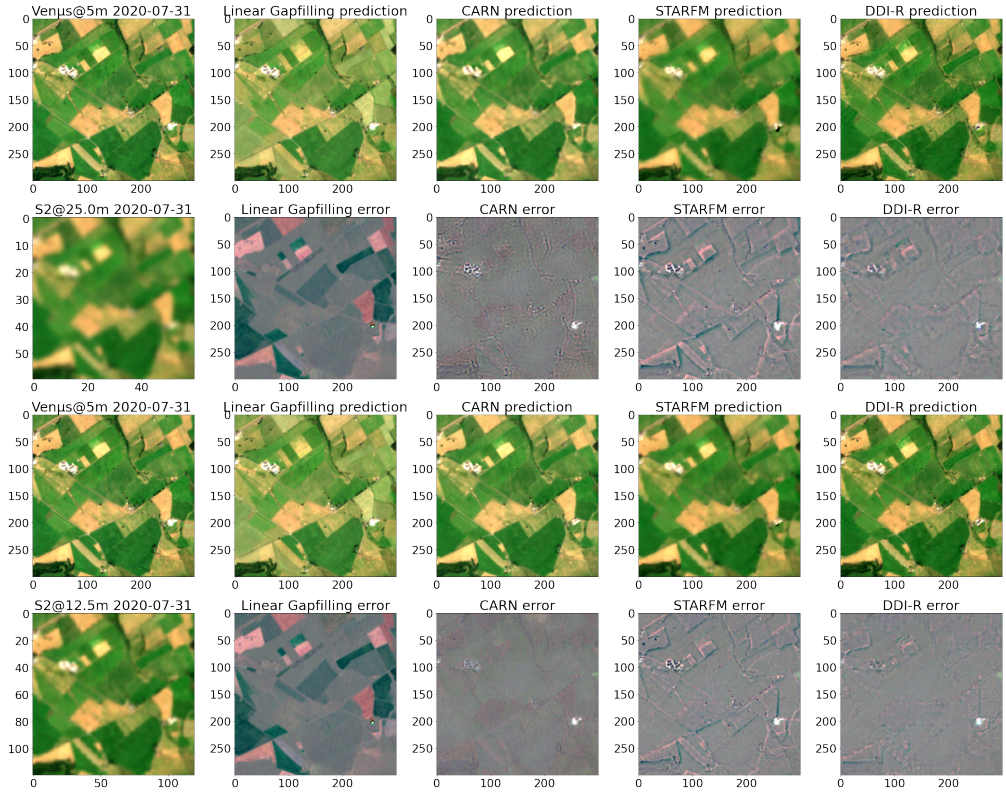

(b) ARM site, resolution ratio of 5 (top) and 2.5 (bottom)

Figure 4.29: Sample predictions for all methods on ARM and FR-LQ1 sites.

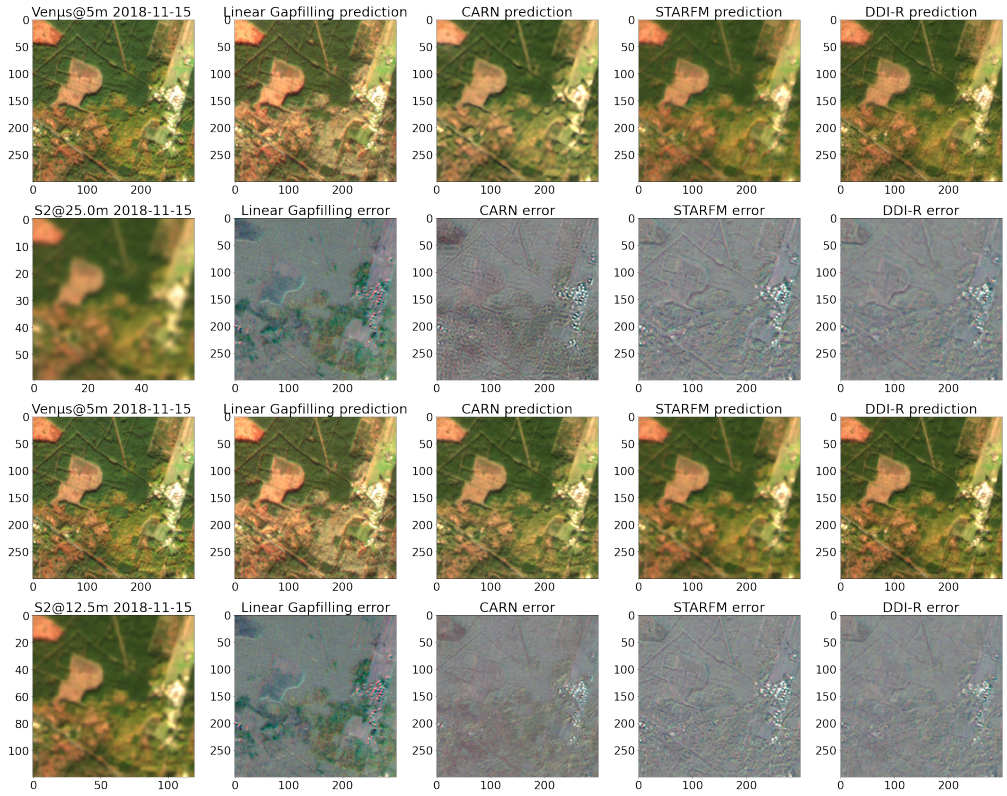

(a) ESGISB-2 site, resolution ratio of 5 (top) and 2.5 (bottom)

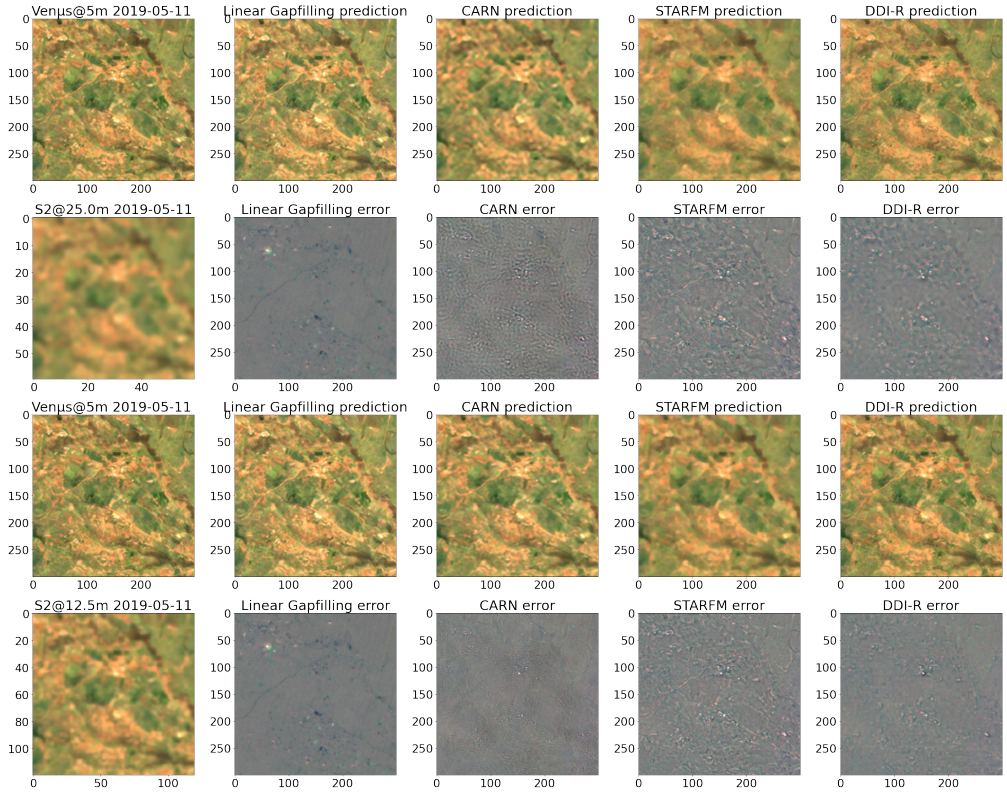

(b) MAD-AMBO site, resolution ratio of 5 (top) and 2.5 (bottom)

Figure 4.30: Sample predictions for all methods on ESGISB-2 and MAD-AMBO sites.

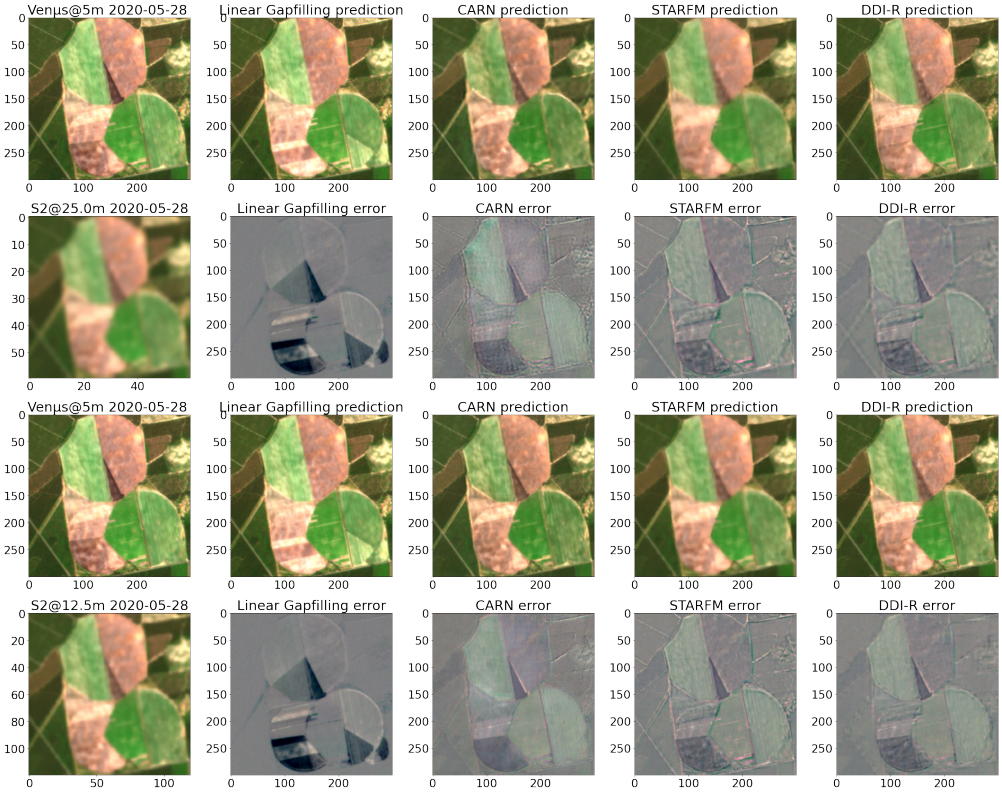

Figure 4.31: Sample predictions for all methods on FR-BIL site, resolution ratio of 5 (top) and 2.5 (bottom)

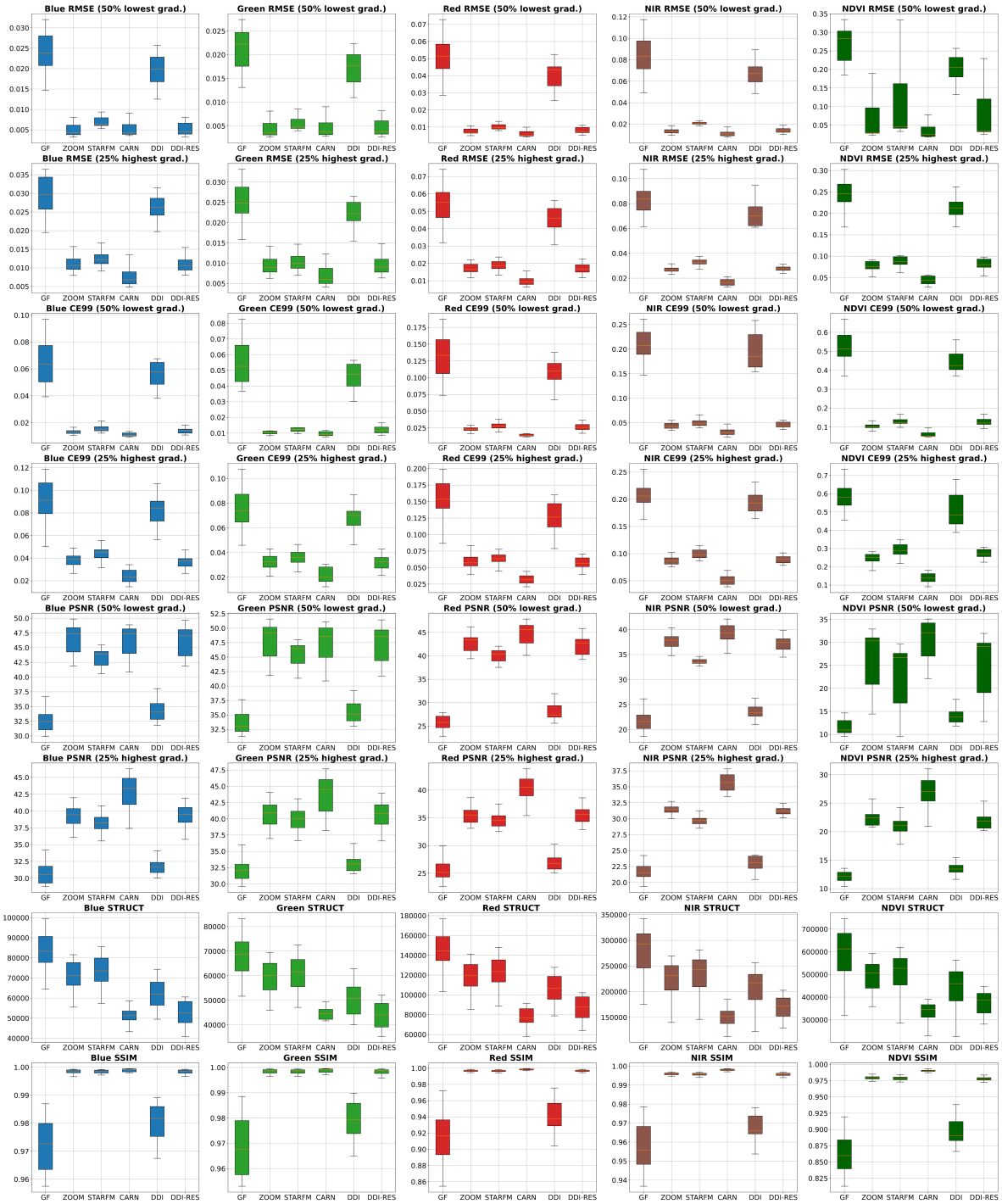

Figure 4.32: Performances on ARM site with a registration noise of 1 pixel magnitude on guide series. Box-plots of RMSE, CE99 absolute error and PSNR for 50% lowest gradients and 25% highest gradients, as well as SSIM and structural error, for Red, Green, Blue, Near Infra-Red and NDVI, on all sites, for methods linear interpolation (GF), cubic zoom (ZOOM), Single Image Super-Resolution (CARN), STARFM (STARFM), Data-Driven Interpolation (DDI) and Data-Driven Interpolation with residuals compensation (DDI-R), with a resolution ratio of 2.5 (12.5m $\rightarrow$ 5m).

4.5 Conclusions

In this section, we investigated the possibility of deriving hybrid products by merging the foreseen Sentinel-HR time-series with Sentinel2 or Sentinel2 NG time-series, in order to get the highest spatial resolution and a better revisit time. This is important for applications that require a revisit better than 20 days, but also because of the gaps caused by the occurrence of clouds.

We demonstrated that this fusion process was possible with acceptable performances, using machine-learning based methods. For a resolution ratio of 5, the DDI method really stands out, with the additional benefit of being able to interpolate partly cloudy scene (but not scenes that will be fully cloudy). For a resolution ratio of 2.5, the Single Image Super-Resolution algorithm (CARN) is a very interesting option given its simplicity: the intensive computations and large data consumption occur in the offline training phase, while only the low resolution image at target date is required). We used the CodeCarbon library to estimate energy consumption of all predictions for ARM series and resolution ratio of 2.5, and DDI indeed appears to be twice has much expensive as CARN (see figure 4.33).

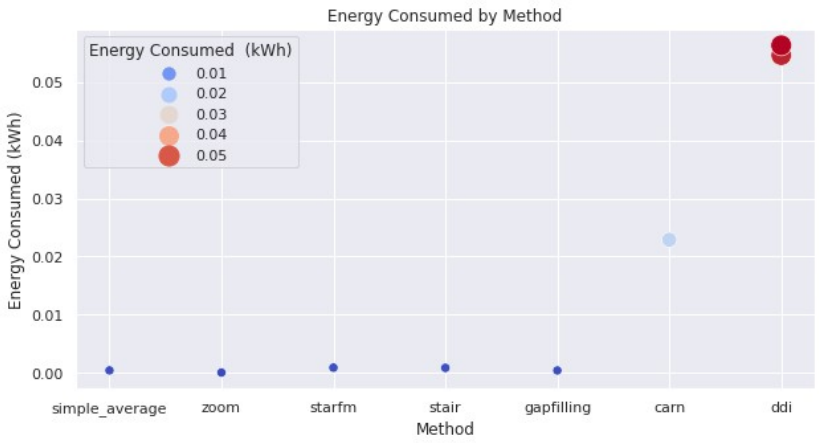

Figure 4.33: Ernergy consumption estimations with CodeCarbon for prediction of the full ARM series with resolution ratio of 2.5

The results presented here, as well as the methodology, have a few limitations. First, we must stress that if CE99 performances are really good for red, green and blue bands, they are twice as worse for near-infra red channel. This can probably be explained by the wider near-infra red 10m band in Sentinel2, compared to the Venμs near infra red bandwidth. Nevertheless, if two time-series from optical satellites have to merged with those methods, it demonstrates that spectral consistency between sensors is important and should be included in the missions design if possible.

We should also stress that we used highly coherent data, with constant viewing angles, and which have been processed by the same software from L1C to L2A. Venμs has a very good multi-temporal spatial registration, and we have seen in section 4.4.4 that performances of DDI would be largely impacted by a registration noise of about 1 pixel in Sentinel-HR series. But the biggest concern is with the resolution: because of the lack of 2 meters resolution data, we worked at 5 meters resolution, and can only infer that those results would apply at the finer resolution of 2 meters. Spatial registration issues and parallax angular effects will

be more important at 2 meters resolution, and those results should be consolidated at this spatial resolution, maybe by leveraging specific commercial VHR acquisitions.

The proposed DDI architecture is quite young, and we envision a lot of research activities to improve its performances, capabilities and efficiency. On the Single Image Super Resolution side, we are currently preparing the release of a data set based on VENµS and S2 data, to be used as a benchmark for the research community. It will help assessing the performances of state of the art methods and working on improving them.

Chapter 5

Conclusions

In this phase 0 study, we investigated Sentinel-HR, a 2 meter resolution optical and stereoscopic mission with a global, constant viewing angle coverage and 20 days revisit, that would serve as a companion to Sentinel2 or Sentinel2 NG depending on the launch date.

5.1 Mission design

We proposed two alternative designs for the Sentinel-HR mission. The first design is based on a pair of ad-hoc satellites flying at 780 kilometers. Though feasible, this design is highly demanding in terms of focal plane design because of the constraints of both large field of view and stereoscopic focal plane. In this case, resolution will be limited to no less than 2 meters and stereoscopic baseline ratio will be no more than 0.035. Simulations show that the expected accuracy of DEM will be well beyong 4 meters CE90 accuracy, if we account for geometric instabilities (focal plane and attitude stability). A less demanding configuration would require to use two different instruments for stereoscopic acquisitions, in which case the instrument can reach 2 meter resolution and there is no constraints on baseline ratio. This solution comes at the expense of the additional weight and volume of the second instrument. This is the solution that was retained, with parameters summarized in table 5.1. In both cases, telemetry will be huge and will require complex systems onboard and on ground.

The second design is based on the re-use of the CO3D constellation small satellites. Along with the C03D engineering team, we estimated that a 2 meters, 3D-enabled Sentinel-HR would be feasible with 12 (6 pairs) of such satellites, orbiting at an altitude of 845km instead of 580km for CO3D. Modifications of those satellites will be required on both the instrument, in order to reduce the focal length and maybe replace the detectors with push-frame matrix to meet radiometric specifications, and orbit, in order to fly at an altitude allowing required coverage. Even with those adaptations, this solution will likely be cheaper than the previous design. Additionally, if we relax the revisit constraint on the 3D part to 40 days, we can save 3 extra satellites and do the mission with only 9 satellites.

An important outcome of this preliminary mission design is that it would be difficult and costly to improve Sentinel-HR resolution to 1m.

At 2 m resolution, the Sentinel-HR mission is feasible, with costs similar to a Sentinel-expansion mission. With the CO3D solution, we could save costs and do the mission in a shorter delay, before 2028 if funding is available quickly.

	Monoscopic Push-frame
Telescope	TMA
Altitude	794 km
Aperture	10.7
Pupil diameter	26 cm
Focal length	1.39 m
Resolution	2m
Detector size	3.5 µm
Field of view	70 km, 5°, 35e3 pixels
B/H	No constraints
Volume	650x1170x1300 mm^3 ×2
Mass	≈ 150 kg ×2
Number of cameras	2 (stereo)

Table 5.1: Main parameters for final design choice

5.2 Hybrid products expected performances

We investigated the potential of combined Sentinel-HR and Sentinel2 (NG) products in order to increase the temporal resolution of high resolution observations, either to compensate for clouds induced gaps or to increase temporal resolution beyond Sentinel-HR native revisit in order to meet requirements of some applications. This study has been carried out by using Venµs and Sentinel2 time series as a proxy.

Our results show that with carefully cross-calibrated and spatially registered, constant viewing angle time series, there is a benefit in using any fusion method with respect to temporal interpolation of the Sentinel-HR series or spatial interpolation of the Sentinel 2 (NG) series. Given the 2 meter resolution outcome of the mission design study, a ratio of 5 in resolution (for Sentinel-HR vs. Sentinel2) and 2.5 in resolution (for Sentinel-HR vs. Sentinel2 NG) have been investigated.

With a resolution ratio of 5, there is a clear interest in combining both series with machine learning driven method such as DDI. This comes with the additional benefit of getting cloud removal for partly cloudy scenes. If the resolution ratio is only 2.5, Single Image Super-Resolution becomes a competitive solution, with less complexity at inference time and performances similar to machine learning fusion of series.

As a conclusion, the study of spatio-temporal fusion of Sentinel-2 and Sentinel-HR concludes on the feasibility and interest of this methodology.

5.3 User requirements

We consolidated the user requirements by setting up a Mission Advisory Group that allowed to identify 11 use cases addressing a wide range of applications, for which the target indicators were identified, along with their coverage, expected accuracy and readiness level. Benefits and limits of Sentinel-HR have been clearly identified. With the outcome of the mission design and hybrid products performances, we can revisit the expected accuracies as well as identify benefits and limitations of Sentinel-HR, summarized in table 5.2.

Theme	Benefits	Limitations
Glaciers	Estimating glacier volume change or mass balance globally with a seasonal frequency and at high resolution. Provide frequent real ortho-images, generated from a synchronous DSM	Stereo capability is mandatory 2m resolution only acceptable with higher baseline ratios Revisit will only allow one clear image per trimester
Ice sheets	Repetitive simultaneous measurements of horizontal displacement and altitude changes. Complement current altimetry data (CryoSat-2, IceSat)	Stereo capability is mandatory
Water Bodies	Map all small water bodies (S2NG resolution will be insufficient)	20 days revisit too high for water bodies dynamics No SWIR band for water detection
Urban	Yearly monitoring achievable Timing of change Description at parcel level	Height accuracy limited for urban changes The smaller resolution the better
Urban vegetation	Revisit makes quarterly monitoring achievable Revisit will give access to phenology Spatial resolution good enough 4m CE90 DEM should allow to monitor urban trees	The smaller resolution the better Number of bands can be limiting for some species
Herbaceous	Seasonal monitoring achievable Metric level description Synergy with S2 (NG) should give monthly monitoring DEM can help delimit encroachments	Revisit insufficient for intra-annual cycle Number of bands can be limiting for some species DEM accuracy is a potential limit for heterogeneous vegetation mosaics
Agricultural	2m resolution along growing season will allow to monitor structural features	Revisit can be insufficient for intra-parcel phenology Resolution can be too coarse for some row cultures Limited number of spectral bands
Forest	Single recurrent source for DSM and metric imagery Constant nadir view angle	No Red-Edge or SWIR Phenological differences between species (< 20 days) will not be detectable Height accuracy and spatial resolution will be inadequate for young trees and some hedgerows
Erosion	Repeating observations with a metric accuracy Time series of DTM	Metric resolution is critical Relative accuracy of DSM is critical and should not exceed the 3m specification
Land-sea cont.	Monthly and seasonal monitoring available Resolution sufficient for bathymetry	Constraints on stereo angle and duration between each stereo image wrt. typical wave kinematic
Geo-hazard	Will allow for 2 months global geohazard monitoring	The smaller resolution the better
Crisis and risks	Up-to-date imagery and derived maps	20 days revisit for crisis images Resolution should be kept $\leq$ 2m Lack of SWIR band

Table 5.2: Summary of Sentinel-HR benefits and limitations for all investigated use cases.

We can see that most of use cases stress the great benefit of having regular nadir observations at metric resolution. In the different fields, this enables applications at global scale that are out of reach with other missions, including the foreseen Sentinel2 NG. A lot of use cases stress that synchronous DSM acquisitions is a key element of the mission which further unlocks monitoring possibilities.

Most limitations fall into one of the four following categories:

- Resolution of 2 meters might be insufficient
- Revisit of 20 days might be insufficient
- Lack of specific spectral bands (Red-Edge, SWIR)
- DSM accuracy might be too low

Regarding resolution, the impact of enhancing spatial resolution to 1 meter is tremendous: in the ad-hoc satellite design, the instrument is highly constrained by the large field of view. A new study would be required, but most probably swath, resolution and in field of view stereoscopy is not feasible with a single instrument. However, if stereoscopy is achieved by using two instruments, reaching 1m resolution might be possible at the expense of weight and volume. In any case, Telemetry will be doubled, which will require even more complex communications. On the CO3D-based design, a resolution of 1 meter might be reachable but will require to at least double the number of satellites, provided the memory, step and stare frequency and telemetry allow the satellite to observe continuously during the orbit.

Regarding the increase of the revisit, and to a less extent, the absence of some specific spectral bands, even if they are not as perfect as real measurements, hybrid products are an interesting option (as mentioned in some use cases). Our study demonstrates that we might be able to generate cloud free time series combining the revisit of Sentinel2 (NG) and the spatial resolution of Sentinel-HR. The question of quality of such hybrid product with respect to requirements of a given application will need to be further investigated. It is noteworthy that some of the investigated methods would be able to estimate high resolution versions of spectral bands available on Sentinel2 (NG) but not on Sentinel-HR.

Last, regarding the DSM accuracy, even within the 4m CE90, even if our experiments showed that this specification might be reachable with a native stereoscopic instrument with baseline ratio of 0.035, this instrument is also very complex to design. This therefore pleads even more for a larger baseline ratio, and for a satellite with two monoscopic instruments in ad-hoc design, or for the design based on the re-use of C03D satellites. Note that the land-sea topography-bathymetry continuum use case relies on the capacity of using bursts of images, which will be limited to 2 images (as in the Venμs case), even in the C03D configurations (CO3D can reach 5 bursts per second), because of the absence of tasking in Sentinel-HR.

To conclude, the work of Sentinel-HR mission group confirms that there is a missing link in the available optical remote sensing chain of missions, related to systematic imagery at 1-2m resolution, producing seasonal cloud free coverage delivered as free and open data.

Bibliography

[AAW09] Selim Aksoy, H Gökhan Akçay, and Tom Wassenaar. Automatic mapping of linear woody vegetation features in agricultural landscapes using very high resolution imagery. *IEEE Transactions on Geoscience and Remote Sensing*, 48(1):511–522, 2009.

[Abi06] R. Abileah. Mapping shallow water depth from satellite. *Proceedings of the ASPRS Annual Conference, Reno, Nevada*, pages 1–7, 2006.

[ABMd19] Rafael Almar, Erwin W.J. Bergsma, Philippe Maisongrande, and Luis Pedro Melo de Almeida. Wave-derived coastal bathymetry from satellite video imagery: A showcase with pleiades persistent mode. *Remote Sensing of Environment*, 231:111263, 2019.

[ACD+16] Iftikhar Ali, Fiona Cawkwell, Edward Dwyer, Brian Barrett, and Stuart Green. Satellite remote sensing of grasslands: from observation to management. *Journal of Plant Ecology*, 9(6):649–671, 2016.

[ACSGPP+16] Jaime Almonacid-Caballer, Elena Sánchez-García, Josep E. Pardo-Pascual, Angel A. Balaguer-Beser, and Jesús Palomar-Vázquez. Evaluation of annual mean shoreline position deduced from landsat imagery as a mid-term coastal evolution indicator. *Marine Geology*, 372:79–88, 2016.

[AH12] Frederic Achard and Matthew C Hansen. *Global forest monitoring from earth observation*. Taylor & Francis, 2012.

[AILB13] Marcela Arias, Jordi Inglada, R Lucas, and Palma Blonda. Hedgerow segmentation on vhr optical satellite images for habitat monitoring. In *2013 IEEE International Geoscience and Remote Sensing Symposium-IGARSS*, pages 3301–3304. IEEE, 2013.

[AK17] Bas Altena and Andreas Kääb. Elevation Change and Improved Velocity Retrieval Using Orthorectified Optical Satellite Data from Different Orbits. *Remote Sensing*, 9(3), 2017.

[AK20] Bas Altena and Andreas Kääb. Ensemble matching of repeat satellite images applied to measure fast-changing ice flow, verified with mountain climber trajectories on Khumbu icefall, Mount Everest. *Journal of Glaciology*, pages 1–11, 2020. Edition: 2020/08/11 Publisher: Cambridge University Press.

[AKB20] Saeed Anwar, Salman Khan, and Nick Barnes. A deep journey into super-resolution: A survey. *ACM Computing Surveys (CSUR)*, 53(3):1–34, 2020.

[AKS18] Namhyuk Ahn, Byungkon Kang, and Kyung-Ah Sohn. Fast, accurate, and lightweight super-resolution with cascading residual network. In *Proceedings of the European Conference on Computer Vision (ECCV)*, pages 252–268, 2018.

[ALDD12] P Allemand, E Lajeunesse, O Devauchelle, and C Delacourt. Erosion under extreme climatic events in tropical climates: the case of the storm helena (1963) in the guadeloupe island (lesser antilles arc). In *EGU General Assembly Conference Abstracts*, page 8835, 2012.

[Alm19] Almeida, LP. and Almar, Rafael and Bergsma, E. and Berthier, E. and Baptista, P.B. and Garel, E. and Dada, O. and Alves, B. High resolution coastal topography from satellite stereo imagery. *Remote sensing of Environment*, 11(5):590, 2019.

[ARN19] Rolland Amandine, Binet Renaud, and Bernardini Nicolo. DEM generation from native stereo Venμs acquisitions, November 2019.

[ASG+11] Philippe Apparicio, Anne-Marie Séguin, Martin Gagnon, et al. Mapping the greenscape and environmental equity in montreal: an application of remote sensing and gis. In *Mapping environmental issues in the city*, pages 30–48. Springer, 2011.

[ASS+12] Radhakrishna Achanta, Appu Shaji, Kevin Smith, Aurelien Lucchi, Pascal Fua, and Sabine Süsstrunk. Slic superpixels compared to state-of-the-art superpixel methods. *IEEE transactions on pattern analysis and machine intelligence*, 34(11):2274–2282, 2012.

[BAM19] Erwin W. J. Bergsma, Rafael Almar, and Philippe Maisongrande. Radon-augmented sentinel-2 satellite imagery to derive wave-patterns and regional bathymetry. *Remote Sensing*, 11(16), 2019.

[BAR+21] Erwin W.J. Bergsma, Rafael Almar, Amandine Rolland, Renaud Binet, Katherine L. Brodie, and A. Spicer Bak. Coastal morphology from space: A showcase of monitoring the topography-bathymetry continuum. *Remote Sensing of Environment*, 261:112469, 2021.

[BBB00] Jacques Baudry, RGH Bunce, and Françoise Burel. Hedgerows: an international perspective on their origin, function and management. *Journal of environmental management*, 60(1):7–22, 2000.

[BBM+17] J. M. C. Belart, E. Berthier, E. Magnússon, L. S. Anderson, F. Pálsson, T. Thorsteinsson, I. M. Howat, G. Aðalgeirsdóttir, T. Jóhannesson, and A. H. Jarosch. Winter mass balance of Drangajökull ice cap (NW Iceland) derived from satellite sub-meter stereo images. *The Cryosphere*, 11(3):1501–1517, 2017.

[BBT+21] José I Barredo, Cristina Brailescu, Anne Teller, Francesco Maria Sabatini, Achille Mauri, and Klara Janouskova. Mapping and assessment of primary and old-growth forests in europe. 2021.

[BCF+19] Stéphanie Battiston, Stephen Clandillon, Robin Faivre, Claire Tinel, and Annett Wania. L'utilisation des services cartographiques numériques d'urgence par satellite à des fins de sécurité intérieure. In *Annales des Mines-Responsabilite et environnement*, number 2, pages 66–73. FFE, 2019.

[BCV+19] Jérôme Benveniste, Anny Cazenave, Stefano Vignudelli, Luciana Fenoglio-Marc, Rashmi Shah, Rafael Almar, Ole Andersen, Florence Birol, Pascal Bonnefond, Jérôme Bouffard, Francisco Calafat, Estel Cardellach, Paolo Cipollini, Gonéri Le Cozannet, Claire Dufau, Maria Joana Fernandes, Frédéric Frappart, James Garrison, Christine Gommenginger, Guoqi Han, Jacob L. Høyer, Villy Kourafalou, Eric Leuliette, Zhijin Li, Hubert Loisel, Kristine S. Madsen, Marta Marcos, Angélique Melet, Benoît Meyssignac, Ananda Pascual, Marcello Passaro, Serni Ribó, Remko Scharroo, Y. Tony Song, Sabrina Speich, John Wilkin, Philip Woodworth, and Guy Wöppelmann. Requirements for a coastal hazards observing system. *Frontiers in Marine Science*, 6:348, 2019.

[BDS14] Mariana Belgiu, Lucian Drăguţ, and Josef Strobl. Quantitative evaluation of variations in rule-based classifications of land cover in urban neighbourhoods using worldview-2 imagery. *ISPRS Journal of Photogrammetry and Remote Sensing*, 87:205–215, 2014.

[BFG+19] Stéphanie Battiston, Monika Friedemann, Daniel Gascón, Alberto Viseras, Adrián Cardil, Miguel Angelo Isidoro Mendes, Jordi Vendrell, Benjamin Barth, Edgar Nebot, Sandro Martinis, et al. Heimdall: A technological solution for multi-hazard management support including wildfires. 2019.

[BGBC14] Benoit Beguet, Dominique Guyon, Samia Boukir, and Nesrine Chehata. Automated retrieval of forest structure variables based on multi-scale texture analysis of vhr satellite imagery. *ISPRS journal of photogrammetry and remote sensing*, 96:164–178, 2014.

[BJTW11] Thomas Blaschke, Kasper Johansen, Dirk Tiede, and Q Weng. Object-based image analysis for vegetation mapping and monitoring. *Advances in environmental remote sensing: Sensors, algorithms, and applications*, 2010:241–272, 2011.

[Bla10] Thomas Blaschke. Object based image analysis for remote sensing. *ISPRS journal of photogrammetry and remote sensing*, 65(1):2–16, 2010.

[BLAD13] Adam M. Booth, Michael P. Lamb, Jean-Philippe Avouac, and Christophe Delacourt. Landslide velocity, thickness, and rheology from remote sensing: La clapiÃšre landslide, france. *Geophysical Research Letters*, 40(16):4299–4304, 2013.

[BLML19] Corentin Bolyn, Philippe Lejeune, Adrien Michez, and Nicolas Latte. Automated classification of trees outside forest for supporting operational management in rural landscapes. *Remote Sensing*, 11(10):1146, 2019.

[BS19] Mariana Belgiu and Alfred Stein. Spatiotemporal image fusion in remote sensing. *Remote sensing*, 11(7):818, 2019.

[BSV+17] Reubens Bert, Broekx Steven, Nelissen Victoria, Pardon Paul, Verheyen Kris, et al. Ecosystem service delivery of agri-environment measures: A synthesis for hedgerows and grass strips on arable land. *Agriculture, Ecosystems & Environment*, 244:32–51, 2017.

[BT05] Elizabeth H. Boak and Ian L. Turner. Shoreline Definition and Detection: A Review. *Journal of Coastal Research*, 2005(214):688 – 703, 2005.

[CA69] Albert Clos-Arceduc. *Essai d'explication des formes dunaires sahariennes.* l'Institut geographique national, 1969.

[CHP+18] Antoine Collin, James L. Hench, Yves Pastol, Serge Planes, Lauric Thiault, Russell J. Schmitt, Sally J. Holbrook, Neil Davies, and Matthias Troyer. High resolution topobathymetry using a pleiades-1 triplet: Moorea island in 3d. *Remote Sensing of Environment*, 208:109–119, 2018.

[CK18] Changhyun Choi and Duk-jin Kim. Optimum baseline of a single-pass in-sar system to generate the best dem in tidal flats. *IEEE Journal of Selected Topics in Applied Earth Observations and Remote Sensing*, 11(3):919–929, 2018.

[CKKM08] Casey Cleve, Maggi Kelly, Faith R Kearns, and Max Moritz. Classification of the wildland–urban interface: A comparison of pixel-and object-based classifications using high-resolution aerial photography. *Computers, Environment and Urban Systems*, 32(4):317–326, 2008.

[CMS+21] Bruno Castelle, Gerd Masselink, Tim Scott, Christopher Stokes, Aikaterini Konstantinou, Vincent Marieu, and Stéphane Bujan. Satellite-derived shoreline detection at a high-energy meso-macrotidal beach. *Geomorphology*, 383:107707, 2021.

[CS02] D Chen and Douglas Stow. The effect of training strategies on supervised classification at different spatial resolutions. *Photogrammetric Engineering and Remote Sensing*, 68(11):1155–1162, 2002.

[CSD+20] M Cournet, E Sarrazin, L Dumas, J Michel, J Guinet, D Youssefi, V Defonte, and Q Fardet. Ground truth generation and disparity estimation for optical satellite imagery. *The International Archives of Photogrammetry, Remote Sensing and Spatial Information Sciences*, 43:127–134, 2020.

[CW18] Gang Chen and Qihao Weng. Remote sensing of our changing landscapes with geographic object-based image analysis (geobia), 2018.

[CW20] Li Chu and Xiao-Jun Wu. Dimensionality reduction on the symmetric positive definite manifold with application to image set classification. *Journal of Electronic Imaging*, 29(4):1 – 13, 2020.

[CYS+15] Mathilde Caspard, Hervé Yesou, Arnaud Selle, Claire Tinel, Pierre Tessier, Arnaud Durand, Stephen Clandillon, and Paul de Fraipont. Forest recolonization monitoring based on hr and vhr imagery: the case of the maido forest fire exploiting pléiades hr and spot kalideos database. *Revue Française de Photogrammétrie et de Télédétection*, (209):149–155, 2015.

[DB13] C. Danilo and R. Binet. Bathymetry estimation from wave motion with optical imagery: influence of acquisition parameters. *IEEE Transactions on Geoscience and Remote Sensing*, pages 1–5, 2013.

[DBB+21] Christopher J Daly, Wassim Baba, Erwin Bergsma, Rafael Almar, and Thierry Garlan. The new era of regional coastal bathymetry from space: A showcase for west africa using sentinel-2 imagery. *Remote Sensing of Environment*, 2021.

[DF16] C. Danilo and M. Farid. Wave period and coastal bathymetry using wave propagation on optical images. *IEEE Transactions on Geoscience and Remote Sensing*, 54.11:6307–6319, 2016.

[DFC02] David Doxaran, J-M Froidefond, and P Castaing. A reflectance band ratio used to estimate suspended matter concentrations in sediment-dominated coastal waters. *International Journal of Remote Sensing*, 23(23):5079–5085, 2002.

[DFST+13] H De Foresta, E Somarriba, A Temu, D Boulanger, H Feuilly, M Gauthier, and D Taylor. Towards the assessment of trees outside forests: a thematic report prepared in the framework of the global forest resources assessment 2010. *Forest Resources Assessment Working Paper (FAO)*, 2013.

[DGG+19] Amaury Dehecq, Noel Gourmelen, Alex S. Gardner, Fanny Brun, Daniel Goldberg, Peter W. Nienow, Etienne Berthier, Christian Vincent, Patrick Wagnon, and Emmanuel Trouvé. Twenty-first century glacier slowdown driven by mass loss in High Mountain Asia. *Nature Geoscience*, 12(1):22–27, 2019.

[DHK+18] Gérard Dedieu, Olivier Hagolle, Arnon Karnieli, Pierric Ferrier, Philippe Crébassol, Philippe Gamet, Camille Desjardins, Moti Yakov, Merav Cohen, and Ehud Hayun. Venμs: Performances and first results after 11 months in orbit. In *IGARSS 2018 - 2018 IEEE International Geoscience and Remote Sensing Symposium*, pages 7756–7759, 2018.

[DRM+18] Jeroen Degerickx, Dar A Roberts, Joe P McFadden, Martin Hermy, and Ben Somers. Urban tree health assessment using airborne hyperspectral and lidar imagery. *International journal of applied earth observation and geoinformation*, 73:26–38, 2018.

[FAB+12] Mathieu Fauvel, Benoit Arbelot, Jón Atli Benediktsson, David Sheeren, and Jocelyn Chanussot. Detection of hedges in a rural landscape using a local orientation feature: from linear opening to path opening. *IEEE Journal of Selected Topics in Applied Earth Observations and Remote Sensing*, 6(1):15–26, 2012.

[FAO15] FAO. Fao forestry paper no. 1, 2015.

[FB84] Richard TT Forman and Jacques Baudry. Hedgerows and hedgerow networks in landscape ecology. *Environmental management*, 8(6):495–510, 1984.

[FBC+17] Denis Felikson, Timothy C Bartholomaus, Ginny A Catania, Niels J Korsgaard, Kurt H Kjær, Mathieu Morlighem, Brice Noël, Michiel Van Den Broeke, Leigh A Stearns, Emily L Shroyer, et al. Inland thinning on the greenland ice sheet controlled by outlet glacier geometry. *Nature Geoscience*, 10(5):366–369, 2017.

[FCD+10] Pierric Ferrier, Philippe Crebassol, Gérard Dedieu, Olivier Hagolle, Aimé Meygret, Francesc Tinto, Yoram Yaniv, and Jacob Herscovitz. Venμs (vegetation and environment monitoring on a new micro satellite). In *2010 IEEE International Geoscience and Remote Sensing Symposium*, pages 3736–3739. IEEE, 2010.

[FDG17] Adrian Fisher, Tim Danaher, and Tony Gill. Mapping trees in high resolution imagery across large areas using locally variable thresholds guided by medium resolution tree maps. *International journal of applied earth observation and geoinformation*, 58:86–96, 2017.

[FHF+19] Daniel Farinotti, Matthias Huss, Johannes J. Fürst, Johannes Landmann, Horst Machguth, Fabien Maussion, and Ankur Pandit. A consensus estimate for the ice thickness distribution of all glaciers on Earth. *Nature Geoscience*, February 2019.

[FLD+20] Mathieu Fauvel, Mailys Lopes, Titouan Dubo, Justine Rivers-Moore, Pierre-Louis Frison, Nicolas Gross, and Annie Ouin. Prediction of plant diversity in grasslands using sentinel-1 and-2 satellite image time series. *Remote Sensing of Environment*, 237:111536, 2020.

[FLS+16] Fabian Ewald Fassnacht, Hooman Latifi, Krzysztof Stereńczak, Aneta Modzelewska, Michael Lefsky, Lars T Waser, Christoph Straub, and Aniruddha Ghosh. Review of studies on tree species classification from remotely sensed data. *Remote Sensing of Environment*, 186:64–87, 2016.

[FM04] Giles M Foody and Ajay Mathur. Toward intelligent training of supervised image classifications: directing training data acquisition for svm classification. *Remote Sensing of Environment*, 93(1-2):107–117, 2004.

[FM18] V Faure-Muntian. Les données géographiques souveraines–rapport au gouvernement. *Paris, ministère de la Transition écologique et solidaire*, 2018.

[FMW+20] Fang Fang, Brenden McNeil, Timothy Warner, Gregory Dahle, and Earl Eutsler. Street tree health from space? an evaluation using worldview-3 data and the washington dc street tree spatial database. *Urban Forestry & Urban Greening*, 49:126634, 2020.

[FRHM21] James M. Fitton, Alistair F. Rennie, Jim D. Hansom, and Freya M.E. Muir. Remotely sensed mapping of the intertidal zone: A sentinel-2 and google earth engine methodology. *Remote Sensing Applications: Society and Environment*, 22:100499, 2021.

[FSM+16a] Mark Fahnestock, Ted Scambos, Twila Moon, Alex Gardner, Terry Haran, and Marin Klinger. Rapid large-area mapping of ice flow using Landsat 8. *Remote Sensing of Environment*, 185:84–94, 2016.

[FSM+16b] Mark Fahnestock, Ted Scambos, Twila Moon, Alex Gardner, Terry Haran, and Marin Klinger. Rapid large-area mapping of ice flow using landsat 8. *Remote Sensing of Environment*, 185:84–94, 2016.

[FSW+18] Peter Friedl, Thorsten C Seehaus, Anja Wendt, Matthias H Braun, and Kathrin Höppner. Recent dynamic changes on fleming glacier after the disintegration of wordie ice shelf, antarctic peninsula. *The Cryosphere*, 12(4):1347–1365, 2018.

[GBALB20] Carlos Granero-Belinchon, Karine Adeline, Aude Lemonsu, and Xavier Briottet. Phenological dynamics characterization of alignment trees with sentinel-2 imagery: a vegetation indices time series reconstruction methodology adapted to urban areas. *Remote Sensing*, 12(4):639, 2020.

[GBvL05] Carla J Grashof-Bokdam and Frank van Langevelde. Green veining: landscape determinants of biodiversity in european agricultural landscapes. *Landscape Ecology*, 20(4):417–439, 2005.

[GKA12] Feng Gao, William P. Kustas, and Martha C. Anderson. A data mining approach for sharpening thermal satellite imagery over land. *Remote Sensing*, 4(11):3287–3319, 2012.

[GMA08] Barnérias C. Germaine M.-A., Puissant A. Intérêt des données images et des sig pour l'extraction et l'identification des formations végétales arborées en milieu bocager. exemples bas-normands. *Revue Forestière Française*, (5):646–651, 2008.

[GMG+19] Massimiliano Gargiulo, Antonio Mazza, Raffaele Gaetano, Giuseppe Ruello, and Giuseppe Scarpa. Fast super-resolution of 20 m sentinel-2 bands using convolutional neural networks. *Remote Sensing*, 11(22):2635, 2019.

[GMSH06] Feng Gao, Jeff Masek, Matt Schwaller, and Forrest Hall. On the blending of the landsat and modis surface reflectance: Predicting daily landsat surface reflectance. *IEEE Transactions on Geoscience and Remote sensing*, 44(8):2207–2218, 2006.

[GPP05] Manuel Garcin, Blanche Poisson, and Richard Pouget. High rates of geomorphological processes in a tropical area: the remparts river case study (réunion island, indian ocean). *Geomorphology*, 67(3-4):335–350, 2005.

[HBM+19] Regine Hock, Andrew Bliss, Ben Marzeion, Rianne H. Giesen, Yukiko Hirabayashi, Matthias Huss, Valentina Radic, and Aimee B. A. Slangen. GlacierMIP - A model intercomparison of global-scale glacier mass-balance models and projections. *Journal of Glaciology*, 65(251):453–467, 2019. Place: Cambridge Publisher: Cambridge Univ Press WOS:000470734900008.

[HdL+18] Gerben Hagenaars, Sierd de Vries, Arjen P. Luijendijk, Wiebe P. de Boer, and Ad J.H.M. Reniers. On the accuracy of automated shoreline detection derived from satellite imagery: A case study of the sand motor mega-scale nourishment. *Coastal Engineering*, 133:113–125, 2018.

[HHF+19] Alexander L Handwerger, Mong-Han Huang, Eric Jameson Fielding, Adam M Booth, and Roland Bürgmann. A shift from drought to extreme rainfall drives a stable landslide to catastrophic failure. *Scientific reports*, 9(1):1–12, 2019.

[HK12] T. Heid and A. Kääb. Evaluation of existing image matching methods for deriving glacier surface displacements globally from optical satellite imagery. *Remote Sensing of Environment*, 118:339–355, March 2012.

[HMB+21a] Romain Hugonnet, Robert McNabb, Etienne Berthier, Brian Menounos, Christopher Nuth, Luc Girod, Daniel Farinotti, Matthias Huss, Ines Dussaillant, Fanny Brun, et al. Accelerated global glacier mass loss in the early twenty-first century. *Nature*, 592(7856):726–731, 2021.

[HMB+21b] Romain Hugonnet, Robert McNabb, Etienne Berthier, Brian Menounos, Christopher Nuth, Luc Girod, Daniel Farinotti, Matthias Huss, Ines Dussaillant, Fanny Brun, and Andreas Kääb. Accelerated global glacier mass loss in the early twenty-first century. *Nature*, 592(7856):726–731, 2021.

[HPC+21] Yousra Hamrouni, Eric Paillassa, Véronique Chéret, Claude Monteil, and David Sheeren. From local to global: A transfer learning-based approach for mapping poplar plantations at national scale using sentinel-2. *ISPRS Journal of Photogrammetry and Remote Sensing*, 171:76–100, 2021.

[HS07] R.A. Holman and J. Stanley. The history and technical capabilities of argus. *Coastal Engineering*, 54(6):477–491, 2007. The CoastView Project: Developing coastal video monitoring systems in support of coastal zone management.

[HSP+19] Yousra Hamrouni, David Sheeren, Eric Paillassa, Veronique Cheret, and Claude Monteil. Active learning for large-scale classification of poplar plantations with sentinels time series. In *ESA Living Planet Symposium 2019*, 2019.

[HZOH+05] C Huggel, S Zgraggen-Oswald, W Haeberli, A Kääb, A Polkvoj, I Galushkin, and SG Evans. The 2002 rock/ice avalanche at kolka/karmadon, russian caucasus: assessment of extraordinary avalanche formation and mobility, and application of quickbird satellite imagery. *Natural Hazards and Earth System Sciences*, 5(2):173–187, 2005.

[IAK12] Markus Immitzer, Clement Atzberger, and Tatjana Koukal. Tree species classification with random forest using very high spatial resolution 8-band worldview-2 satellite data. *Remote sensing*, 4(9):2661–2693, 2012.

[IAS20] Joubert-Boitat Inès, Wania Annett, and Dalmasso Simone. Manual for cems-rapid mapping products. 2020.

[JH15] P. Jagalingam and Arkal Vittal Hegde. A review of quality metrics for fused image. *Aquatic Procedia*, 4:133–142, 2015. INTERNATIONAL CONFERENCE ON WATER RESOURCES, COASTAL AND OCEAN ENGINEERING (ICWRCOE'15).

[JSSF20] Ian Joughin, David E Shean, Benjamin E Smith, and Dana Floricioiu. A decade of variability on jakobshavn isbræ: ocean temperatures pace speed through influence on mélange rigidity. *The cryosphere*, 14(1):211–227, 2020.

[J10] Bohumír Janský, Miroslav Šobr, and Zbyněk Engel. Outburst flood hazard: Case studies from the tien-shan mountains, kyrgyzstan. *Limnologica*, 40(4):358–364, 2010.

[KAD+19] Md Jamal Uddin Khan, MD Nazmuddoha Ansary, Fabien Durand, Laurent Testut, Marufa Ishaque, Stéphane Calmant, Yann Krien, A.K.M. Saiful Islam, and Fabrice Papa. High-resolution intertidal topography from sentinel-2 multi-spectral imagery: Synergy between remote sensing and numerical modeling. *Remote Sensing*, 11(24), 2019.

[KC21] R Knowelden and AG Castriotta. Copernicus sentinel data access 2020 annual report. *available online*, 2021.

[KD05] Karim Kelfoun and Timothy H Druitt. Numerical modeling of the emplacement of socompa rock avalanche, chile. *Journal of Geophysical Research: Solid Earth*, 110(B12), 2005.

[KDF+19] Nicolas Karasiak, Jean-François Dejoux, Mathieu Fauvel, Jérôme Willm, Claude Monteil, and David Sheeren. Statistical stability and spatial instability in mapping forest tree species by comparing 9 years of satellite image time series. *Remote Sensing*, 11(21):2512, 2019.

[KEF19] Teja Kattenborn, Jana Eichel, and Fabian Ewald Fassnacht. Convolutional neural networks enable efficient, accurate and fine-grained segmentation of plant species and communities from high-resolution uav imagery. *Scientific reports*, 9(1):1–9, 2019.

[KHC+20] Michalea D King, Ian M Howat, Salvatore G Candela, Myoung J Noh, Seongsu Jeong, Brice PY Noël, Michiel R van den Broeke, Bert Wouters, and Adelaide Negrete. Dynamic ice loss from the greenland ice sheet driven by sustained glacier retreat. *Communications Earth & Environment*, 1(1):1–7, 2020.

[KHCK+16] Harshinie Karunarathna, Jose Horrillo-Caraballo, Yoshiaki Kuriyama, Hajime Mase, Roshanka Ranasinghe, and Dominic E. Reeve. Linkages between sediment composition, wave climate and beach profile variability at multiple timescales. *Marine Geology*, 381:194–208, 2016.

[KHD06] François Kayitakire, C Hamel, and Pierre Defourny. Retrieving forest structure variables based on image texture analysis and ikonos-2 imagery. *Remote sensing of environment*, 102(3-4):390–401, 2006.

[KJS+17] LM Kehrl, Ian Joughin, DE Shean, Dana Floricioiu, and Lukas Krieger. Seasonal and interannual variabilities in terminus position, glacier velocity, and surface elevation at helheim and kangerlussuaq glaciers from 2008 to 2016. *Journal of Geophysical Research: Earth Surface*, 122(9):1635–1652, 2017.

[KL21] Ioannis Kotaridis and Maria Lazaridou. Remote sensing image segmentation advances: A meta-analysis. *ISPRS Journal of Photogrammetry and Remote Sensing*, 173:309–322, 2021.

[KLZ+21] Ya Kang, Zhong Lu, Chaoying Zhao, Yuankun Xu, Jin-woo Kim, and Alan J Gallegos. Insar monitoring of creeping landslides in mountainous regions: A case study in eldorado national forest, california. *Remote Sensing of Environment*, 258:112400, 2021.

[Kom98] P.D. Komar. *Beach Processes and Sedimentation, 2nd edition.* Prentice-Hall, 1998.

[KRS+11] David Kleijn, Maj Rundlöf, Jeroen Scheper, Henrik G Smith, and Teja Tscharntke. Does conservation on farmland contribute to halting the biodiversity decline? *Trends in ecology & evolution*, 26(9):474–481, 2011.

[KZAB20] Mahmoud M Khattab, Akram M Zeki, Ali A Alwan, and Ahmed S Badawy. Regularization-based multi-frame super-resolution: A systematic review. *Journal of King Saud University-Computer and Information Sciences*, 32(7):755–762, 2020.

[Lac16] Pascal Lacroix. Landslides triggered by the gorkha earthquake in the langtang valley, volumes and initiation processes. *Earth, Planets and Space*, 68(1):1–10, 2016.

[LAC17] Mathieu Lepot, Jean-Baptiste Aubin, and François HLR Clemens. Interpolation in time series: An introductive overview of existing methods, their performance criteria and uncertainty assessment. *Water*, 9(10):796, 2017.

[LAL+18] Marc Lang, Samuel Alleaume, Sandra Luque, Nicolas Baghdadi, and Jean-Baptiste Féret. Monitoring and characterizing heterogeneous mediterranean landscapes with continuous textural indices based on vhsr imagery. *Remote Sensing*, 10(6):868, 2018.

[LCHL+20] L Lebegue, E Cazala-Hourcade, F Languille, S Artigues, and O Melet. Co3d, a worldwide one one-meter accuracy dem for 2025. *The International Archives of Photogrammetry, Remote Sensing and Spatial Information Sciences*, 43:299–304, 2020.

[LDH+16] Vincent Lonjou, Camille Desjardins, Olivier Hagolle, Beatrice Petrucci, Thierry Tremas, Michel Dejus, Aliaksei Makarau, and Stefan Auer. Maccs-atcor joint algorithm (maja). In *Remote Sensing of Clouds and the Atmosphere XXI*, volume 10001, page 1000107. International Society for Optics and Photonics, 2016.

[LDWS19] Riccardo de Lutio, Stefano D'aronco, Jan Dirk Wegner, and Konrad Schindler. Guided super-resolution as pixel-to-pixel transformation. In *Proceedings of the IEEE/CVF International Conference on Computer Vision*, pages 8829–8837, 2019.

[LFG17] Adrien Lagrange, Mathieu Fauvel, and Manuel Grizonnet. Large-scale feature selection with gaussian mixture models for the classification of high dimensional remote sensing images. *IEEE Transactions on Computational Imaging*, 3(2):230–242, 2017.

[LFO01] F. Lahet, P. Forget, and S. Ouillon. Application of a colour classification method to quantify the constituents of coastal waters from in situ reflectances sampled at satellite sensor wavebands. *International Journal of Remote Sensing*, 22(5):909–914, 2001.

[LGP18] Yunan Luo, Kaiyu Guan, and Jian Peng. Stair: A generic and fully-automated method to fuse multiple sources of optical satellite data to generate a high-resolution, daily and cloud-/gap-free surface reflectance product. *Remote Sensing of Environment*, 214:87–99, 2018.

[LGew] Antoine Lucas and Eric Gayer. Decennal geomorphic transport from archived time series digital elevation models: a cookbook for tropical and alpine environments. *IEEE Geoscience and Remote Sensing Magazine*, pages GRSM–2021–00026.R1, in review.

[LMMB11] Antoine Lucas, Anne Mangeney, Daniel Mège, and François Bouchut. Influence of the scar geometry on landslide dynamics and deposits: Application to martian landslides. *Journal of Geophysical Research: Planets*, 116(E10), 2011.

[LNR+15] Antoine Lucas, Clément Narteau, Sébastien Rodriguez, Olivier Rozier, Yann Callot, Amandine Garcia, and Sylvain Courrech du Pont. Sediment flux from the morphodynamics of elongating linear dunes. *Geology*, 43(11):1027–1030, 2015.

[LTS20] Camille CD Lelong, Urcel Kalenga Tshingomba, and Valérie Soti. Assessing worldview-3 multispectral imaging abilities to map the tree diversity in semi-arid parklands. *International Journal of Applied Earth Observation and Geoinformation*, 93:102211, 2020.

[LWDF11] Anat Levin, Yair Weiss, Fredo Durand, and William T Freeman. Understanding blind deconvolution algorithms. *IEEE transactions on pattern analysis and machine intelligence*, 33(12):2354–2367, 2011.

[LYD+20] Kai Li, Shenghao Yang, Runting Dong, Xiaoying Wang, and Jianqiang Huang. Survey of single image super-resolution reconstruction. *IET Image Processing*, 14(11):2273–2290, 2020.

[MCP+17a] Sandro Martinis, Mathilde Caspard, Simon Plank, Stephen Clandillon, and Sadri Haouet. Mapping burn scars, fire severity and soil erosion susceptibility in southern france using multisensoral satellite data. In *2017 IEEE*

International Geoscience and Remote Sensing Symposium (IGARSS), pages 1099–1102. IEEE, 2017.

[MCP+17b] Sandro Martinis, Stephen Clandillon, Simon Plank, André Twele, Claire Huber, Mathilde Caspard, Jérôme Maxant, Wenxi Cao, Sadri Haouet, and Eva-Maria Fuchs. Asapterra-advancing sar and optical methods for rapid mapping. 2017.

[MFA07] Renaud Mathieu, Claire Freeman, and Jagannath Aryal. Mapping private gardens in urban areas using object-oriented techniques and very high-resolution satellite imagery. *Landscape and urban planning*, 81(3):179–192, 2007.

[MGG+19] Sergio Marconi, Sarah J Graves, Dihong Gong, Morteza Shahriari Nia, Marion Le Bras, Bonnie J Dorr, Peter Fontana, Justin Gearhart, Craig Greenberg, Dave J Harris, et al. A data science challenge for converting airborne remote sensing data into ecological information. *PeerJ*, 6:e5843, 2019.

[MGK00] D. C. Mason, C. Gurney, and M. Kennett. Beach topography mapping: A comparison of techniques. *Journal of Coastal Conservation*, 6(1):113–124, 2000.

[MHH+15] Jeffrey G Masek, Daniel J Hayes, M Joseph Hughes, Sean P Healey, and David P Turner. The role of remote sensing in process-scaling studies of managed forest ecosystems. *Forest Ecology and Management*, 355:109–123, 2015.

[MI21] J Michel and J Inglada. Learning harmonised pleiades and sentinel-2 surface reflectances. *The International Archives of Photogrammetry, Remote Sensing and Spatial Information Sciences*, 43:265–272, 2021.

[MJA+18] Larry Mayer, Martin Jakobsson, Graham Allen, Boris Dorschel, Robin Falconer, Vicki Ferrini, Geoffroy Lamarche, Helen Snaith, and Pauline Weatherall. The nippon foundation—gebco seabed 2030 project: The quest to see the world's oceans completely mapped by 2030. *Geosciences*, 8(2), 2018.

[MJSH12] T Moon, I Joughin, B Smith, and I Howat. 21st-century evolution of greenland outlet glacier velocities. *Science*, 336(6081):576–578, 2012.

[MLE+17] Joachim Maack, Marcus Lingenfelder, Christina Eilers, Thomas Smaltschinski, Holger Weinacker, Dirk Jaeger, and Barbara Koch. Estimating the spatial distribution, extent and potential lignocellulosic biomass supply of trees outside forests in baden-wuerttemberg using airborne lidar and openstreetmap data. *International journal of applied earth observation and geoinformation*, 58:118–125, 2017.

[MLS+16] Malcolm McMillan, Amber Leeson, Andrew Shepherd, Kate Briggs, Thomas WK Armitage, Anna Hogg, Peter Kuipers Munneke, Michiel Van Den Broeke, Brice Noel, Willem Jan van de Berg, et al. A high-resolution record of greenland mass balance. *Geophysical Research Letters*, 43(13):7002–7010, 2016.

[MMR+19] Romain Millan, Jérémie Mouginot, Antoine Rabatel, Seongsu Jeong, Diego Cusicanqui, Anna Derkacheva, and Mondher Chekki. Mapping Surface Flow Velocity of Glaciers at Regional Scale Using a Multiple Sensors Approach. *Remote Sensing*, 11(21), 2019.

[MRB+19] Jérémie Mouginot, Eric Rignot, Anders A Bjørk, Michiel Van den Broeke, Romain Millan, Mathieu Morlighem, Brice Noël, Bernd Scheuchl, and Michael Wood. Forty-six years of greenland ice sheet mass balance from 1972 to 2018. *Proceedings of the National Academy of Sciences*, 116(19):9239–9244, 2019.

[MRGW21] Eylül Malkoç, Marius Rüetschi, Christian Ginzler, and Lars T Waser. Countrywide mapping of trees outside forests based on remote sensing data in switzerland. *International Journal of Applied Earth Observation and Geoinformation*, 100:102336, 2021.

[MRSM17] Jeremie Mouginot, Eric Rignot, Bernd Scheuchl, and Romain Millan. Comprehensive annual ice sheet velocity mapping using landsat-8, sentinel-1, and radarsat-2 data. *Remote Sensing*, 9(4):364, 2017.

[MTLC+20] A. Melet, P. Teatini, G. Le Cozannet, C. Jamet, A. Conversi, J. Benveniste, and Rafael Almar. Earth observations for monitoring marine coastal hazards and their drivers. *Surveys in Geophysics*, [Early access]:[46 p.], 2020.

[MTZ+20] Bjarke Madsen, Urs A Treier, András Zlinszky, Arko Lucieer, and Signe Normand. Detecting shrub encroachment in seminatural grasslands using uas lidar. *Ecology and evolution*, 10(11):4876–4902, 2020.

[MWW10] Brice Mora, Michael A Wulder, and Joanne C White. Identifying leading species using tree crown metrics derived from very high spatial resolution imagery in a boreal forest environment. *Canadian Journal of Remote Sensing*, 36(4):332–344, 2010.

[Nab18] Jean Nabucet. *Apport des données de télédétection à très haute résolution spatiale pour la cartographie de la végétation en milieu urbain.* PhD thesis, Rennes 2, 2018.

[NK11] C. Nuth and A. Kääb. Co-registration and bias corrections of satellite elevation data sets for quantifying glacier thickness change. *The Cryosphere*, 5(1):271–290, 2011.

[NRD+15] Jean Nabucet, Simon Rougier, Julien Deniau, Léo Vétillard, Emilie Hanson, Omar Benarchid, Eléonore Wolff, Laurence Hubert-Moy, and Anne Puissant. Multi-scale methodology to map grey and green structures in urban areas using pléiades images and existing geographic data. *Revue Française de Photogrammétrie et de Télédétection*, (209):95–101, 2015.

[ODA04] Sylvain Ouillon, Pierre Douillet, and Serge Andréfouët. Coupling satellite data with in situ measurements and numerical modeling to study fine suspended-sediment transport: a study for the lagoon of new caledonia. *Coral Reefs*, 23(1):109–122, 2004.

[OP05] Sylvain Ouillon and Anne A Petrenko. Above-water measurements of reflectance and chlorophyll-a algorithms in the gulf of lions, nw mediterranean sea. *Optics Express*, 13(7):2531–2548, 2005.

[Pas21a] Ferrant S. Selles A. Marechal J.C. Gascoin S. Merlin Pascal, C. High resolution mapping of rainwater harvesting system capacity from satellite derived products in south india. In *IGARSS 2021*, 2021.

[Pas21b] Ferrant S. Selles A. Pena Luque S. Marechal J.C. Gascoin S. Merlin O. Pascal, C. Dem-based true bathymetry retrieval for surface water volume monitoring of rainwater harvesting system in south india. 2021.

[PBK+15] Frank Paul, Tobias Bolch, Andreas Kääb, Thomas Nagler, Christopher Nuth, Killian Scharrer, Andrew Shepherd, Tazio Strozzi, Francesca Ticconi, Rakesh Bhambri, Etienne Berthier, Suzanne Bevan, Noel Gourmelen, Torborg Heid, Seongsu Jeong, Matthias Kunz, Tom Rune Lauknes, Adrian Luckman, John Peter Merryman Boncori, Geir Moholdt, Alan Muir, Julia Neelmeijer, Melanie Rankl, Jeffrey VanLooy, and Thomas Van Niel. The glaciers climate change initiative: Methods for creating glacier area, elevation change and velocity products. *Remote Sensing of Environment*, 162:408–426, 2015.

[PCF07] Christophe Proisy, Pierre Couteron, and François Fromard. Predicting and mapping mangrove biomass from canopy grain analysis using fourier-based textural ordination of ikonos images. *Remote Sensing of Environment*, 109(3):379–392, 2007.

[PFW+13] Henrique Miguel Pereira, Simon Ferrier, M Walters, Gary N Geller, RHG Jongman, Robert J Scholes, Michael William Bruford, N Brummitt, SHM Butchart, AC Cardoso, et al. Essential biodiversity variables. *Science*, 339(6117):277–278, 2013.

[PIDMR16] Adrien Poupardin, Déborah Idier, Marcello De Michele, and Daniel Raucoules. Water Depth Inversion From a Single SPOT-5 Dataset. *IEEE Transactions on Geoscience and Remote Sensing*, 2016.

[PL19] Ruiliang Pu and Shawn Landry. Evaluating seasonal effect on forest leaf area index mapping using multi-seasonal high resolution satellite pléiades imagery. *International Journal of Applied Earth Observation and Geoinformation*, 80:268–279, 2019.

[PL21] Ferrant S. Cordeiro M.C.R. Martinez J.M. Peña-Luque, S. Regional sentinel-12 multitemporal water detection accuracies, evaluated at reservoirs level. 2021.

[PMG+19] Livia Piermattei, Mauro Marty, Christian Ginzler, Markus Pöchtrager, Wilfried Karel, Camillo Ressl, Norbert Pfeifer, and Markus Hollaus. Pléiades satellite images for deriving forest metrics in the alpine region. *International Journal of Applied Earth Observation and Geoinformation*, 80:240–256, 2019.

[PRS14] Anne Puissant, Simon Rougier, and André Stumpf. Object-oriented mapping of urban trees using random forest classifiers. *International Journal of Applied Earth Observation and Geoinformation*, 26:235–245, 2014.

[PWK+16] Frank Paul, Solveig H. Winsvold, Andreas Kääb, Thomas Nagler, and Gabriele Schwaizer. Glacier Remote Sensing Using Sentinel-2. Part II: Mapping Glacier Extents and Surface Facies, and Comparison to Landsat 8. *Remote Sensing*, 8(7), 2016.

[QMH+20] Mengjiao Qin, Sébastien Mavromatis, Linshu Hu, Feng Zhang, Renyi Liu, Jean Sequeira, and Zhenhong Du. Remote sensing single-image resolution improvement using a deep gradient-aware network with image-specific enhancement. *Remote Sensing*, 12:758, 02 2020.

[RBC+10] Duccio Rocchini, Niko Balkenhol, Gregory A Carter, Giles M Foody, Thomas W Gillespie, Kate S He, Salit Kark, Noam Levin, Kelly Lucas, Miska Luoto, et al. Remotely sensed spectral heterogeneity as a proxy of species diversity: recent advances and open challenges. *Ecological Informatics*, 5(5):318–329, 2010.

[RCL04] Duccio Rocchini, Alessandro Chiarucci, and Steven A Loiselle. Testing the spectral variation hypothesis by using satellite multispectral images. *Acta Oecologica*, 26(2):117–120, 2004.

[RPSL16] Simon Rougier, Anne Puissant, André Stumpf, and Nicolas Lachiche. Comparison of sampling strategies for object-based classification of urban vegetation from very high resolution satellite images. *International Journal of Applied Earth Observation and Geoinformation*, 51:60–73, 2016.

[RPZ+17] Zhibin Ren, Ruiliang Pu, Haifeng Zheng, Dan Zhang, and Xingyuan He. Spatiotemporal analyses of urban vegetation structural attributes using multitemporal landsat tm data and field measurements. *Annals of Forest Science*, 74(3):1–14, 2017.

[RSB+21] Duccio Rocchini, Nicole Salvatori, Carl Beierkuhnlein, Alessandro Chiarucci, Florian de Boissieu, Michael Förster, Carol X Garzon-Lopez, Thomas W Gillespie, Heidi C Hauffe, Kate S He, et al. From local spectral species to global spectral communities: A benchmark for ecosystem diversity estimate by remote sensing. *Ecological informatics*, 61:101195, 2021.

[SADB16] André Stumpf, Emmanuel Augereau, Christophe Delacourt, and Julien Bonnier. Photogrammetric discharge monitoring of small tropical mountain rivers: A case study at rivière des pluies, réunion island. *Water Resources Research*, 52(6):4550–4570, 2016.

[SAM+16] David E Shean, Oleg Alexandrov, Zachary M Moratto, Benjamin E Smith, Ian R Joughin, Claire Porter, and Paul Morin. An automated, open-source pipeline for mass production of digital elevation models (dems) from very-high-resolution commercial stereo satellite imagery. *ISPRS Journal of Photogrammetry and Remote Sensing*, 116:101–117, 2016.

[SASK15] Sebastian Schnell, Dan Altrell, Göran Ståhl, and Christoph Kleinn. The contribution of trees outside forests to national tree biomass and carbon stocks—a comparative study across three continents. *Environmental monitoring and assessment*, 187(1):1–18, 2015.

[SBF14] Claire Marais Sicre, Frédéric Baup, and Rémy Fieuzal. Determination of the crop row orientations from formosat-2 multi-temporal and panchromatic images. *ISPRS journal of photogrammetry and remote sensing*, 94:127–142, 2014.

[SBO+09] David Sheeren, N Bastin, Annie Ouin, Sylvie Ladet, Gérard Balent, and J-P Lacombe. Discriminating small wooded elements in rural landscape from aerial photography: a hybrid pixel/object-based analysis approach. *International Journal of Remote Sensing*, 30(19):4979–4990, 2009.

[SC12] Tony Schenk and Beata Csatho. A new methodology for detecting ice sheet surface elevation changes from laser altimetry data. *IEEE Transactions on Geoscience and Remote Sensing*, 50(9):3302–3316, 2012.

[SCH08] Rosanna Sosio, Giovanni B Crosta, and Oldrich Hungr. Complete dynamic modeling calibration for the thurwieser rock avalanche (italian central alps). *Engineering Geology*, 100(1-2):11–26, 2008.

[SFA+19] Edward Salameh, Frédéric Frappart, Rafael Almar, Paulo Baptista, Georg Heygster, Bertrand Lubac, Daniel Raucoules, Luis Pedro Almeida, Erwin W. J. Bergsma, Sylvain Capo, Marcello De Michele, Deborah Idier, Zhen Li, Vincent Marieu, Adrien Poupardin, Paulo A. Silva, Imen Turki, and Benoit Laignel. Monitoring beach topography and nearshore bathymetry using spaceborne remote sensing: A review. *Remote Sensing*, 11(19), 2019.

[SFG+20] Ben Smith, Helen A Fricker, Alex S Gardner, Brooke Medley, Johan Nilsson, Fernando S Paolo, Nicholas Holschuh, Susheel Adusumilli, Kelly Brunt, Bea Csatho, et al. Pervasive ice sheet mass loss reflects competing ocean and atmosphere processes. *Science*, 368(6496):1239–1242, 2020.

[SFM+18] Edward Salameh, Frédéric Frappart, Vincent Marieu, Alexandra Spodar, Jean-Paul Parisot, Vincent Hanquiez, Imen Turki, and Benoit Laignel. Monitoring sea level and topography of coastal lagoons using satellite radar altimetry: The example of the arcachon bay in the bay of biscay. *Remote Sensing*, 10(2), 2018.

[SFRRA+18] JJ Santiago-Freijanes, A Rigueiro-Rodríguez, JA Aldrey, G Moreno, M den Herder, Paul Burgess, and MR Mosquera-Losada. Understanding agroforestry practices in europe through landscape features policy promotion. *Agroforestry Systems*, 92(4):1105–1115, 2018.

[SGPVPP+20] E. Sánchez-García, J.M. Palomar-Vázquez, J.E. Pardo-Pascual, J. Almonacid-Caballer, C. Cabezas-Rabadán, and L. Gómez-Pujol. An efficient protocol for accurate and massive shoreline definition from mid-resolution satellite imagery. *Coastal Engineering*, 160:103732, 2020.

[SJD+19] David E Shean, Ian R Joughin, Pierre Dutrieux, Benjamin E Smith, and Etienne Berthier. Ice shelf basal melt rates from a high-resolution digital elevation model (dem) record for pine island glacier, antarctica. *The Cryosphere*, 13(10):2633–2656, 2019.

[SKL+20] Francesco M Sabatini, William S Keeton, Marcus Lindner, Miroslav Svoboda, Pieter J Verkerk, Jürgen Bauhus, Helge Bruelheide, Sabina Burrascano, Nicolas Debaive, Inês Duarte, et al. Protection gaps and restoration opportunities for primary forests in europe. *Diversity and Distributions*, 26(12):1646–1662, 2020.

[SKS15] Sebastian Schnell, Christoph Kleinn, and Göran Ståhl. Monitoring trees outside forests: a review. *Environmental monitoring and assessment*, 187(9):1–17, 2015.

[SLP+15] Cornelius Senf, Pedro J Leitão, Dirk Pflugmacher, Sebastian van der Linden, and Patrick Hostert. Mapping land cover in complex mediterranean landscapes using landsat: Improved classification accuracies from integrating multi-seasonal and synthetic imagery. *Remote Sensing of Environment*, 156:527–536, 2015.

[SMA+15] André Stumpf, J-P Malet, Pascal Allemand, Marc Pierrot-Deseilligny, and Grzegorz Skupinski. Ground-based multi-view photogrammetry for the monitoring of landslide deformation and erosion. *Geomorphology*, 231:130–145, 2015.

[SMC+12] David Sheeren, Antoine Masse, Fanny Collard, Stéphane May, Danielle Ducrot, and Mathieu Fauvel. La télédétection pour la cartographie de la trame verte en milieu agricole. évaluation des potentialités d'images multi-angulaires à très haute résolution spatiale. *Rev. Int. Géomatique*, 22(4):539–563, 2012.

[SMD17] André Stumpf, Jean-Philippe Malet, and Christophe Delacourt. Correlation of satellite image time-series for the detection and monitoring of slow-moving landslides. *Remote sensing of environment*, 189:40–55, 2017.

[SMS+17] Fabian D Schneider, Felix Morsdorf, Bernhard Schmid, Owen L Petchey, Andreas Hueni, David S Schimel, and Michael E Schaepman. Mapping functional diversity from remotely sensed morphological and physiological forest traits. *Nature communications*, 8(1):1–12, 2017.

[SRB05] James M Suttie, Stephen G Reynolds, and Caterina Batello. *Grasslands of the World*, volume 34. Food & Agriculture Org., 2005.

[STAL20] Martin Sudmanns, Dirk Tiede, Hannah Augustin, and Stefan Lang. Assessing global sentinel-2 coverage dynamics and data availability for operational earth observation (eo) applications using the eo-compass. *International Journal of Digital Earth*, 13(7):768–784, 2020.

[TA92] R. Tateishi and A. Akutsu. Relative dem production from spot data without gcp. *International Journal of Remote Sensing*, 13(14):2517–2530, 1992.

[TAB+21] Adélaïde Taveneau, Rafaël Almar, Erwin W. J. Bergsma, Boubou Aldiouma Sy, Abdoulaye Ndour, Mamadou Sadio, and Thierry Garlan. Observing and predicting coastal erosion at the langue de barbarie sand spit around saint louis (senegal, west africa) through satellite-derived digital elevation model and shoreline. *Remote Sensing*, 13(13), 2021.

[TCA+09] Kevin Tansey, Ian Chambers, Andrew Anstee, Anthony Denniss, and Alistair Lamb. Object-oriented classification of very high resolution airborne imagery for the extraction of hedgerows and field margin cover in agricultural areas. *Applied geography*, 29(2):145–157, 2009.

[THAB21] Ian L. Turner, Mitchell D. Harley, Rafael Almar, and Erwin W.J. Bergsma. Satellite optical imagery in coastal engineering. *Coastal Engineering*, 167:103919, 2021.

[TLH13] Jan Tigges, Tobia Lakes, and Patrick Hostert. Urban vegetation classification: Benefits of multitemporal rapideye satellite data. *Remote Sensing of environment*, 136:66–75, 2013.

[TP05] Sakari Tuominen and Anssi Pekkarinen. Performance of different spectral and textural aerial photograph features in multi-source forest inventory. *Remote sensing of Environment*, 94(2):256–268, 2005.

[TRP+09] Devis Tuia, Frédéric Ratle, Fabio Pacifici, Mikhail F Kanevski, and William J Emery. Active learning methods for remote sensing image classification. *IEEE Transactions on Geoscience and Remote Sensing*, 47(7):2218–2232, 2009.

[VCVDW07] Frieke MB Van Coillie, Lieven PC Verbeke, and Robert R De Wulf. Feature selection by genetic algorithms in object-based classification of ikonos imagery for forest mapping in flanders, belgium. *Remote Sensing of Environment*, 110(4):476–487, 2007.

[VDG11] An Van Delm and Hubert Gulinck. Classification and quantification of green in the expanding urban and semi-urban complex: Application of detailed field data and ikonos-imagery. *Ecological Indicators*, 11(1):52–60, 2011.

[VHM08] Clémence Vannier and Laurence Hubert-Moy. Detection of wooded hedgerows in high resolution satellite images using an object-oriented method. In *IGARSS 2008-2008 IEEE International Geoscience and Remote Sensing Symposium*, volume 4, pages IV–731. IEEE, 2008.

[VKST14] Charles Verpoorter, Tiit Kutser, David A Seekell, and Lars J Tranvik. A global inventory of lakes based on high-resolution satellite imagery. *Geophysical Research Letters*, 41(18):6396–6402, 2014.

[VL12] Pieter Vermeesch and Sebastien Leprince. A 45-year time series of dune mobility indicating constant windiness over the central sahara. *Geophysical Research Letters*, 39(14), 2012.

[VLDM12] Vincent Vantrepotte, Hubert Loisel, David Dessailly, and Xavier Mériaux. Optical classification of contrasted coastal waters. *Remote Sensing of Environment*, 123:306–323, 2012.

[VMD+18] Anton Vrieling, Michele Meroni, Roshanak Darvishzadeh, Andrew K Skidmore, Tiejun Wang, Raul Zurita-Milla, Kees Oosterbeek, Brian O'Connor, and Marc Paganini. Vegetation phenology from sentinel-2 and field cameras for a dutch barrier island. *Remote Sensing of Environment*, 215:517–529, 2018.

[WBE+08] LT Waser, Emmanuel Baltsavias, K Ecker, H Eisenbeiss, E Feldmeyer-Christe, C Ginzler, M Küchler, and L Zhang. Assessing changes of forest area and shrub encroachment in a mire ecosystem using digital surface models and cir aerial images. *Remote Sensing of Environment*, 112(5):1956–1968, 2008.

[WCDD04] Jan Walstra, JH Chandler, N Dixon, and TA Dijkstra. Extracting landslide movements from historical aerial photographs. *Landslides: evaluation and stabilization. Taylor & Francis, London*, pages 843–850, 2004.

[WCW+16] Joanne C White, Nicholas C Coops, Michael A Wulder, Mikko Vastaranta, Thomas Hilker, and Piotr Tompalski. Remote sensing technologies for enhancing forest inventories: A review. *Canadian Journal of Remote Sensing*, 42(5):619–641, 2016.

[WF03] Michael A Wulder and Steven E Franklin. *Remote Sensing of Forest Environments: Concepts and Case Studies*. Springer Science & Business Media, 2003.

[WMC+12] Michael A Wulder, Jeffrey G Masek, Warren B Cohen, Thomas R Loveland, and Curtis E Woodcock. Opening the archive: How free data has enabled the science and monitoring promise of landsat. *Remote Sensing of Environment*, 122:2–10, 2012.

[WSA+19] Anne-Cathrin Wölfl, Helen Snaith, Sam Amirebrahimi, Colin W. Devey, Boris Dorschel, Vicki Ferrini, Veerle A. I. Huvenne, Martin Jakobsson, Jennifer Jencks, Gordon Johnston, Geoffroy Lamarche, Larry Mayer, David Millar, Terje Haga Pedersen, Kim Picard, Anja Reitz, Thierry Schmitt, Martin Visbeck, Pauline Weatherall, and Rochelle Wigley. Seafloor mapping – the challenge of a truly global ocean bathymetry. *Frontiers in Marine Science*, 6:283, 2019.

[WSVS09] Craig E Williamson, Jasmine E Saros, Warwick F Vincent, and John P Smol. Lakes and reservoirs as sentinels, integrators, and regulators of climate change. *Limnology and Oceanography*, 54(6part2):2273–2282, 2009.

[XSY08] Yichun Xie, Zongyao Sha, and Mei Yu. Remote sensing imagery in vegetation mapping: a review. *Journal of plant ecology*, 1(1):9–23, 2008.

[Xu18] Nan Xu. Detecting coastline change with all available landsat data over 1986–2015: A case study for the state of texas, usa. *Atmosphere*, 9(3), 2018.

[YQY+20] Xiucheng Yang, Qiming Qin, Hervé Yésou, Thomas Ledauphin, Mathieu Koehl, Pierre Grussenmeyer, and Zhe Zhu. Monthly estimation of the surface water extent in france at a 10-m resolution using sentinel-2 data. *Remote Sensing of Environment*, 244:111803, 2020.

[ZCTW18] Xiaolin Zhu, Fangyi Cai, Jiaqi Tian, and Trecia Kay-Ann Williams. Spatiotemporal fusion of multisource remote sensing data: Literature survey, taxonomy, principles, applications, and future directions. *Remote Sensing*, 10(4):527, 2018.

[ZFJ10] Xiuying Zhang, Xuezhi Feng, and Hong Jiang. Object-oriented method for urban vegetation mapping using ikonos imagery. *International Journal of Remote Sensing*, 31(1):177–196, 2010.

Appendices

(a) Guide, target and reference time-series time sampling and clear pixels coverage

(b) Guide time-series

(c) Target and reference time-series

Figure 5.1: Guide, target and reference time-series for MAD-AMBO site

(a) Guide, target and reference time-series time sampling and clear pixels coverage

(b) Guide time-series

(c) Target and reference time-series

Figure 5.2: Guide, target and reference time-series for FR-LQ1 site

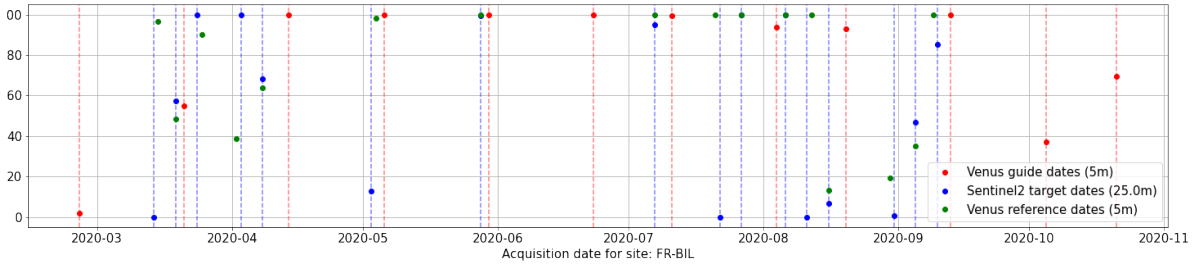

(a) Guide, target and reference time-series time sampling and clear pixels coverage

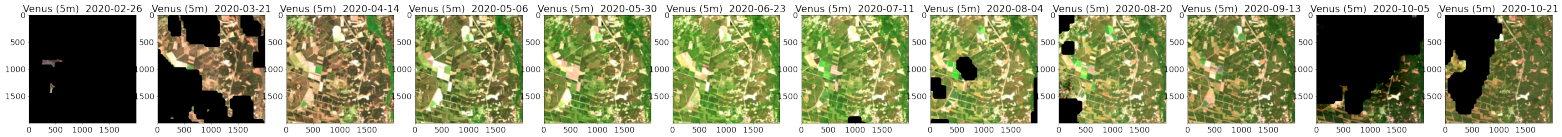

(b) Guide time-series

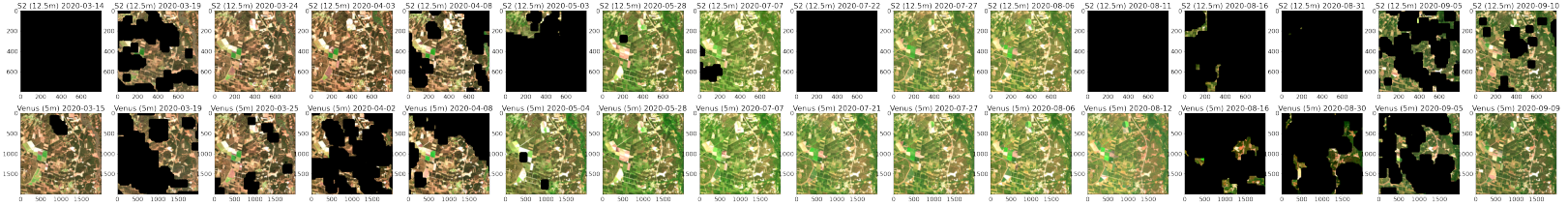

(c) Target and reference time-series

Figure 5.3: Guide, target and reference time-series for FR-BIL site

(a) Guide, target and reference time-series time sampling and clear pixels coverage

(b) Guide time-series

(c) Target and reference time-series

Figure 5.4: Guide, target and reference time-series for ARM site

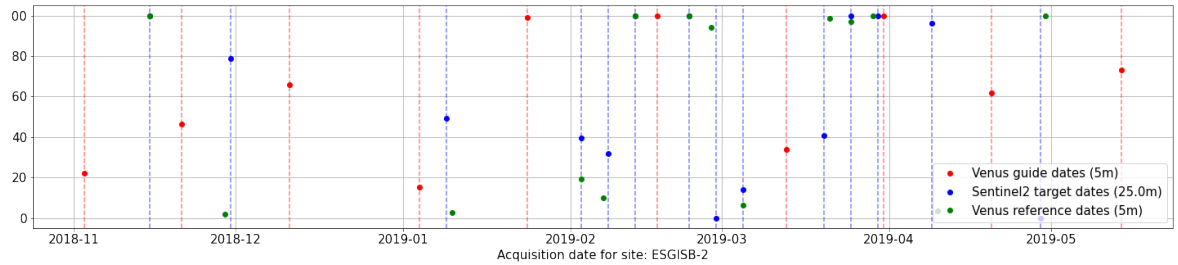

(a) Guide, target and reference time-series time sampling and clear pixels coverage

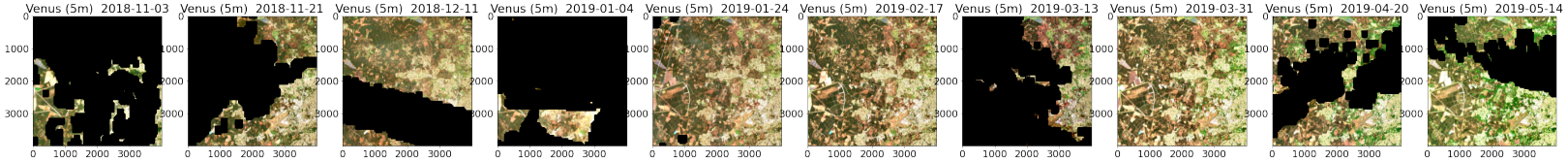

(b) Guide time-series

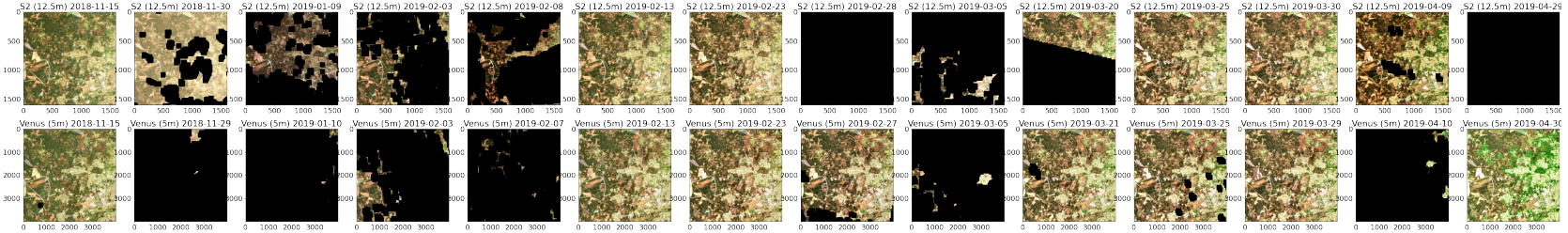

(c) Target and reference time-series

Figure 5.5: Guide, target and reference time-series for ESGISB-2 site